**The Thesis Committee for Nicholas Daniel Griffith**
**Certifies that this is the approved version of the following thesis:**

# Nanoparticle-Stabilized Natural Gas Liquid Emulsions for Heavy Oil Recovery

**APPROVED BY**
**SUPERVISING COMMITTEE:**

**Supervisor:**

Hugh Daigle

Kishore Mohanty

# Nanoparticle-Stabilized Natural Gas Liquid Emulsions for Heavy Oil Recovery

**by**

**Nicholas Daniel Griffith, B.S.**

**Thesis**

Presented to the Faculty of the Graduate School of

The University of Texas at Austin

in Partial Fulfillment

of the Requirements

for the Degree of

**Master of Science in Engineering**

**The University of Texas at Austin**

**May 2017**

# Dedication

To my parents.

# Acknowledgements

I would like to thank my advisor, Dr. Hugh Daigle, for his guidance, support, and comedic relief during my graduate studies and research. I would also like to thank Dr. Chun Huh and Dr. Kishore Mohanty for their help and insight throughout my research.

I would like to thank Chris Griffith for his company in the lab and insightful discussions about tiny things. Also, I would like to thank Saebom Ko and Ijung Kim for bestowing their knowledge of nanoparticles on me. Special thanks to Yusra Ahmad for showing me the ropes in the lab. Many thanks to the Yates family for sponsoring me as a graduate student and SURI program participant.

I would also like to thank Glen Baum and Gary Miscoe for their help with lab equipment and preparation for experiments.

Finally, I would like to thank the Nanoparticle for Subsurface Engineering consortium for funding this research.

# Abstract

## Nanoparticle-Stabilized Natural Gas Liquid Emulsions for Heavy Oil Recovery

Nicholas Daniel Griffith, M.S.E.

The University of Texas at Austin, 2017

Supervisor: Hugh Daigle

The transport of nanoparticle-stabilized emulsions through porous media and its effects on enhanced oil recovery are only marginally understood. This thesis explores the characteristics of nanoparticle-stabilized emulsion flow in porous media, especially in respect to its residual oil recovery capabilities.

Widely available, low-cost natural gas liquids were emulsified in brines using polyethylene glycol-coated silica nanoparticles. Emulsions with various aqueous nanoparticle phases and oil phases were generated via beadpack co-injection or sonication at varying salinities for observations of emulsion characteristics. In general it was found that high-salinity emulsions generated via sonication were more robust: statically and dynamically more stable than their lower salinity counterparts. Emulsions generated via beadpack co-injection displayed non-Newtonian shear-thinning rheology and larger droplet sizes. Emulsions generated via sonication displayed Newtonian rheology and much smaller droplet sizes.

Coreflood experiments were conducted to assess the effects of different emulsion properties on residual oil recovery of heavy oils, effective permeability reduction capabilities (i.e. conformance control), and in-situ emulsion stability. During low salinity

emulsion floods, no emulsion was produced in the effluent. However, by increasing the salinity, emulsion was produced in the effluent and up to 89% residual mineral oil was recovered at low injection rates (~16 ft/day). Increases in residual oil recovery during high salinity floods can be explained by DLVO and Filtration theory. By increasing the ionic concentration, the magnitude of repulsive electrostatic double layer forces are decreased, leading to increased droplet interception on grain surfaces. This results in more efficient droplet-pore throat blockage, therefore, redirecting displacing fluids into less permeable zones. Increasing the magnitude of the zeta-potential of injected emulsions resulted in marginal increases in oil recovery, significant reductions in effective permeability, and in-situ emulsion stability. It was concluded that at high zeta-potentials, emulsion droplets are likely repulsed via electrostatic repulsive forces rather than through mechanical bridging of aggregates between droplets, as observed in high salinity emulsions. The increase in permeability reduction in the high zeta-potential case occurs due to the droplets' increased resistance to flow through a pore throat, a product of increased repulsive forces between droplets and grains encountered at tight constrictions.

# Table of Contents

# List of Tables

# List of Figures

# Chapter 1

# Introduction

As an alternative to conventional surfactant-stabilized emulsion for enhanced oil recovery, solids-stabilized oil and water emulsions have garnered interest in the oil and gas industry for some time. While colloidal particles >100 nm in diameter may plug pore throats and be retained indefinitely in porous media inhibiting long range transport into reservoirs, recent advances in nanotechnology have led to decreases in particle size (to the nanometer range). Furthermore, increases in nanoparticle stability and degree of customizable surface coatings for specific downhole environments make field use of this technology feasible. Due to their high-specific surface areas and range of available materials and surface coatings, ultra-robust nanoparticles can be designed for stability in extreme conditions such as high salinity and high temperature. The relative high cost of nanoparticles compared to surfactants is expected to decrease as research and development initiatives evolve into mass production. Furthermore, the cost of using nanoparticle-stabilized emulsions in the field can be reduced by employing low-cost and widely available natural gas liquids as the oil phase.

When used as an enhanced oil recovery technique after waterflooding procedures, injected emulsions plug high permeability zones and redirect flow elsewhere, resulting in a more piston-like displacement front and increased sweep efficiencies. When displacing heavy oils, injected emulsions decrease the mobility ratio aiding in further recovery of otherwise trapped viscous oil. Also, by injecting an emulsified oil phase, the relative permeability to oil increases, increasing the fractional flow of residual oil. Just as nanoparticles are highly customizable, so too are the emulsions that they stabilize. Factors such as nanoparticle type, droplet size, oil type, phase concentrations, droplet

concentration, salinity, injection rate, etc. can be designed to optimize oil recovery potential in varying downhole environments. In order to better understand the flow behavior and stability of nanoparticle-stabilized emulsions during flow through porous media, this thesis will investigate the effects of emulsion droplet size, injection rate, generation technique, zeta-potential, and salinity on static and in-situ stability, as well as effective permeability reduction and residual oil recovery.

## 1.1 Thesis Outline

This thesis is composed of five chapters. The first chapter serves as an introduction to the capabilities and feasibility of nanoparticle-stabilized emulsions for enhanced oil recovery in the oil and gas industry. The second chapter is a literature review, detailing pertinent research related to the scope of this thesis. The third chapter investigates the static stability of nanoparticle-stabilized natural gas liquid-in-water emulsions. The fourth chapter provides a detailed analysis on a set of coreflood tests, investigating how various emulsion characteristics effect in-situ stability and flow behavior. The fifth, and final chapter summarizes the conclusions of this research and provides recommendations for future work.

# Chapter 2

# Literature Review

## 2.1 Nanoparticles and their Role as Emulsifying Agents

An emulsion is a mixture of two otherwise immiscible liquids. It consists of a dispersed and continuous phase, in which the dispersed phase is found in droplet form, distributed in the continuous phase. If two immiscible fluids are mixed, say water and oil, and small oil droplets become dispersed in water, the droplets will eventually coalesce and the two phases will separate without the use of a stabilizing agent. The interface between the normally immiscible dispersed and continuous phases requires an emulsifying agent to stabilize the system. Conventional oil-water emulsions used in the oil and gas industry have been stabilized by surfactants. Surfactants stabilize droplet interfaces by reducing the interfacial tension between the phases. On the contrary, adsorption of solid, colloidal to nano-sized particles to droplet interfaces have proven to be a robust alternative to surfactant emulsifying agents. First characterized by S.U. Pickering in 1907 (Pickering, 1907), these emulsions have garnered recent attention in the oil and gas industry, in part because of accelerated advances in nanotechnology over the past decade. While colloidal particles (>100 nm in diameter) may plug pore throats and be retained in porous media, nanoparticles are small enough to pass through these pores. Furthermore, nanoparticles, with their a high surface area-to-volume ratio and specialized surface coatings can be used to create robust emulsions, with capabilities of enduring harsh reservoir conditions such as high salinity, pressure, and temperature, which often destabilize conventional surfactant-stabilized emulsions.

Most of the nanoparticles used to stabilize oil-water emulsions in oil field applications, including the ones used in this thesis, are spherical and made of silica, with

diameters ranging in the tens of nanometers. The silica nanoparticles used in this study are coated with polyethylene glycol or proprietary surface groups. The nanoparticles coated with polyethylene glycol will be referred to as PEG-coated, while many of the proprietary coatings are likely variations of PEG-coated nanoparticles. While bare silica nanoparticles do not decrease the interfacial tension between oil and water, grafted polymer chains on the nanoparticles penetrate the oil-water interface, reducing the interfacial tension between the phases (Saleh et al., 2005). The nanoparticles adhere to immiscible, polar/non-polar phases due to their partially wetting nature, and when shear is applied to this boundary, droplets can form, stabilized by nanoparticles that have now found themselves in a surface energy well as a result of asymmetric charge distributions and large electrical dipole forces (Pieranski, 1980). In addition to reductions in interfacial tension, dendritic PEG-coated nanoparticles enhance inter-droplet stability and resistance to coalescence via increased steric and electrostatic repulsive forces (Saigal et al., 2010)

The wettability of the nanoparticles is controlled by the extent of the silanol group coverage on the particle surface (Binks, 2002). Silica nanoparticles that contain over 90% silanol groups are hydrophilic (soluble in polar solutions) and will form oil-in-water emulsions. They will have a contact angle of <90° at the oil-water interface. Conversely, nanoparticles with less than 10% silanol groups are hydrophobic (soluble in non-polar solutions) and will form water-in-oil emulsions and have a contact angle of >90°. Nanoparticles partially coated with silanol groups (percent coverage between 10% and 90%) are described as having “intermediate hydrophobicity”. The type of emulsion formed will be dependent on the polarity of the oil phase: non-polar oils result in oil-in-water emulsions and polar oils result in water-in-oil emulsions (Zhang et al., 2010). A schematic description of this phenomenon is shown in Figure 2.1.

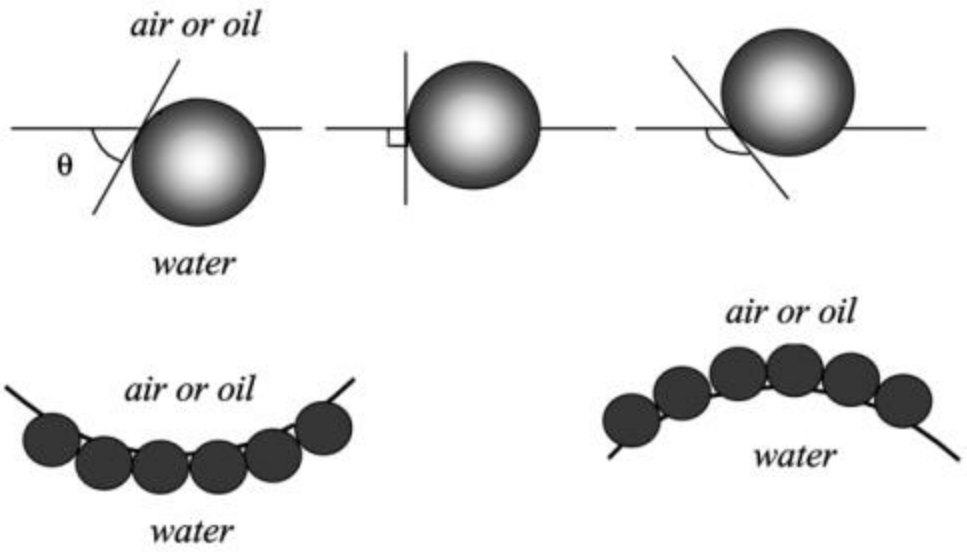


Figure 2.1: (Upper) Position of a small spherical particle at a planar fluid-water interphase. Contact angle measured through the aqueous phase. Contact angle is less than 90° for a hydrophilic particle (left), equal to 90° for an intermediate particle (center), greater than 90° for a hydrophobic particle (right). Oil-in-water emulsion (left). Water-in-oil emulsion (right). (Binks, 2002).

## 2.2 EMULSION STABILITY AND RHEOLOGY

Due to the increased interest in nanoparticle-stabilized emulsions, many studies have been done on emulsion characterization. These include droplet size, bulk viscosity, zeta potential, interfacial properties, and degree of stability in extreme conditions. A variety of studies have been conducted on factors affecting both static and dynamic emulsion behavior. In general, an emulsion will destabilize or completely break (coalescence) via separation into bulk immiscible phases. This process is governed by four different precursors to droplet coalescence: Brownian flocculation, creaming, sedimentation flocculation, and disproportion, otherwise known as Ostwald ripening (Particle Sciences, 2011). Emulsion creaming, a precursor to droplet coalescence, occurs as the continuous phase separates from the emulsion phase due to density differences. Flocculation occurs as

droplets tend to aggregate due to weak, attractive forces between one another. Finally, disproportionation or Ostwald ripening occurs due the diffusion of smaller droplets to larger droplets through the continuous phase. A summary of these processes is shown below in Figure 2.2.

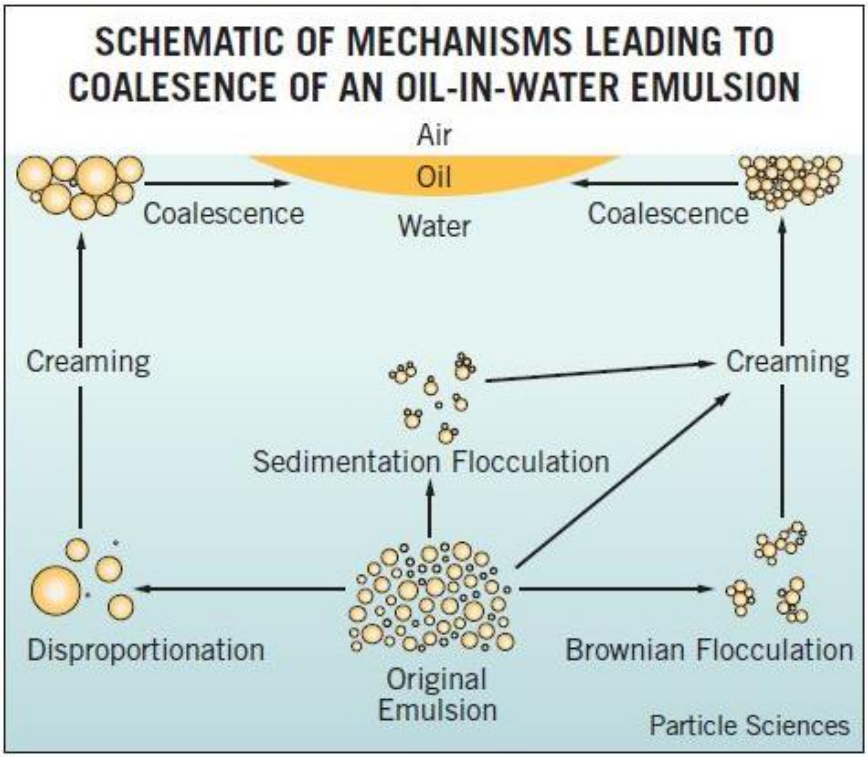


Figure 2.2: Summary of processes responsible for oil-in-water emulsion coalescence (Particle Sciences, 2011).

Research has been conducted on the effects of nanoparticle size, wettability, and concentration, ionic strength of the aqueous phase, pH, and oil type. Binks and Lumsdon (2000a) found that very hydrophobic and very hydrophilic nanoparticles created very large, unstable emulsion droplets, whereas particles exhibiting intermediate hydrophobicity generated small, stable emulsion droplets. Unlike surfactant-stabilized emulsions whose

preferential emulsion type depends on the initial location of the emulsifying agent, nanoparticles with intermediate hydrophobicity have been found to be more hydrophilic, preferring oil-in-water emulsions in the presence of non-polar oils (Binks and Lumsdon, 2000b).

Horozov et al. (2007) investigated the effects of pH and electrolyte concentration on overall emulsion stability and rheological properties. The critical flocculation concentration was defined as the electrolyte concentration at which there was a significant increase in the turbidity and acceleration of sedimentation in the suspension. As the electrolyte concentration was increased, nanoparticles began to aggregate due to reductions in the electrostatic double layer (EDL) potential between particles. This is consistent with colloidal stability theory developed by Derjaguin, Landau, Verwey, and Overbeek (DLVO) for increases in ionic concentration (Derjaguin, et al., 1993; Verwey et al., 1999). Emulsions generated using nanoparticle dispersions with high electrolyte concentrations were shown to possess higher apparent viscosities and greater stability, i.e. greater resistance to creaming (Horozov et al., 2007). This was attributed to the aggregation of nanoparticles in the dispersion phase, resulting in the formation of a three-dimensional network of interconnected droplets and aggregates. Work by Kostakis et al. (2005) also supports these findings, with observed increases in the stability of nanoparticle-stabilized foams with increasing ionic concentration. Interestingly, not all salts at similar ionic strengths resulted in enhanced stability of the foams. Rather than decreases in EDL potential as DLVO theory would predict, the effective hydrophobicity of nanoparticles at immiscible interfaces was increased, dependent on the type of ions in solution. The findings of these studies are best summarized by Figure 2.3.

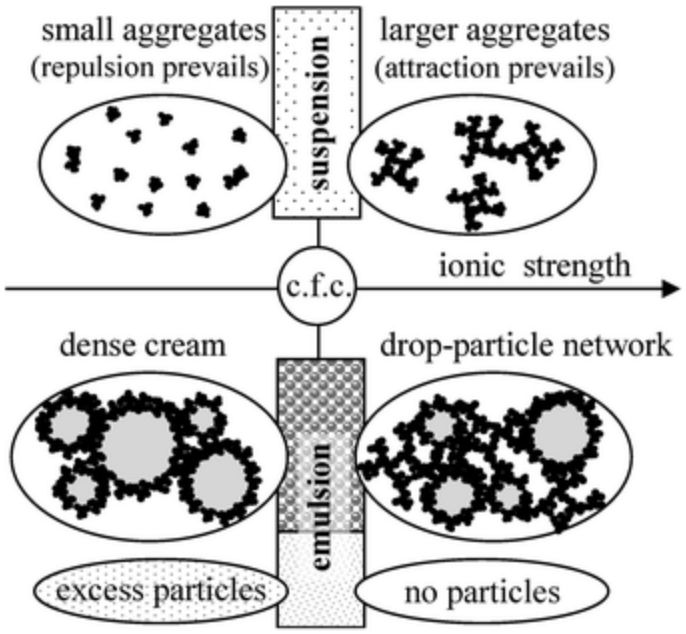


Figure 2.3: Schematic summarizing the effect of electrolyte concentration on the electrostatic repulsion of nanoparticles in the aqueous suspension (top) and in the oil-in-water nanoparticle-stabilized emulsions (bottom) at ionic strengths below (left) and above (right) the critical flocculation concentration of the aqueous suspension (Horozov et al., 2007).

Furthermore, Stancik (2004) showed that droplet-droplet zipping can occur in which a monolayer of bridging nanoparticles can connect multiple droplets. Horozov (2008) proposed three possible mechanisms for nanoparticle-stabilized droplet-droplet interactions: monolayers of bridging particles, bilayers of close-packed particles, or networks of particle aggregates between the interfaces (as in the high salinity cases discussed previously). Graphical representations of these proposed mechanisms are shown in Figure 2.4.

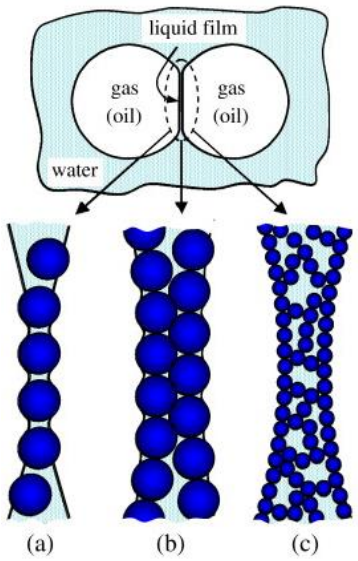


Figure 2.4: Possible mechanisms of Pickering emulsion droplet-to-droplet interactions and stabilization by: (a) a monolayer of bridging particles; (b) a bilayer of close-packed particles and (c) a network of particle aggregates (gel) between the interfaces (Horozov, 2008).

Emulsions utilizing the synergistic stabilizing effects of nanoparticles and surfactants have come to recent attention in the last several years. Pilapil et al. (2016) investigated applications of these synergistic emulsifiers, finding increases in the stability of oil-in-water emulsions to coalescence when used. It was concluded that the surfactants had a large role in initializing the emulsion droplet formation by reducing interfacial tension, while the nanoparticles aided in the mechanical stability of the droplets. Furthermore, the location of the nanoparticles in respect to oil-water interfaces was determined. Extremely hydrophilic nanoparticles acted as a cushion in between droplets (no adsorption to interfaces), adding resistance to droplet-droplet contact, while partially hydrophobic nanoparticles actually adsorbed to droplet interfaces, providing a mechanical barrier to coalescence. The synergy of nanoparticles and surfactants as emulsion stabilizers

decreased the total concentration of emulsifying agent needed to generate stable emulsions. This is appealing for field use due to potential total cost reductions for emulsifying agents.

Both Zhang et al. (2010) and Gabel (2014) observed that silica nanoparticle-stabilized oil-in-water emulsions generated via beadpack co-injection were highly shear-thinning power-law fluids. As the shear rate increased, the apparent viscosity of the emulsion decreased. Ultimately, the shear-thinning behavior of nanoparticle-stabilized emulsions is due to the weak-attractive forces between droplets, giving rise to the formation of a weak elastic, gel-like network (Dickinson, 1992). As shear stress is applied to the emulsion, the distance between droplets begins to increase. An emulsion's resistance to flow begins to decrease as the weak attractive forces are overcome with increasing shear stress, leading to this shear-thinning behavior (Torres et al., 2007). Gabel showed that the apparent viscosity was independent of the nature of the oil phase, rather highly dependent on emulsion droplet size – with increasing apparent viscosity as droplet size decreased. Zhang et al. (2010) also hypothesized that the apparent viscosity could be dependent on the extent of droplet surface coverage with particles and the average distance between droplets.

### 2.3 Emulsion Flow Through Porous Media

In the past, work on nanoparticle-stabilized emulsion flow through porous media has described the flow mechanism as dominated by a front of coalescence and regeneration of droplets (Gabel, 2014; Ahmad, 2015). On the contrary, nanoparticle-stabilized emulsion flow through porous media is likely more similar to that of surfactant-stabilized emulsions, where droplet-pore blockage mechanisms dominate, dependent on droplet to pore throat diameter distributions and injection rates. Research on surfactant-stabilized emulsion flow through porous media has been heavily documented, dating back to McAuliffe (1973)

studying the effect of droplet size and injection rates on effective permeability reduction and conformance control.

Likely the most comprehensive and well-developed model for general emulsion flow through porous media is filtration theory developed by Soo (1981) for dilute, stable emulsions. Filtration theory proposes two methods of droplet capture in porous media: straining and interception. Filtration theory is similar but differs from conventional deep-bed filtration theory in that relative droplet to grain size ratios in emulsion flow through porous media are much larger than typical colloid or nano-sized particles used to develop deep-bed theory. Straining occurs when droplets become lodged in pore throats that are smaller than the droplets' diameter. Furthermore, it addresses at what critical states droplets will become re-entrained or squeezed through the pore-throats due to local pressure gradients (governed by the Young-Laplace equation) or droplet breakup/re-generation. It was found that as the capillary number was decreased and/or the droplet-to-pore throat diameter was increased, more droplets were able to block pore throats leading to larger effective permeability reduction in sandpacks. The model also takes into account the effect of interception capture which is similar to deep-filtration theory. The two main mechanisms of this phenomenon are droplet surface capture due to surface forces such as Van der Waals and electric double-layer forces, or mechanical droplet wedging and dead-space capture. The model shows that even droplets smaller than pore throats can be captured in porous media due to crevices where flow is stagnant, or through droplet-to-grain surface interactions, stuck in primary or secondary energy wells, as described by extended DLVO theory. A critical re-entrapment velocity for a droplet attached to a grain can be calculated depending on assumptions made about the ionic concentration, type of emulsifier, and surface chemistry of the system. By isolating the size of the droplets in the experiments, effective permeability reduction from droplet straining and interception capture

mechanisms were verified separately in experiments of surfactant-stabilized emulsion flow through Berea sandstone. While filtration theory was developed specifically for dilute emulsions (the work in this thesis focuses on dense emulsions), this should serve as an effective analogue going forward.

More recently, advances in micromodel science have allowed researchers to observe particle and emulsion flow through complex geometries and constrictions, analogous to phenomena seen in porous media and many biological systems. Researchers have characterized different types of microchannel blocking mechanisms for particles and droplets as shown in Figure 2.5.

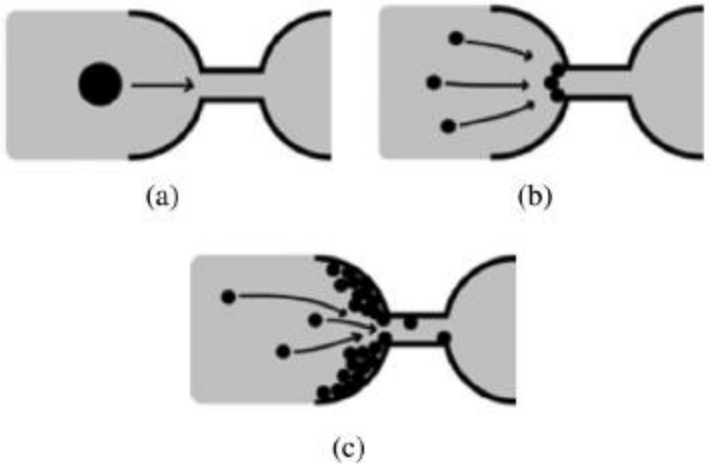


Figure 2.5: Examples of droplet/particle microchannel clogging mechanisms: (a) sieving, (b) bridging, (c) aggregation. Resulting mechanism(s) at constrictions depend on droplet/particle size distribution relative to the constriction diameter, concentration of suspension, and particle-wall and particle-particle interactions (Dressaire and Sauret, 2017)

Cobos et al. (2009) investigated flow of surfactant-stabilized emulsions through a constricted capillary tube. They found that for emulsion droplets smaller than capillary throat diameters, effective permeability reduction does not vary with capillary number, rather dependent on bulk emulsion characteristics such as: phase viscosity ratio, surfactant

concentration, and drop size distribution. Conversely, for emulsions with drops larger than the constriction, large oil droplets partially blocked the capillary, leading to greater effective permeability reductions at lower capillary numbers. Xu et al. (2016) developed dual-permeability micromodels representing fracture-matrix pore systems and injected nanoparticle and/or surfactant-stabilized emulsions observing the effects of emulsion droplet behavior in these micromodels. The nanoparticle and surfactant-stabilized emulsion exhibited enhanced, synergistic capabilities compared to those stabilized by a single emulsifying agent, namely denser packing in high permeability regions and enhanced stability. This research displayed the potential of synergistic emulsions for increased sweep efficiencies and conformance control in respect to enhanced oil recovery applications.

### 2.4 NANOPARTICLE-STABILIZED EMULSIONS FOR ENHANCED OIL RECOVERY

The ultimate motivation for research on nanoparticle-stabilized emulsions in the scope of oilfield operations is for improved oil recovery. After reservoirs have been depleted either through primary production and/or waterflooding procedures, over 50% of the original oil in place (OOIP) may remain in the ground. Poor sweep efficiencies are often the strongest factor in preventing oil from being produced in field operations. These poor sweep efficiencies are often due to heterogeneities in reservoir geology where a majority of injected fluids are directed to high permeability channels, and/or unfavorable mobility ratios leading to viscous fingering. The mobility ratio for immiscible displacements is defined as the ratio of the mobility of the displacing to the displaced fluid, as shown below:

$$M = \frac{\lambda_{water}}{\lambda_{oil}} = \frac{k_{r_{water}} \cdot \mu_{oil}}{k_{r_{oil}} \cdot \mu_{water}}, \quad (1)$$

where $\lambda$ is the mobility of each respective phase, $k_r$ is the relative permeability of each phase, and $\mu$ is the phase viscosity. Improvements in oil recovery can be obtained through methods that have been classified as enhanced oil recovery (EOR) procedures. EOR is typically characterized by the injection of materials that would otherwise not be present in reservoirs (Lake, 1989). From a mobility ratio standpoint, emulsion injection can decrease the mobility ratio via increases in the viscosity of the displacing fluid and increases in relative oil permeability, preventing viscous fingering leading to more piston-like displacements. Emulsions can also plug high permeability thief zones, increasing the sweep efficiency of the displacing front by redirecting injected fluids to otherwise un-swept regions of the reservoir. This phenomenon is otherwise known as conformance control.

Using solids as emulsion stabilizers for viscous oil recovery was first conceived and patented by J.R. Bragg (Bragg, 1999). In a pilot test in the Celtic field of Saskatchewan, Canada, ExxonMobil injected what they termed as solids-stabilized emulsions (SSE) into a high permeability reservoir containing oil with a viscosity of approximately 3000 cp (Kaminsky et al., 2010). The pilot not only showed the potential success of using particle-stabilized emulsions for EOR, but also the process's feasibility in terms of facilities and cost. In fact, the water-in-crude oil emulsions were simply stabilized by natural asphaltenes and other surface active components in the crude oil, with added mineral fines to help stabilize these components. Economical particle-stabilized EOR successes have also included the use of water-in-used engine oil emulsions, stabilized by the soot particles in engine oil (Fu and Mamora, 2010).

Gabel (2014) demonstrated the efficacy of using nanoparticle-stabilized oil-in-water emulsions for residual oil recovery in sandstone cores. These emulsions exhibited potential for improved conformance and mobility control through the potential plugging of high permeability thief zones. Furthermore, Ahmad (2016) demonstrated the ability of

nanoparticle-stabilized natural gas liquid-in-water emulsions to recover heavy residual oil in high permeability sandstone cores. Pei et al. (2015) showed an increase in emulsion stability and residual heavy oil recovery through the addition of nanoparticles to previously surfactant-stabilized emulsions. In this study of the synergistic effects of using both surfactants and nanoparticles to stabilize oil-in-water emulsions, micromodel tests were conducted that indicated more desirable mobility ratios due to increases in emulsion viscosity, resulting from the addition of nanoparticles. Compared to waterflooding and pure surfactant emulsions, the addition of nanoparticles greatly decreased viscous fingering phenomenon, improving micromodel sweep efficiencies.

# Chapter 3

## Static Stability of Nanoparticle-Stabilized Natural Gas Liquid-in-Water Emulsions

To optimize the features of nanoparticle-stabilized emulsions for residual oil recovery at reservoir conditions, it is vital to understand both their limitations and advantages in extreme environments such as high temperature, pressure and salinity. The effects of salinity on emulsion rheology and overall stability will be addressed in this section. Understanding the effect that the ionic concentration in the aqueous phase has on both nanoparticle dispersions and emulsions is essential to characterizing the flow of nanoparticle-stabilized emulsion through porous media, and its consequences on oil recovery.

To better understand these effects, particle and droplet size analysis, rheology, and general emulsion stability tests were constructed to determine the effects of salinity on pentane and liquid butane nanoparticle-stabilized emulsions. Two hydrophilic nanoparticle dispersions were used with particle diameters ranging from 13-46 nm in diameter (the nanoparticles are assumed spherical) with pH ranging from 3-9.65 for the concentrated dispersions. Salinity was varied from 0-20 wt% API brine in the aqueous nanoparticle dispersions, and the effects on hydrodynamic nanoparticle size were recorded. By co-injecting pentane or butane with the aqueous nanoparticle dispersions into a beadpack, water-in-oil emulsions were generated. Emulsion characteristics such as droplet size, stability and rheology were recorded at varying salinities.

Gabel (2014) demonstrated the efficacy of using nanoparticle-stabilized octane-in-water emulsions for residual oil recovery in sandstone cores. Khan (2016) continued this research, showing that residual oil recovery of up to 82% light mineral oil was possible using pentane-in-water nanoparticle stabilized emulsions.

## 3.1 MATERIALS AND EXPERIMENTAL METHODS

### 3.1.1 Materials Used

***Nanoparticle Dispersions***

Two brands of partially hydrophilic silica nanoparticles were used in the experiments. DP9711, from Nyacol Nano Technologies, is an aqueous dispersion of partially hydrophilic nanoparticles (30.5 wt%) with a measured particle size of 46 nm. The surface coating of the nanoparticles is proprietary. The concentrated solution of DP9711 nanoparticles has a pH of 3. This dispersion has a viscosity of 1.06 cp and density of 1.03 $g/cm^3$. The second concentrated nanoparticle dispersion contained partially hydrophilic, polyethylene glycol (PEG)-coated nanoparticles (18.1 wt%) with a measured particle size of 13 nm at the concentration supplied. Its pH is 9.65. This dispersion had a viscosity of 2.53 cp. The density of this nanoparticle dispersion was assumed to be near that of water, as in the case of the DP9711 dispersion. It is known that small traces of surfactant are in the PEG-coated nanoparticle dispersion and may or may not be in the DP9711 dispersion.

Deionized water was used to dilute the nanoparticle dispersions. Reagent grade sodium chloride and calcium chloride were used to create API standard brine. API brine contains a 4:1 ratio of sodium chloride to calcium chloride by mass (e.g., 5 wt% API contains 5 wt% NaCl and 1.25 wt% $CaCl_2$).

***Organic Phases***

Reagent grade n-butane and pentane were used for the oil phase in the emulsions. The pentane had a viscosity of 0.25 cp and a density of 0.626 $g/cm^3$. The vapor density of the n-butane was 2.1 (air = 1). The organic phases were purchased from Fisher Scientific.

### *Procedure to Measure Hydrodynamic Nanoparticle Size*

A distribution of hydrodynamic nanoparticle diameters for each unique dispersion was measured using the Malvern Dynamic Light Scattering Zetasizer Nano ZS. The DLS obtains particle size distributions by measuring the scattering intensity of a nanoparticle dispersion sample measured by a photon detector, when the sample is exposed to a mono-chromatic laser (Hackley and Clogston, 2011). The hydrodynamic particle size was determined for varying API brine concentrations while the nanoparticle concentration was held constant at 2 wt%. The API brine concentration for the DP9711 dispersions was varied from 0-20 wt% in increments of 2 wt%. Hydrodynamic nanoparticle size distributions were determined for these dispersions within one hour of initial preparation. A transient analysis of the particle size distributions of the DP9711 dispersions was made over the course of two days for salinities varying from 0-20 wt% in increments of 5 wt%. A transient analysis of particle size for dispersions containing PEG-coated nanoparticles was conducted for salinities ranging from 0-20 wt% in increments of 5 wt% over the span of two days.

### *Beadpack and Beads*

A high pressure column from HiP (High Pressure Equipment Company) was filled with 180 μm spherical hydrophilic glass beads. The column is 6 inches in length with an inner diameter of 0.173 inches. Wire mesh is placed on the inlets and outlets of the beadpack to ensure that no flux of glass beads occurs. It should be noted that the beads are small enough to assume that very little flow occurs in the irregular space between the column walls and the glass beads, rather through the void space or semi-uniform pore throats between beads. Gabel (2014) was able to show that for different bead sizes and varying types of aqueous nanoparticle and oleic phases a critical shear rate exists for emulsion generation to occur.

### 3.1.2 Beadpack Co-injection Set-up

***Nanoparticle-stabilized Pentane Emulsions***

A general overview of the experimental set-up is seen in Figure 3.1. To make pentane emulsions the DP9711 or PEG-coated nanoparticle dispersions were prepared at a constant 2 wt% nanoparticles at API brine concentrations varying from 5 wt% to 20 wt% in 5 wt% increments. Pentane and nanoparticle dispersion were co-injected at a 1:1 volume ratio into a high pressure column filled with 180 μm hydrophilic glass beads. The flow through the glass beads provided the shearing forces needed to create emulsion in the effluent. Flow of each phase was held constant at 12 mL/min from two Teledyne ISCO syringe pumps. To prevent the nanoparticles from directly contacting the elements of the pump, a piston-type stainless steel accumulator was used. One of the pumps was filled with pentane, while the other was filled with DI water used to drive the piston in the accumulator containing the aqueous nanoparticle dispersion. Nanoparticle-stabilized pentane emulsions were collected in a series of graded tubes from the effluent of the beadpack.

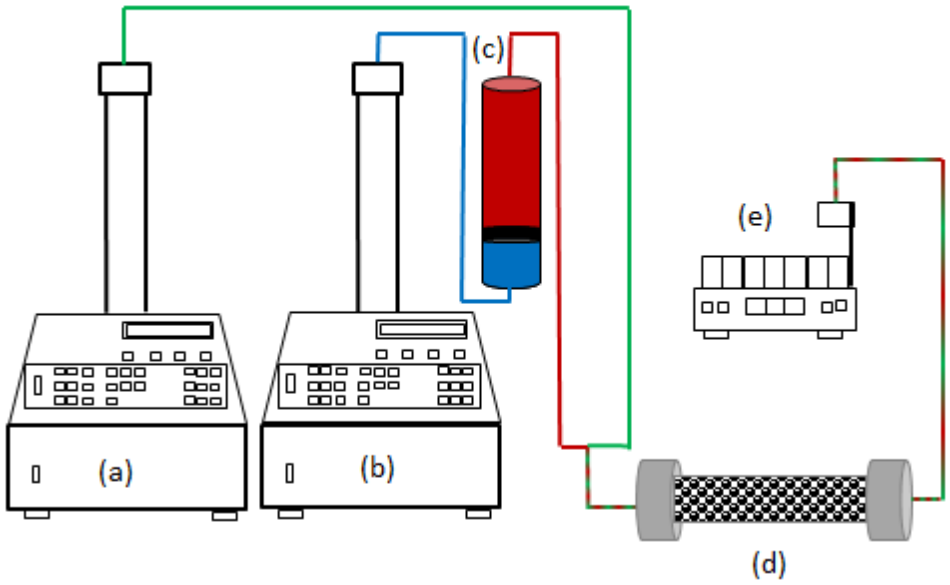


Figure 3.1: Experimental schematic: (a) Syringe pump for oleic phase, (b) Syringe pump for displacing nanoparticle dispersion using brine, (c) Accumulator containing nanoparticle dispersion, (d) Beadpack, (e) Fraction collector for effluent emulsion (Gabel, 2014)

***Nanoparticle-stabilized Butane Emulsions***

Due to the volatility of butane, a gas cylinder containing n-butane at 20 psi was inverted to maximize the amount of liquid butane that could be pulled from the cylinder. By inverting the cylinder, denser liquid butane phase settled to the bottom, and flow from the cylinder was driven by gas-phase expansion (on top). Before conducting butane emulsion experiments, liquid n-butane was drawn from the gas cylinder into a stainless steel piston-type accumulator, and pressurized to 150 psi. A schematic of the experimental set-up for these experiments is shown in Figure 3.2.

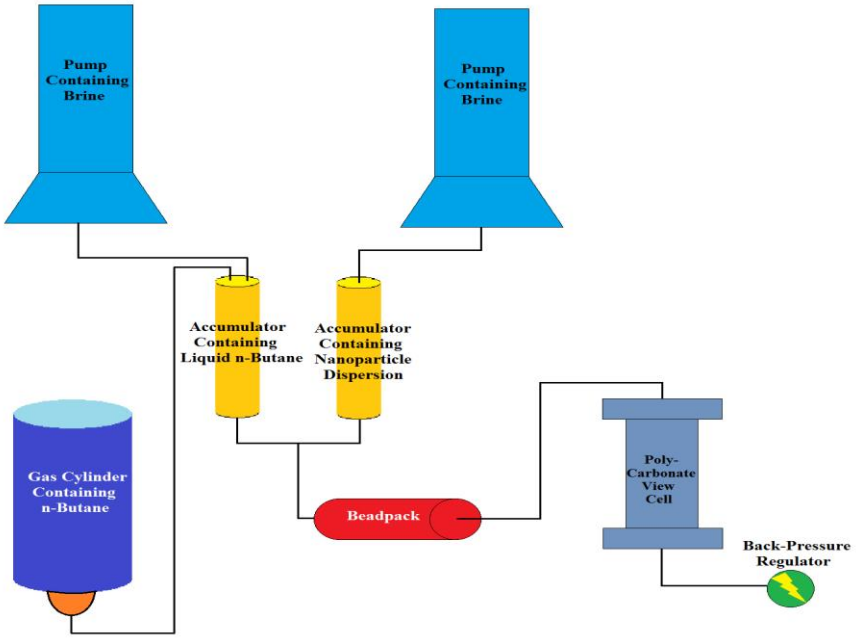


Figure 3.2: Experimental schematic for nanoparticle-stabilized butane emulsion generation experiments.

Two Teledyne ISCO syringe pumps were used to either hold a constant pressure in the system or supply a determined flow rate of brine, which acted as a power fluid for the accumulators. Two steel accumulators were used to drive the liquid n-butane and nanoparticle dispersion. The flow from each accumulator was co-injected into a beadpack filled with 180 µm hydrophilic glass beads. The effluent flow from the beadpack was collected in a custom-made polycarbonate view cell, which was connected to a back-pressure regulator calibrated to 100 psi.

The DP9711 nanoparticles were used as the aqueous phase for these butane emulsions, prepared in dispersions of varying salinity. The first dispersion consisted of 2 wt% nanoparticles and 3 wt% NaCl prepared in DI water. Four other dispersions were created with constant nanoparticle concentrations (2 wt%) at varying API brine salinities at 5 wt%, 10 wt%, 15 wt% and 20 wt% in DI water.

### 3.1.3 Measuring Emulsion Droplet Size

Immediately following co-injection of pentane and nanoparticle dispersion into the beadpack, samples of effluent emulsion were collected and used for measuring the median droplet size of the emulsions. A Nikon Labophot-Pol microscope with a Nikon Digital Sight DS-Fil camera connected to a computer was used to obtain microscopic images of emulsion droplets. An imaging software called Nikon NIS-Elements was used to capture photographic stills of the droplet images and to set the scale bars for appropriate droplet sizing given the scope in use.

Immediately after emulsion generation, an emulsion sample was placed on a glass microscope slide and a cover glass was lightly placed on the emulsion sample to spread the droplets thinly as get clearer images of droplets. Having multiple layers of droplets in the image was a common problem, not allowing enough light to pass through the emulsion and creating focus issues for clearly defined droplet edges. Depending on the size of the emulsion droplets, images were taken with a magnification aperture of 10x or 40x. At 40x magnification the images clearly define droplets from 1-100 microns, and at 10x magnification, 4-400 microns. The images were then transferred to a laptop and droplet distributions were obtained using ImageJ, an open source image processing software. If fewer than fifty droplets were available for droplet size processing, multiple images were used to calculate the droplet size distribution.

### 3.1.4 Measuring Emulsion Rheology

Immediately after an emulsion was generated, rheology tests were conducted using an AR-G2 magnetic bearing rheometer from TA Instruments. Cone-plate geometry was used in the rheology experiments. The data obtained from these experiments was used to generate plots of viscosity versus shear rate for emulsions of different dispersion types and at varying salinities.

### 3.1.5 Quantifying Emulsion Stability

Once steady-state emulsion generation was reached from the effluent of the beadpack, roughly 10 mL of emulsion was collected in a plastic 15 mL centrifuge tube. To quantify general, static emulsion stability, phase volume fractions were recorded with time.

## 3.2 DATA ANALYSIS

### 3.2.1 Permeability and Shear Rate of Beadpack

The permeability of the beadpack used for co-injection emulsion generation was calculated using the following equation:

$$k = \frac{1}{72\tau}\frac{\phi^3 D_p^2}{(1-\phi)^2}, \quad (2)$$

where $k$ is the permeability, $\tau$ is the tortuosity, $\phi$ is the porosity, and $D_p$ is the bead diameter. The value for the tortuosity is assumed to be 25/12, which is suggested for a bed of randomly packed spheres (Lake, 1989). The porosity was assumed to be 0.36 as done in similar work conducted by Zhang et al. (2006). For the 180 micron beadpack being used in these experiments the permeability was calculated to be roughly 27 D (Darcies).

Approximations of the shear rate through the beadpack were calculated using the following equation (Lake, 1989):

$$\dot{\gamma_{eq}} = 4v\left(\frac{\phi}{8k}\right)^{0.5} = \frac{4q}{A\sqrt{8k\phi}}, \quad (3)$$

where $\dot{\gamma_{eq}}$, is the shear rate in the beadpack ($s^{-1}$), $v = q/A/\phi$ is the interstitial velocity (cm/s), $q$ is the volumetric flow rate ($cm^3/s$), $A$ is the cross-sectional area ($cm^2$), $k$ is the permeability ($cm^2$), and $\phi$ is the porosity of the beadpack. This equation assumes the capillary bundle of tubes model to predict rheological properties of non-Newtonian fluids flowing through porous media. While this may not serve as a perfect approximation given droplet-pore throat blocking behavior, this is an appropriate approximation for determining the critical shear rate required to generate a stable emulsion. In the experiments in this

section the injection rate for each phase was 12 mL/min, for a total injection rate of 24 mL/min. This corresponds to a shear rate of 12,500 $s^{-1}$. Figure 3.3 displays the shear rate as a function of total injection rate into the beadpack filled with 180 micron glass beads.

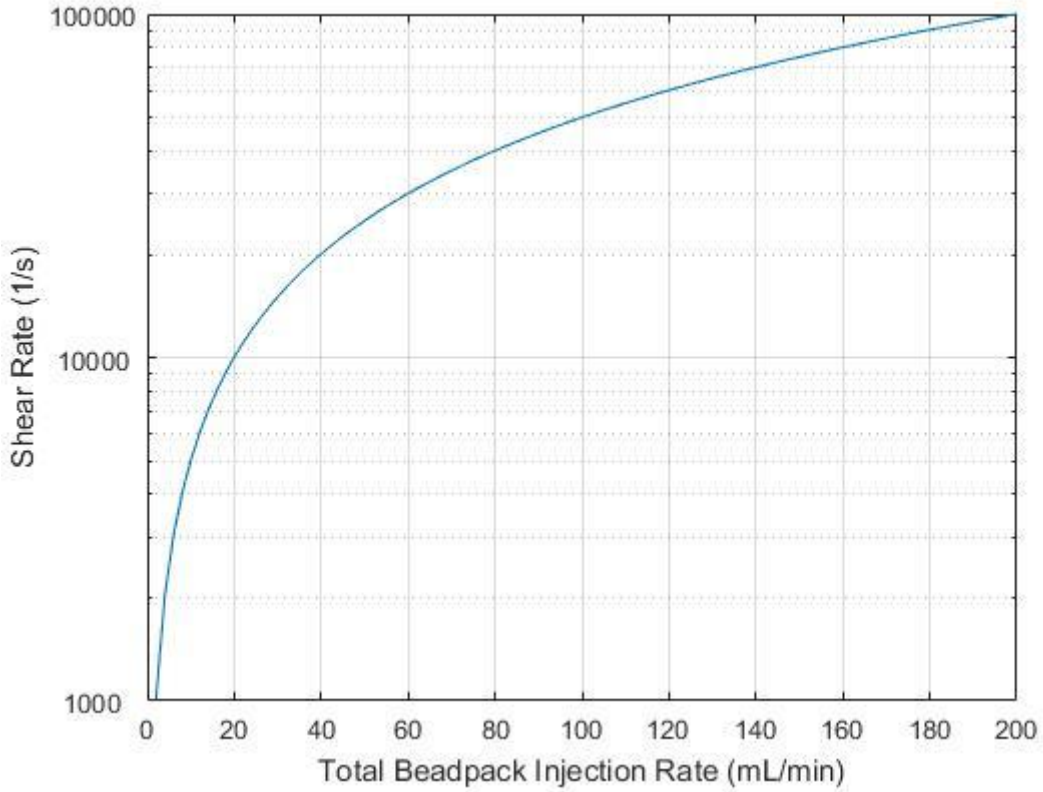


Figure 3.3: Shear rate as a function of total beadpack injection rate (Eq. 2) for HiP beadpack filled with 180 micron beads.

### 3.2.2 Emulsion Viscosity

The nanoparticle-stabilized pentane-in-water emulsions generated via the beadpack co-injection method in this section are highly shear-thinning power law fluids. They can be represented by the following power-law model:

$$\tau = K\dot{\gamma}^{n}, \tag{4}$$

where τ is the shear stress, K is the consistency index, $\dot{\gamma}$ is the shear rate, and n is the flow behavior index.

## 3.3 Results and Discussion

### 3.3.1 Hydrodynamic Nanoparticle Size Analysis

The effect of salinity on the hydrodynamic particle size in the nanoparticle dispersions was analyzed first, as the hydrodynamic size would affect certain emulsion characteristics discussed later on. As the ionic concentration increases, the hydrodynamic nanoparticle size was expected to increase due to reductions in electrostatic double layer repulsive forces between negatively-charged silica nanoparticles causing nanoparticles to aggregate (Stumm and Morgan, 1996).

The results for the effects of salinity on the hydrodynamic nanoparticle size for the DP9711 and PEG-coated nanoparticle dispersions of 2 wt% nanoparticles and 0-20 wt% API brines are shown in Table 3.1.

| API Brine wt% | 0% | 5% | 10% | 15% | 20% |
|---|---|---|---|---|---|
| DP9711 | 46 | 51 | 59 | 71 | 155* |
| pH | - | 5.571 | 6.634 | 7.116 | 7.562 |
| PEG-Coated | 13 | 22 | 26 | 43 | 50 |
| pH | - | 8.803 | 8.725 | 8.695 | 8.567 |

Table 3.1: Hydrodynamic nanoparticle size for DP9711 and 3M nanoparticles in nanometers (nm) at 2 wt% for varying API brine concentrations. Corresponding pH for each nanoparticle phase is shown below (*DP9711 at 20 wt% API was unstable transiently as shown in Fig. 3.3)

Table 3.1 displays an average of the hydrodynamic diameter measurements for each nanoparticle dispersion from the transient tests, except for the 20 wt% API DP9711 dispersion, in which case the initial hydrodynamic nanoparticle size is displayed. Figure 3.3 shows the hydrodynamic size of the DP9711 and the PEG-coated nanoparticles as the

salinity was varied from 0-20 wt% API in increments of 2 wt% and 5 wt% (respectively), measured immediately after preparation.

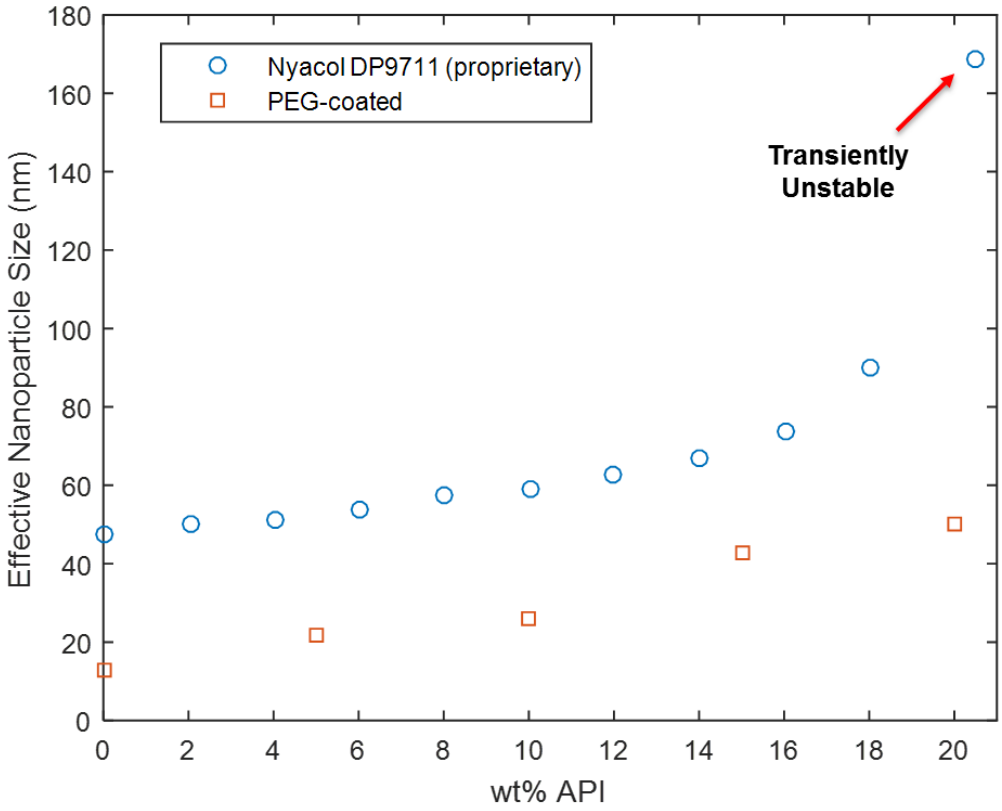


Figure 3.3: Hydrodynamic nanoparticle size for DP9711 and 3M nanoparticles at 2 wt% for varying API brine concentrations. (*DP9711 at 20 wt% API was transiently unstable)

Before continuing, it should be noted that the transient tests revealed that while the 20 wt% API DP9711 dispersion lost its stability with time, all other lower-salinity dispersions showed only minor, non-transient, aggregation behavior for the two-day duration of tests. As time passed, the turbidity of the 20 wt% API DP9711 dispersion increased, and after seven days a noticeable sediment began to develop at the bottom of the

vial due to particle aggregates precipitating out of solution. The results for the transient test of the 20 wt% API DP9711 dispersion are shown in Figure 3.4.

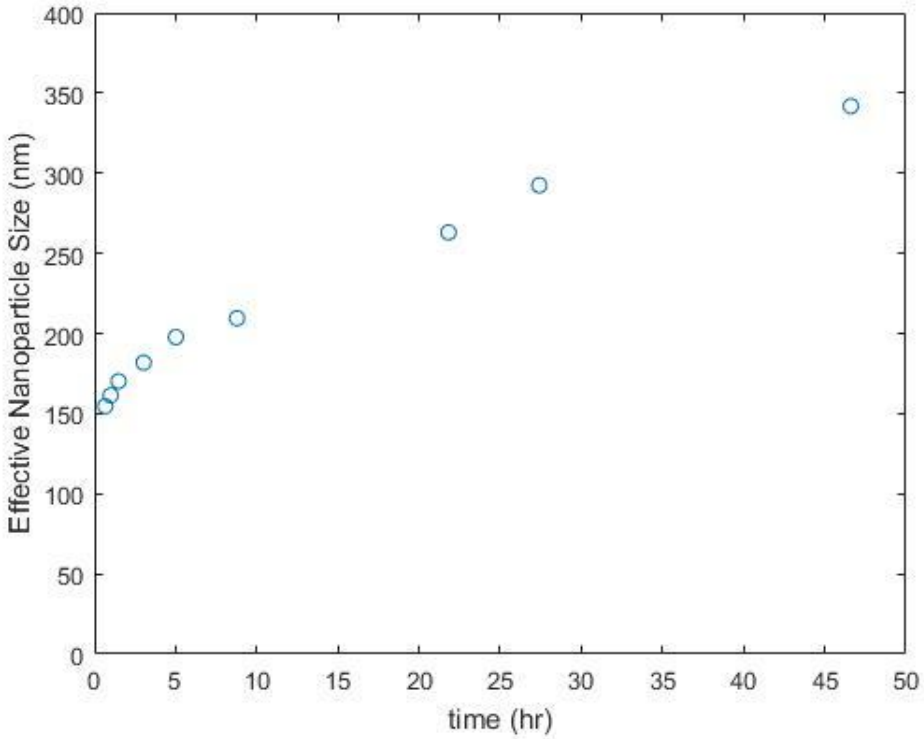


Figure 3.4: Transient changes in hydrodynamic nanoparticle size for unstable 2 wt% DP9711, 20 wt% API nanoparticle dispersion. Nanoparticles eventually aggregated and settled out of solution.

As shown in Figure 3.3, as the salinity of the nanoparticle dispersion increased, there was a noticeable upward trend in hydrodynamic particle size. As the electrolyte concentration increased, the electrostatic repulsion between particles decreased. As salinity increases, aggregation of particles intensifies due to Brownian motion and van Der Waals attractive forces between particles becoming greater than the electrostatic double layer repulsive forces (Azadgoleh and Kharrat, 2014), leading to larger observed hydrodynamic particle sizes. This is reflected in the results seen in Table 3.1. Slight

changes in turbidity were seen as the salinity was increased for the DP9711 dispersions, but no changes in turbidity were seen in the PEG-coated nanoparticle dispersions. Changes in dispersion turbidity were a result of nanoparticle aggregation. The changes in the turbidity of the DP9711 dispersions were more pronounced than the PEG dispersions likely due to the fact that the DP9711 concentrated dispersion had a light blue fluorescent color, while the PEG-coated concentrated nanoparticle dispersion were entirely translucent. This was likely due to differences in surface coatings. Thus, as the nanoparticles tended to aggregate more abundantly with increasing salinity, changes in turbidity of the DP9711 dispersions were more pronounced than the PEG-coated nanoparticle dispersions.

There are several possible reasons as to why the DP9711 nanoparticles began to destabilize at 20 wt% API and the PEG-coated nanoparticles did not. Reasons could include differences in pH, initial nanoparticle size, and surface coating. Kobayashi et al. (2005) showed that for 30 nm particles, the particles aggregate at higher pH and are completely stable at low pH when salinity is increased. The opposite is true for the dispersions being compared in this case: the concentrated DP9711 dispersion is provided at a pH of 3, while the concentrated PEG-coated nanoparticle dispersion is provided at a pH of 9.65. It should be noted that as the salinity is increased, the pH of the dispersions approached toward neutral, as is the nature of adding salts to acidic or alkaline solutions. The surface coatings are also likely different, but are incomparable due to DP9711's proprietary coating. Without knowing the nature of DP9711's surface coating, it is difficult to explain the aggregation behavior in terms of interaction forces between particles.

### 3.3.2 Effects of Salinity on Pentane Emulsion Characteristics

***Droplet Size Analysis***

Pentane emulsions were generated via beadpack co-injection using the DP9711 and PEG-coated nanoparticle dispersions, each at 2 wt% in their respective aqueous phases. Droplet images for each emulsion are shown in Figure 3.5.

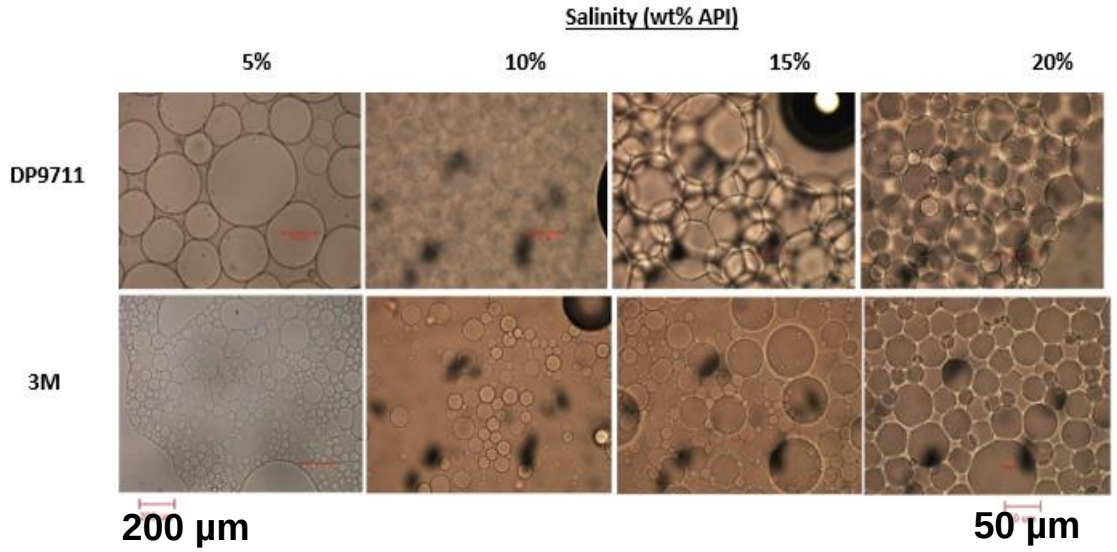


Figure 3.5: Droplet images for pentane-in-water emulsions with varied nanoparticle phase and salinity. The images in the first column are at 20x magnification (200µm scale bar) while the rest are at 40x magnification (50µm scale bar).

Droplet size distributions for pentane emulsions stabilized by DP9711 and PEG-coated nanoparticle dispersions were obtained via ImageJ's droplet size analysis software. These distributions are displayed in Figures 3.6 and 3.7.

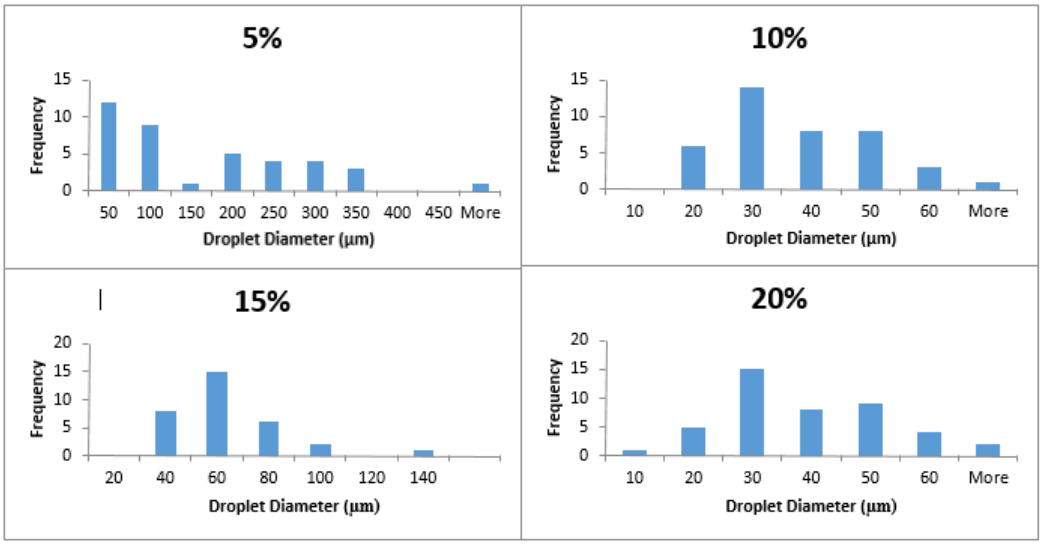


Figure 3.6: Emulsion droplet size distributions for varying API brine wt% stabilized by the DP9711 nanoparticle dispersion.

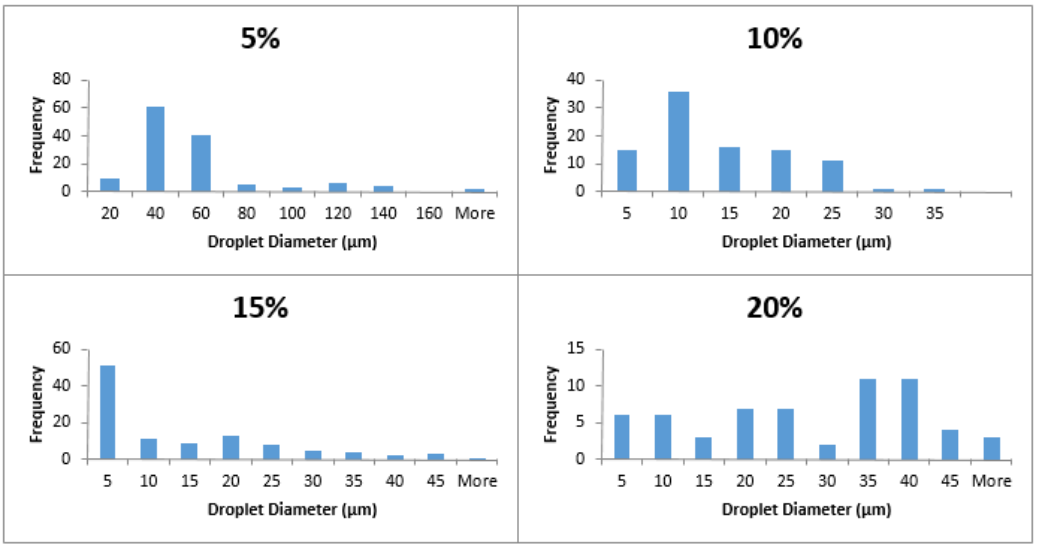


Figure 3.7: Emulsion droplet size distributions for varying API brine wt% stabilized by the PEG-coated nanoparticle dispersion.

Finally, the median droplet sizes values were plotted against corresponding API brine concentrations in Figures 3.8 and 3.9. Median droplet size was used to quantify the overall

droplet size of each emulsion, because some emulsion images had one or two droplets that were much larger than the others, skewing the value of the mean.

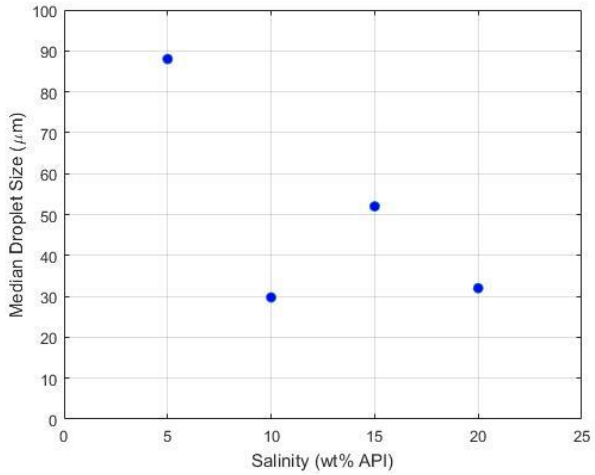


Figure 3.8: Median droplet size of pentane emulsions stabilized with DP9711 nanoparticle dispersion at varying API brine wt%.

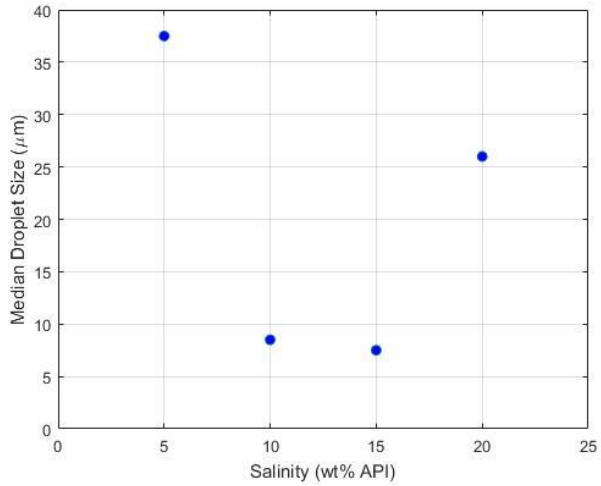


Figure 3.9: Median droplet size of pentane emulsions stabilized with PEG-coated nanoparticle dispersion at varying API brine wt%.

A significant decrease in median droplet size was observed for both emulsions when the salinity was increased from 5 wt% to 10 wt% as shown in Figure 3.8 and 3.9.

The DP9711 emulsion experienced a 65% decrease in median droplet size, while the PEG-coated nanoparticle-stabilized emulsion experienced a 75% decrease. However, as the salinity was increased further, less recognizable trends were apparent. Comparing the DP9711 and PEG emulsions, the median droplet size for the PEG emulsions was smaller for all ionic concentrations tested. This may imply a relationship wherein as hydrodynamic nanoparticle size decreases, emulsion droplet size decreases, as documented by Kim *et al.* (2015). Recall that the PEG-coated nanoparticle dispersions had roughly half the hydrodynamic particle diameter of the DP9711 dispersions at all ionic concentrations. However, assessing each type of emulsion exclusively, as the hydrodynamic particle size increased with incremental increases in salinity from 10 wt% to 20 wt%, there were no distinct trends in droplet size. This implies that the hydrodynamic size of the nanoparticles is not the only factor influencing the droplet size, especially at higher concentrations of salinity. Gabel (2014) and Zhang (2010) showed that with increasing shear rate through the beadpack and increasing nanoparticle concentration, emulsion droplet size decreased, respectively. However, in this study these factors (co-injection rates and aqueous phase nanoparticle concentration) were held constant. Other factors may have included the surface coating of the nanoparticles and more likely, the effects of a three-dimensional network of interconnected droplets and aggregates proposed by Horozov *et al.* (2007) for emulsions with substantial ionic concentration. In fact, at salinities greater than 10 wt% API these indefinite trends in droplet size were likely resultant of a combination of interdependent factors that include but are not limited to: pH, particle size, droplet coverage, surface coating of the nanoparticles, and the extent of the three-dimensional droplet-aggregate network.

***Emulsion pH***

Table 3.2 shows the pH values of the nanoparticle dispersions for the PEG-coated and DP9711 dispersions. It is interesting to note that there was no change in pH in the emulsion phase when compared to the stabilizing nanoparticle dispersion's pH values. This is likely an artifact of the way the pH is measured via a pH probe. When inserted into the emulsion the probe does not break the emulsion droplets, thus measuring the pH of the aqueous nanoparticle dispersion phase of the emulsion. As the salinity of each dispersion increases, the pH of the dispersion becomes more neutral as is expected. There is no noticeable trend between pH and droplet size.

| pH | | |
|---|---|---|
| Salinity (wt% API) | DP9711 | PEG |
| 5% | 8.803 | 5.571 |
| 10% | 8.725 | 6.634 |
| 15% | 8.695 | 7.116 |
| 20% | 8.567 | 7.562 |

Table 3.2: pH measurements of nanoparticle dispersions.

***Emulsion Stability***

As for stability, all emulsions remained stable if kept pressurized in an accumulator at 100 psi. Due to the volatility of pentane, the emulsions would coalesce and destabilize if kept at atmospheric pressure. The pentane emulsions made with the DP9711 nanoparticles with salinities ranging from 5-15 wt% API brine destabilized relatively quickly – within two hours of generation at atmospheric pressure. Upon generation of pentane emulsion with DP9711 nanoparticle dispersion at 20 wt% API, a noticeably viscous gel-like substance was formed, while droplets were visible post-generation, after one day no droplets were visible. It is hypothesized that a bicontinuous gel or "bijel" formed. Even though no droplets were visible under a microscope after one day, the gel

remained opaque, and was much more viscous than its respective nanoparticle dispersion phase.

The PEG-coated nanoparticle emulsions were much more stable. The 5 wt% API brine emulsion was stable for approximately 2 days (~48 hours), while the 10 wt% and 15 wt% API brine emulsions were stable for approximately 1 day (~24 hours). The 20 wt% API brine emulsion also formed a bicontinuous gel after 1 day and remained in that state indefinitely, much like the DP9711 emulsion at 20 wt% API brine. Again, no droplets were visible under the microscope after one day.

The occurrence of gel formation, instead of droplet coalescence and separation into two phases (nanoparticle dispersion and oil phase), for the emulsions generated at 20 wt% API was likely due to the following. Because of the high electrolyte concentration in the aqueous dispersion phase, the nanoparticles tend to aggregate and form nanoparticles of larger hydrodynamic size. In the DP9711 dispersion the hydrodynamic size of the nanoparticles was shown to increase over time, while the hydrodynamic size of the PEG-coated nanoparticles remained constant. However, further agitation by flow through the beadpack may have an effect on the previously observed stability of the PEG-coated nanoparticle hydrodynamic size, resulting in increased aggregation. As emulsion droplets coalesced it is thought that large transiently unstable nanoparticle aggregates prevented pentane from separating to the top of the vial (where it would have evaporated), dispersing aspherical shaped pentane phase, creating a bijel (Cates and Clegg, 2008). This semi-continuous pentane, no longer in droplet form, rises slowly (if at all) to the top of this gel and evaporates, leaving a denser, more viscous gel-like substance behind. Approximately a day after emulsion generation, this gel likely consists of highly aggregated nanoparticles, high-salinity water, and residual amounts of trapped pentane no longer in droplet form.

The formation of more stable emulsions from using the PEG-coated nanoparticle dispersions could be due to a handful of factors. Overall smaller droplets, different surface coatings, and smaller hydrodynamic nanoparticle size may comparatively increase the stability of the emulsions. Because the surface coating of the DP9711 nanoparticles is unknown, it is difficult to quantify the effects that pH and other nanoparticle characteristics may have on emulsion stability.

***Rheology***

Rheology measurements were made within ten minutes of emulsion generation for the emulsions generated using the DP9711 and PEG-coated nanoparticle dispersions at salinities varying from 5-20 wt% API. The effective viscosity of the emulsions was measured as the shear rate was varied from 1 to 1000 1/s is shown in Figures 3.10 and 3.11.

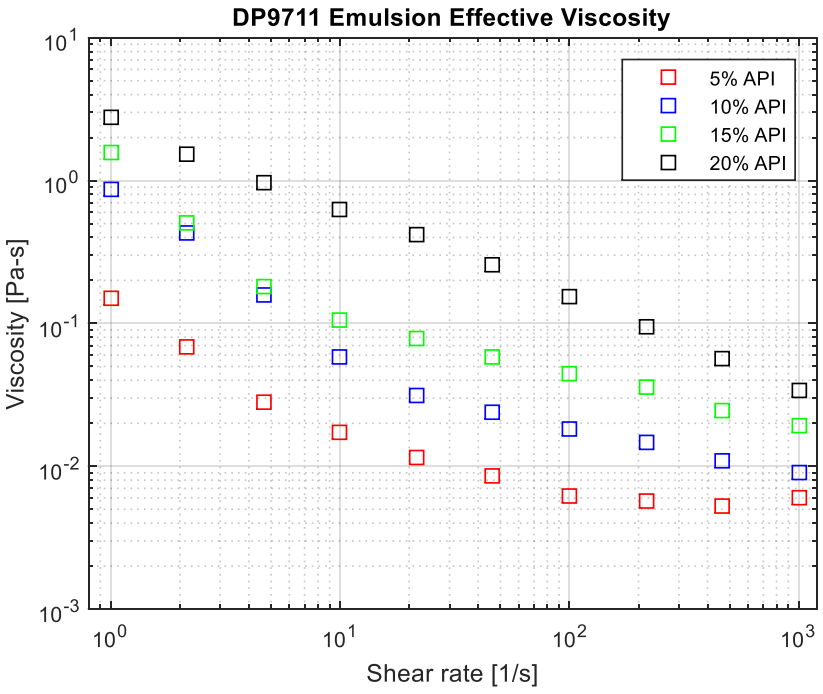


Figure 3.10: Rheology results for pentane emulsions made with DP9711 nanoparticle dispersion at varying salinities.

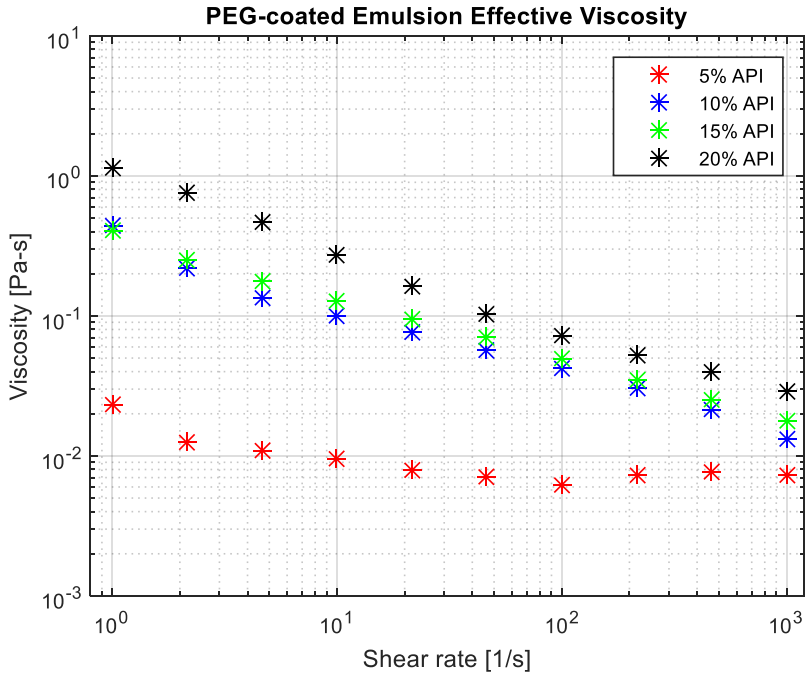


Figure 3.11: Rheology results for pentane emulsions made with PEG-coated nanoparticle dispersion at varying salinities.

These emulsions were found to be highly shear-thinning fluids which can be represented by the power-law model as detailed in Eq. 3. The power-law model values for each emulsion are shown in Tables 3.3 and 3.4, along with the corresponding $R^2$ values.

| Salinity (wt% API) | *K* (cp-s$^n$) | n | $R^2$ |
|---|---|---|---|
| 5% | 0.07 | -0.461 | 0.8522 |
| 10% | 0.4541 | -0.650 | 0.905 |
| 15% | 0.6634 | -0.566 | 0.9029 |
| 20% | 2.6944 | -0.626 | 0.9987 |

Table 3.3: Power-law model parameters from experimental rheology data for pentane emulsions generated with DP9711 nanoparticle dispersions: where K is the consistency index, n is flow behavior, and $R^2$ is the coefficient of determination from the model generated in Excel.

| Salinity (wt% API) | K (cp-s$^n$) | n | R2 |
|---|---|---|---|
| 5% | 1.0192 | -0.545 | 0.9888 |
| 10% | 0.3664 | -0.438 | 0.998 |
| 15% | 0.3318 | -0.459 | 0.9852 |
| 20% | 0.0147 | -0.137 | 0.6688 |

Table 3.4: Power-law model parameters from experimental rheology data for pentane emulsions generated with PEG-coated nanoparticle dispersions: where K is the consistency index, n is flow behavior, and $R^2$ is the coefficient of determination from the model generated in Excel.

As the salinity was increased, the effective emulsion viscosity also increased for both types of emulsions. The emulsions generated using the DP9711 nanoparticle dispersions were characterized as having higher viscosities than those using the PEG-coated nanoparticle dispersions. Gabel (2014) found that the effective viscosity of an emulsion increased as the droplet size decreased. It appears that this hypothesis cannot be applied to comparing the viscosities of emulsions created with two similar but different nanoparticle dispersions – considering the fact that the median droplet sizes for the PEG emulsions were smaller. The differences in viscosity may be a result of differences in pH of the aqueous phase, surface coating of the nanoparticles, or droplet particle coverage. These factors could affect the overall droplet composition and how the droplets interact with each other (i.e., the composition of a three-dimensional droplet-aggregate network).

The observation that the effective viscosity of an emulsion increased as the droplet size decreases is briefly discussed here. The relationship for the PEG emulsions will be explored first. As seen in Figure 3.10, there is a large decrease in median droplet size as the salinity was increased from 5 wt% to 10 wt% API. This corresponds to a large jump in effective viscosity as seen in Figure 3.11. Only a slight increase in effective viscosity is seen as the salinity was increased from 10 wt% to 15 wt% API. This corresponds to a very slight decrease in droplet size. As the salinity was increased to 20 wt% API, the droplet

size increases, while a substantial increase was seen in the effective viscosity. As discussed above, this increase in viscosity may be due to the formation of a strong network of interconnected droplets and aggregates. The transient formation of such droplet-aggregate networks should not be disregarded when considering the increases seen in emulsion viscosity at salinities less than 20 wt% API. Analysis of the effects of salinity on the viscosity of the DP9711 emulsions is not so clear, but the discussion on the PEG emulsions may assist in explaining the fundamentals of what is happening. Like the PEG emulsions, there was a large decrease in droplet size as the salinity was increased from 5 wt% to 10 wt% API for the DP9711 emulsion, corresponding to a relatively moderate increase in viscosity. However, as the salinity was increased from 10 wt% to 15 wt% API there was an increase in droplet size and an increase in viscosity. The formation of the droplet-aggregate network may have a greater effect on the viscosity of the DP9711 emulsions than the PEG emulsions. Finally, as the salinity was increased from 15 wt% to 20 wt% API there was a decrease in droplet size, and another subsequent increase in apparent viscosity for the DP9711 emulsion.

In summary, it was found that as the salinity of the emulsion increases, viscosity also increases. This can be attributed to the initial decrease in droplet size and the formation of a three-dimensional network of interconnected droplets and aggregates. Thus, at lower salinities (<10 wt% API) the droplet size has a more significant effect on the characteristics of the emulsion viscosity. However, as the salinity increases above a certain threshold value, the droplet size seems to have less influence on emulsion viscosity and the increasing formation of a droplet-aggregate network tends to dominate the apparent viscosity increase.

### 3.3.3 Effects of Salinity on Butane Emulsion Characteristics

To maintain its stability, effluent emulsion from the beadpack was kept under pressure (approximately 100 psi) to keep the liquid n-butane in the emulsion from evaporating. A viewing cell was created to quantify the effects of salinity on the overall emulsion composition. While rheological measurements were not feasible due to the volatile nature of butane, quantifications regarding the fraction of emulsion produced in the effluent, overall emulsion stability, and qualitative comparisons of viscosity could be made.

Using the DP9711 nanoparticle dispersion (3 wt% sodium chloride, no calcium chloride), a butane-in-water emulsion was generated, as pictured in Figure 3.12. The effluent from the beadpack had a very small fraction of emulsion phase. The emulsion phase coalesced completely within five minutes while under pressure. Compared to the other emulsions, this appeared the least viscous.

As the salinity was increased for the other emulsions (5 wt% through 20 wt% API ratio brine), an increasing fraction of emulsion phase was observed. Images of the emulsions created using API brines can be observed in Figure 3.12. Note that the emulsion phase is the opaque, white phase between the clear liquid butane phase on top and the slightly translucent aqueous nanoparticle dispersion below. Also, as the salinity of the dispersions increased, the time to complete coalescence increased as well. In other words, increasing salinity resulted in increased emulsion stability. Lastly, by observing the flow into the view cell it was apparent that with increasing salinity, the viscosity of the emulsion appeared to increase. While there was no way to accurately quantify the differences in viscosity between emulsions, there was a significant qualitative increase in viscosity observed based on overall appearance. This agrees with the rheological results from the pentane emulsions. As the salinity is increased, the increasing fraction of emulsion phase

can be contributed to increasing emulsion stability brought about by the growth of the formation of the three-dimensional network of interconnected droplets and aggregates.

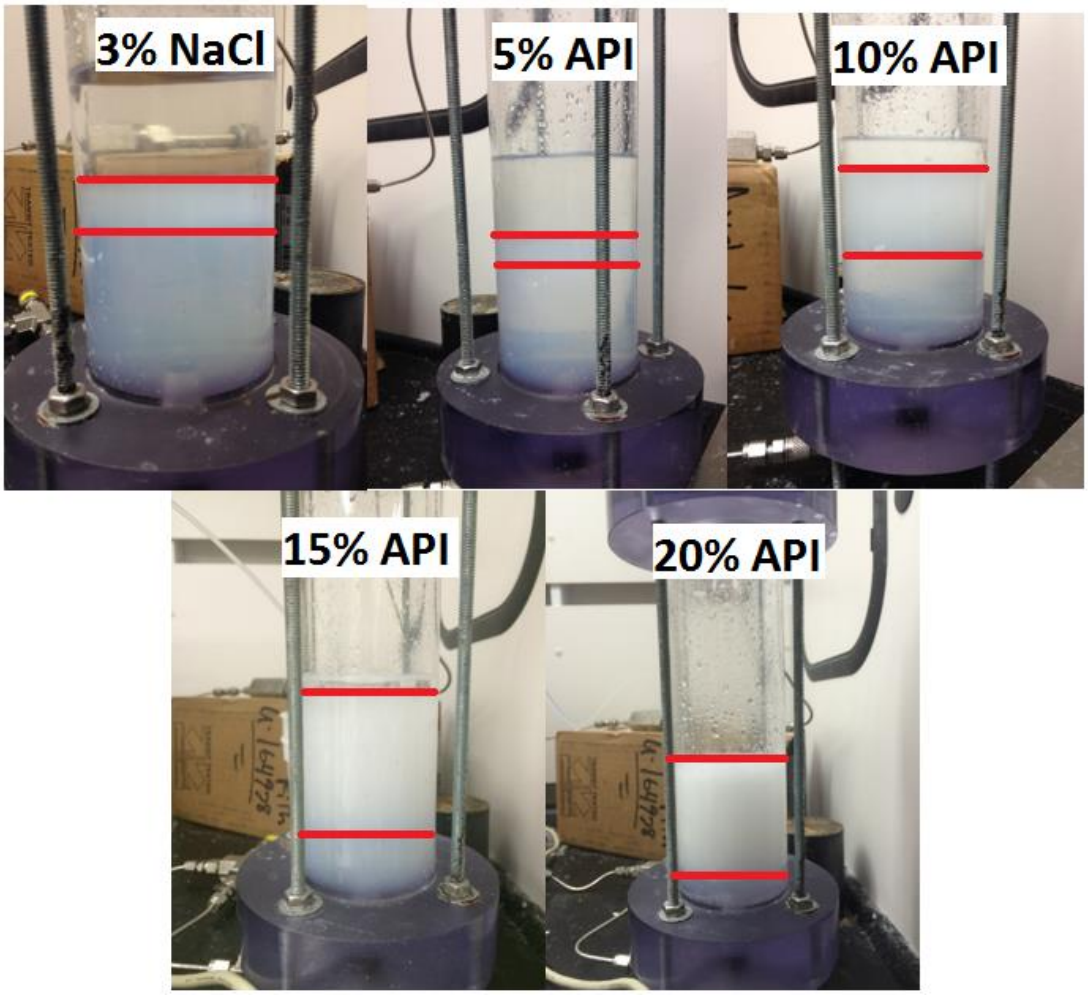


Figure 3.12: Butane emulsion generated at varying salinities using DP9711 dispersion. Red lines distinguish the emulsion phase. Above the top red line: liquid excess n-butane phase. Below the bottom red line: excess nanoparticle dispersion phase.

### 3.4 CONCLUSION

As the salinity was increased from 0-20 wt% API for the DP9711 and the PEG-coated nanoparticle dispersions a noticeable increasing trend in hydrodynamic nanoparticle

diameter was observed. These increases in nanoparticle aggregation can be explained by the reduction in repulsion potential between particles from decreases in electrostatic double layer forces with increasing ionic concentrations.

A significant decrease in median droplet size was observed for the pentane-in-water emulsions when the salinity was increased from 5 wt% to 10 wt% API, but less distinct trends were observed for salinities greater than 10 wt% API. For all salinities (5-20 wt% API), pentane emulsions were shown to remain stable if pressurized at 100 psi. When kept at room temperature and pressure, the emulsions would destabilize within 2 days, except for the emulsions at 20 wt% salinity due to the formation of a bicontinuous gel consisting of nanoparticle aggregates, high-salinity water, and residual amounts of trapped pentane. Pentane emulsion rheology was observed to be strongly shear-thinning. As the salinity of the emulsions increased, an increase in effective viscosity was observed.

Butane emulsions were generated using nanoparticle dispersions ranging from 5-20 wt% API salinity. As the salinity was increased, an increase in fraction of emulsion phase, stability, and viscosity was observed.

# Chapter 4

## Coreflood Experiments through Sandstone Cores

While emulsion stability has been characterized in the preceding chapters in static terms, in-situ stability is much more complicated given dynamic droplet-pore throat interactions. For example, while a high salinity emulsion with large droplets (40-50 microns in diameter) may seem to display static stability to coalescence, it may show dynamic instabilities during multi-step rheology experiments. Furthermore, in porous medium where pore throats are much smaller than droplet diameters, emulsion droplets may coalesce rapidly, affecting the uniformity of the displacing front. Although research has shown that increasing the droplet to pore throat diameter ratio of surfactant emulsions increases effective permeability reduction and has little effect on emulsion stability in porous media, the behavior of nanoparticle-stabilized emulsions in porous media such as complete emulsion coalescence or extremely late breakthrough time has only been partially explained at best (Gabel 2014, Ahmad 2015). Previously, transient-state pressure drops and lack of effluent emulsion in coreflood experiments have been attributed to emulsion coalescence and regeneration fronts. Reanalysis of the aforementioned work, indicates that if emulsions were obtained in coreflood effluents, injection rates and capillary numbers have been extremely high (on the order of 70 ft/day), unrealistic of field EOR injection rates.

Research on surfactant-stabilized emulsions has shown droplet-pore throat blockage to be the primary mechanism for increasing pressure drops and enhanced residual oil recovery, where stable effluent emulsions were produced. The experiments conducted in this thesis show that through optimizing nanoparticle-stabilized emulsions for enhanced oil recovery purposes, in-situ emulsion stability can be achieved and increasing amounts

of residual oil will be produced. Furthermore, models for describing in-situ behavior of surfactant-stabilized emulsions can also be applied to nanoparticle-stabilized emulsions.

The corefloods were conducted using Boise sandstone cores. These cores serve as an analogue to field uses of nanoparticle-stabilized emulsions to plug heterogeneous formations with high permeability thief zones or in reservoirs with heavy oil and poor mobility ratios. Field studies where pre-generated surfactant or colloidal-stabilized emulsions were injected into high permeability thief zones in heavy oil reservoirs, have shown to be effective in increasing oil recovery and reducing water-oil ratios by penetrating and plugging high permeability zones, improving sweep efficiencies and conformance control (McAuliffe, 1973b; Kaminsky, 2010). While many of the corefloods in this study were conducted to show increasing amounts of residual oil recovery when certain emulsion characteristics were altered, some of the corefloods were conducted without a residual oil phase to obtain a better understanding of general nanoparticle-stabilized emulsion flow and stability in porous media. All experiments were conducted at ambient temperature with 0 psig at the producing end of the core. Injection rates were typically kept at 0.5 mL/min (~16 ft/day), unless otherwise stated.

## 4.1 MATERIALS

### *Sandstone Cores*

Boise sandstone cores were used in all of the coreflood experiments. Boise sandstone cores were used for a variety of reasons including: ready availability, low clay content, relatively low heterogeneity, and high permeability. The cores used in these experiments were roughly 12” in length and 1” in diameter. Typical pore volumes were in the 40 to 45 mL range with porosities observed in the 0.25 to 0.35 range.

### *Nanoparticle-Stabilized Emulsions*

Depending on the particular experiment, emulsions with different characteristics were prepared and used accordingly. Emulsions were generated either through co-injecting nanoparticles and an organic phase into the HiP beadpack filled with 180 micron glass beads or by sonicating the nanoparticles and organic phases until emulsified. The emulsions were prepared at a 1:1 ratio of nanoparticle to organic phase by volume. To vary the droplet size of the emulsions the flow rates were varied within the 12-100 mL/min range, with higher flow rates leading to smaller droplet size. Emulsions with median droplet diameters in the 15-50 micron range could be generated using the beadpack co-injection method. Using the sonicating gun, emulsions were generated in 100 mL batches, where the sonicating tip was set to operate at different frequencies, depending on the desired size of emulsions droplets, until nearly all the organic phase had been emulsified. The amplitude of the sonicating tip was varied between 45-100%. Increasing the amplitude generally resulted in generating smaller emulsion droplets. Emulsions with median droplet sizes in the 1-15 micron range could be generated using this method. The emulsions injected in these coreflood experiments were stabilized using 2 wt% PEG-coated silica nanoparticles at varying API brine salinities (4:1 sodium chloride to calcium chloride by weight) and organic phases (which will be specified in the individual experiment descriptions).

### *Organic Phases and Aqueous Phases*

Different organic phases were used for a variety of purposes in these coreflood experiments. Pentane and n-octane were used as the oil phase in the emulsions, while light mineral oil was used as residual oil for the residual oil recovery coreflood experiments. Finally, isopropyl alcohol was used as the oil solvent during core cleaning procedures. The viscosity properties are delineated in the table below:

| **Oil** | Light mineral oil | n-Octane | Pentane | Isopropyl alcohol |
|---|---|---|---|---|
| **Viscosity (cp)** | 41.5 | 0.49 | 0.24 | 2.27 |

Table 4.1: Bulk viscosity of organic phases used in corefloods

Brine was used for permeability measurement experiments and for saturating and waterflooding the core. The brine used for these procedures was 5% API and was prepared in large batches.

***Effluent Collection***

15 mL centrifuge tubes were used to collect effluent from the corefloods using a fraction collector to automate the process of switching tubes. Depending on the injection rate of the emulsion, the timer on the fraction collector was set so that approximately 12-13 mL of effluent would be collected in each centrifuge tube. Depending on the porosity of the core, each centrifuge tube was equivalent to 0.27-0.33 pore volumes of produced fluid. Combinations of multiple phases can be obtained in the effluent or in the centrifuge tube: aqueous nanoparticle dispersion, residual oil (mineral oil), emulsion, and oil phase that has separated from the emulsion.

***Pressure Transducers and Data Acquisition***

Three Rosemount pressure transducers (model 3051CD5A22A1A) were able to measure the pressure drop across the entire length of the core during the coreflood procedures. The transducers were calibrated for pressure differentials of 200, 1000, and 2000 psi. Depending on pressure drop expected across the core, the appropriate transducer was chosen to provide the most accuracy within that range. A National Instruments data acquisition card was connected to the transducers and communicated that information to the computer. The computer was able to display and record the differential pressure data

via a LABView program. Prior to data analysis, a correction was applied to the data to remove any offset from the transducers when no flow was occurring (i.e. expected pressure drop of 0 psig).

### 4.2 Coreflood Experimental Methods

This section will describe the experimental set-up and specific equipment used in the coreflood experiments.

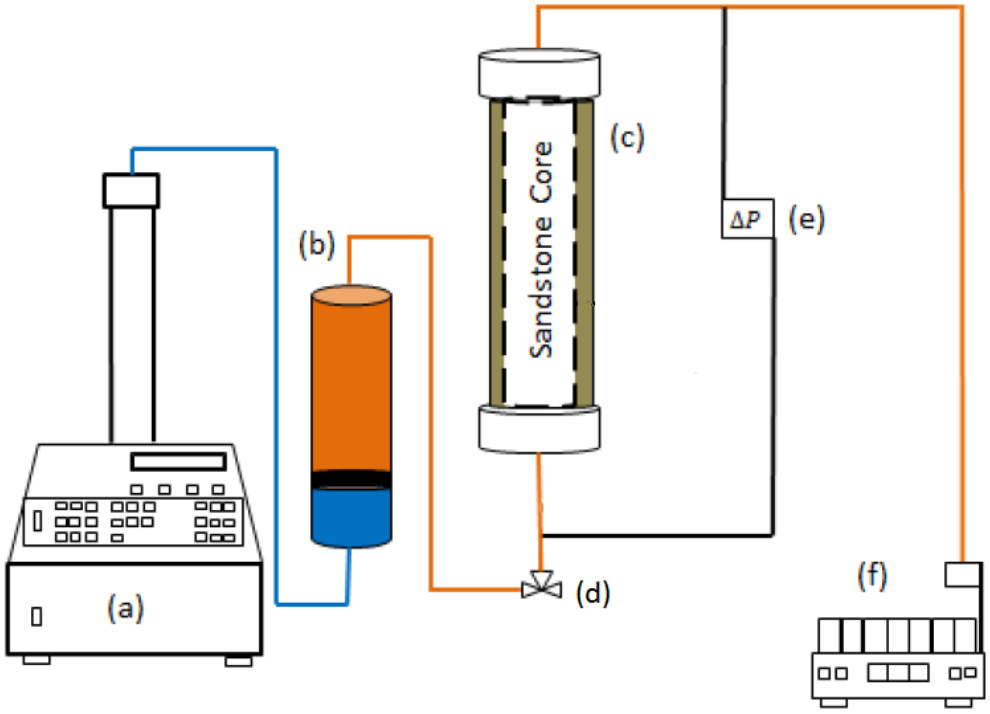


Figure 4.1: Schematic of coreflood set-up: (a) Teledyne ISCO syringe, pump, (b) steel accumulator, (c) core holder with sandstone core, (d) three-way valve, (e) differential pressure transducer to measure pressure drop across the core, and (f) fraction collector. The accumulator was used to prevent emulsion and nanoparticles from occupying the syringe pump. The accumulator was bypassed when injecting water or oil into the core.

The set-up shown above in Figure 4.1 was used to inject emulsion contained in a steel accumulator into a sandstone core. After generation, the emulsion is loaded into the steel accumulator (b) with its piston in the bottom position. The accumulator has the capacity to hold 400 mL of fluid. Brine is pumped via the Teledyne ISCO syringe pump (a) at a constant flow rate, in order to push the accumulator piston upward, injecting emulsion into the core holder (c) containing the sandstone core. The effluent fluids from the core holder are collected in the fraction collector (f), while the Rosemount differential pressure transducers measure the pressure drop across the core and communicate that information back to the computer via a National Instruments data acquisition card.

A similar set-up was used for preliminary permeability measurements and oil injection, except the accumulator is bypassed and fluids are injected directly into the sandstone core via the ISCO pump. With information about the flow rate and pressure drop across the core, calculations of the core's permeability can be made.

***Core Holder***

A Hassler type core holder was used for all the coreflood experiments in this thesis. Manufactured by Phoenix Instruments Inc., the coreholder is designed to hold cores up to 1" in diameter and 12" in length. It has a working pressure and temperature of 2000 psi and 156°C, respectively. The core holder was mounted vertically on metal frames made by Unistrut. Moreover, this orientation allows for injection from either the top or bottom of the core to prevent gravity driven flow depending on the saturating and injecting fluids. The core holder has an inner rubber sleeve made of Viton. This rubber sleeve holds and seals the core, preventing injected fluids from channeling in flow-paths around the edges of the core. Confining pressure is applied to the exterior of the Viton sleeve holding the core via a mechanical hand pump, in order to prevent leakage. The core holder is equipped

with 5 equidistant pressure taps spaced across the length of the core and has the capability to measure the pressure along multiple sections of the core if desired. However, in all the experiments conducted in this thesis, the pressure drop across the entire core was monitored.

## 4.3 COREFLOOD PROCEDURE

This section describes the general steps taken in the coreflood experiments described in this thesis. The procedures described in this section include core preparation, loading and pressurizing, permeability measurements, saturating the core with oil, reducing the core to residual oil saturation, and preparing the core for reuse.

### 4.3.1 Core Preparation

The Boise sandstone cores used during these coreflood experiments were cut from larger blocks of this sandstone obtained from outcrops near the surface. When the cores are being cut from these large rocks, water is used to cool the core cutting equipment and the rocks may become slightly saturated with water. Because of this, the cores were dried in an oven for approximately 24 hours to evaporate any residual water in the core, before the dry weight was measured for purposes of calculating the pore volume and porosity. To remove trapped air from the core, the cores are placed in a plastic, vacuum-tight, cylindrical container and vacuumed for approximately 24 hours using 1402 Welch Duoseal vacuum pump. The cores were then saturated with brine by submerging each sample for approximately 3-4 hours under a vacuum in the same container used to evacuate the cores of trapped air. The water-saturated core is then removed from the vacuum-sealed container and is weighed to obtain the wet weight of the core. This measurement was also used to calculate the pore volume of the core.

### 4.3.2 Loading and Unloading Core into Core Holder

After saturating the core with brine and measuring the wet weight of the core, the core loading procedure is immediately commenced as to limit the amount of water that may evaporate from the core. The core holder has two cylindrical end caps that screw in and hold the core in place. These are removed before loading the core. Before inserting the core, the endcaps and lines running to and from the core are flushed with brine to remove any dead volume that may exist from previous core floods. The core is slid into place by hand from the top section of the core holder, coming into contact with the depressurized internal Viton sleeve. The bottom end cap's three prongs are then slid and locked into place creating a seal on the bottom of the core holder. The top end cap is then inserted and a screw-piece is tightened to provide axial confining pressure on the core.

Once the core is axially secured in place, radial confining pressure is applied around the core via the Viton sleeve by pumping mechanical pump oil into the annulus of the core holder using an Enerpac P-392 hydraulic hand pump. This pump is capable of applying up to 10,000 psi. A pressure gauge displays the confining pressure being applied on the core. The cores were pressured to approximately 2,500 psi for these experiments.

Once coreflood procedures were completed, the confining pressure is released via turning a three-way valve connected to the annulus of the core holder. The mechanical pump oil is allowed to drain for several minutes. The top end cap is unscrewed and removed. Then the bottom end cap is unlocked and removed, taking care to not let the core drop rapidly and potentially break. If the core does not slide out on its own, a small diameter steel rod is used to carefully push the core from the core holder. Finally, the insides of the coreholder are rinsed with Contrex powdered labware detergent at DI water and prepared for another core flood.

### 4.3.3 Permeability Measurements

After loading the core into place and applying appropriate confining pressure to the core, the permeability of the core was measured using the following procedure. Before beginning the procedure, brine was pumped into the core using the ISCO syringe pump while the differential pressure transducers were disconnected, as to remove any air from the lines connected to the transducer ports. Once air had been removed from these lines, they were reconnected to the transducers. Brine was then injected at a constant flow rate through the bottom of the core until a steady-state pressure drop was achieved. The pressure drop across the core was recorded using LABView and was used to calculate the permeability at each respective flow rate. The permeability was calculated for at least three different flow rates, and taken as an average of these calculations. If there was a small differential pressure offset being recorded when no flow was occurring across the core, this value was noted and the proper adjustment to the pressure drop data was made during analysis.

### 4.3.4 Saturating Core with Oil

If a residual oil recovery experiment was being conducted, the following steps were taken to bring the core to residual oil saturation. To prevent gravity-driven flow, the desired residual oil phase was injected into the top of the core using the ISCO syringe pump designated for oil. If injection of oil is done from the bottom of the core, density differences between the oil and water phases can cause the less dense oil to non-uniformly displace water in the core. Effluent fluids during oil injection floods were collected in 15 mL centrifuge tubes via the fraction collector. Injection of the oil phase was continued until no subsequent brine was recovered in the effluent or in other words until residual water saturation ($S_{wr}$) had been reached. This normally took approximately 10 pore volumes of oil injection to achieve. The amount of water collected in the effluent was recorded to

calculate the residual water saturation. The inlet and outlet lines to the pressure transducers were switched for oil injection into the top of the core, as to ensure a positive recorded pressure drop.

### 4.3.5 Waterflooding the Core to Residual Oil Saturation

Waterflooding the core with brine was conducted to achieve residual oil saturation ($S_{or}$). This state of residual oil saturation simulates a depleted oil field where no incremental oil production is feasible using subsequent waterflooding procedures. Brine was injected at the bottom of the core to prevent gravity-driven flow, and achieve a more uniform displacement of oil. Brine injection rates were incrementally increased from 2 mL/min to 12 mL/min. These flow rates, on the order of 60-400 ft/day, don't realistically reflect typical ~1 ft/day waterflood rates seen in the field (Pope, 2007), rather were used to reduce the oil saturation to that of an extremely depleted oil field. Starting from 2 mL/min, injection is continued until no oil is present in the effluent. The brine injection rate is then increased and oil production initially resumes due to increases in the capillary number. Eventually no substantial incremental increases in oil production occurred with increases in brine injection rates (< 0.25 mL). The amount of oil collected in the effluent was recorded after the waterflood procedure to calculate the residual oil saturation. Typically, injection rates for the waterflood procedure started at 2 mL/min and were increased to 4, 8, and 12 mL/min.

### 4.3.6 Core Cleaning Procedure for Reuse

After a majority of the coreflood experiments, a core cleaning procedure was conducted so that the same core could be reused for a subsequent, and often comparative, experiment. Approximately 20 pore volumes of isopropyl alcohol (IPA) were injected at high flow rates (~10 mL/min) into the core, to remove organic phases from the core.

Following the injection of IPA, about 10 pore volumes of brine were injected into the core at high flow rates (~10 mL/min) to flush the core of IPA, while saturating the core with brine. Finally, permeability calculations were made by injecting at various flow rates and observing the coinciding pressure drop across the core. If the permeability of the cleaned core matched was within 10% of the initial permeability calculated during first coreflood experiment, the core was deemed fit for the next coreflood experiment. All cores satisfied this condition, indicative of minimal retention or adsorption of nanoparticles.

## 4.4 DATA ANALYSIS

### 4.4.1 Core Pore Volume

Using the dry and wet weight core measurements described earlier in this chapter, the pore volume of each core was calculated. The pore volume of a core is defined as the volume of the void space open to fluid occupation, otherwise the total porous volume of the core. The core pore volume, *PV*, in units of mL was calculated using the following equation:

$$PV = \frac{M_{wet} - M_{dry}}{\rho_{brine}}, \tag{4}$$

where $M_{wet}$ is mass of the core when saturated with brine (g), $M_{dry}$ is the mass of the core after being dried and vacuumed (g), and $\rho_{brine}$ is the density of the brine (g/mL). The pore volumes of the Boise sandstone cores typically ranged from 40 to 45 mL corresponding to porosities ranging from 0.25 to 0.35, as calculated by the following equation:

$$\phi = \frac{Pore\ Volume}{Bulk\ Volume}, \tag{5}$$

### 4.4.2 Core Permeability

The permeability of each core, $k$ (D), was calculated using Darcy's Law as shown below:

$$k = \frac{\mu L Q}{A \Delta P}, \tag{6}$$

where $\mu$ is the viscosity of the injected brine (Pa-s), $L$ is the length of the core (cm), $Q$ is flow rate ($cm^3/s$), $A$ is the cross-sectional area of the core ($cm^2$), and $\Delta P$ is the pressure drop across the length of the core (atm).

Brine was injected at a constant flow rate, and the pressure drop across the core was recorded once it reached a steady state. At minimum, three flow rate-pressure drop measurements were used to calculate an average value for the permeability of each core. To ensure consistent permeability measurements, $R^2$ values from linear regression were used to verify that the permeability of the core was nearly constant at different flow rates.

### 4.4.3 Residual Water Saturation

Recall that to reduce the core to residual water saturation, oil was injected from the top of the core until no more brine was produced. The value for residual water saturation, $S_{wr}$, was calculated by comparing the total produced water in this procedure to the pore volume of the core using the following equation:

$$S_{wr} = \frac{PV - displaced\ brine\ during\ oil\ injection}{PV}, \tag{7}$$

where $PV$ is the pore volume of the core.

As seen in Figure 4.2, the fractional flow of water quickly decreases to nearly zero, at which the oil injection displacing the brine from the core was stopped. The mineral oil was dyed red with an oil soluble dye as to help distinguish it from the brine.

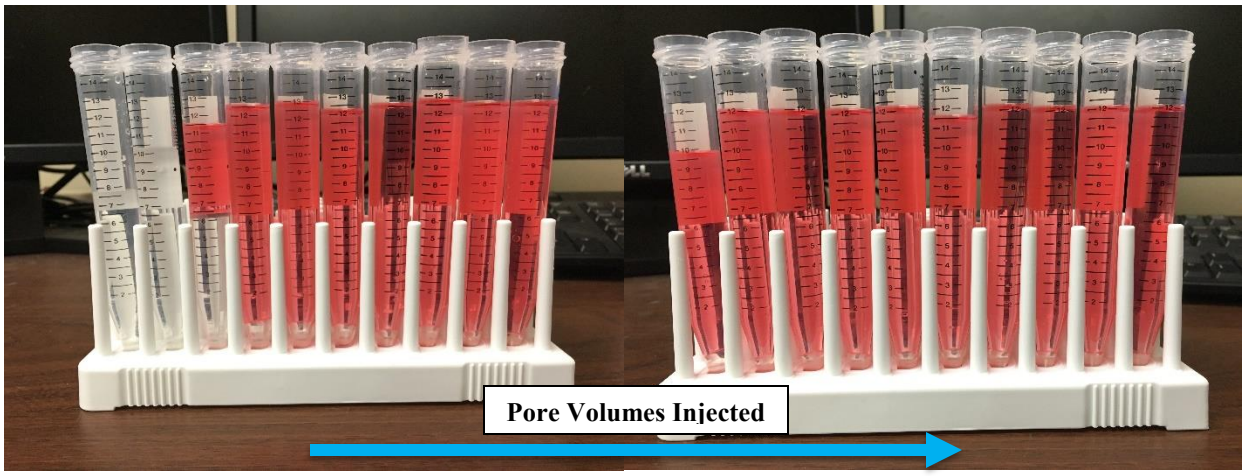


Figure 4.2: Example of effluent from residual water saturation procedure (injection of mineral oil into brine saturated core). This figure displays roughly 5 pore volumes of mineral oil injection. Mineral oil has been dyed red.

The first few pore volumes (~3-5 PVs) were collected in 15 mL centrifuge tubes in the fraction collector in order to provide accurate estimations of the total amount of displaced brine during oil injection. After little to no brine was being produced from the core, injection of mineral oil continued to a total of 10 PVs and the effluent was collected in a large container. Typical residual water saturations for the cores used in this thesis range between 30-40%.

### 4.4.4 Residual Oil Saturation

Recall, that to reduce the core to residual oil saturation, brine was injected into the bottom of the core (previously reduced to residual water saturation) until no more mineral oil was produced. The value for residual oil saturation, $S_{or}$, was calculated by comparing the total produced oil in this waterflood procedure to the fraction of the pore volume available to flow, using the following equation:

$$S_{or} = \frac{PV(1-S_{wr}) - oil\ displaced\ during\ waterflood}{PV}, \quad (8)$$

where $PV$ is the pore volume of the core and $S_{wr}$ is the residual water saturation

Brine was injected at incrementally increasing flow rates into the bottom of the core, until the fractional flow of oil from the core was zero. At this point, the core was considered to be at residual water saturation, representing a depleted reservoir where enhanced oil recovery techniques are needed to produce oil. An example of the effluent collected during the procedure to reduce the core to residual oil saturation is shown below in Figure 4.3. After increasing the injection rate to 12 mL/min, no incremental increase in oil recovery was observed, so the procedure was terminated.

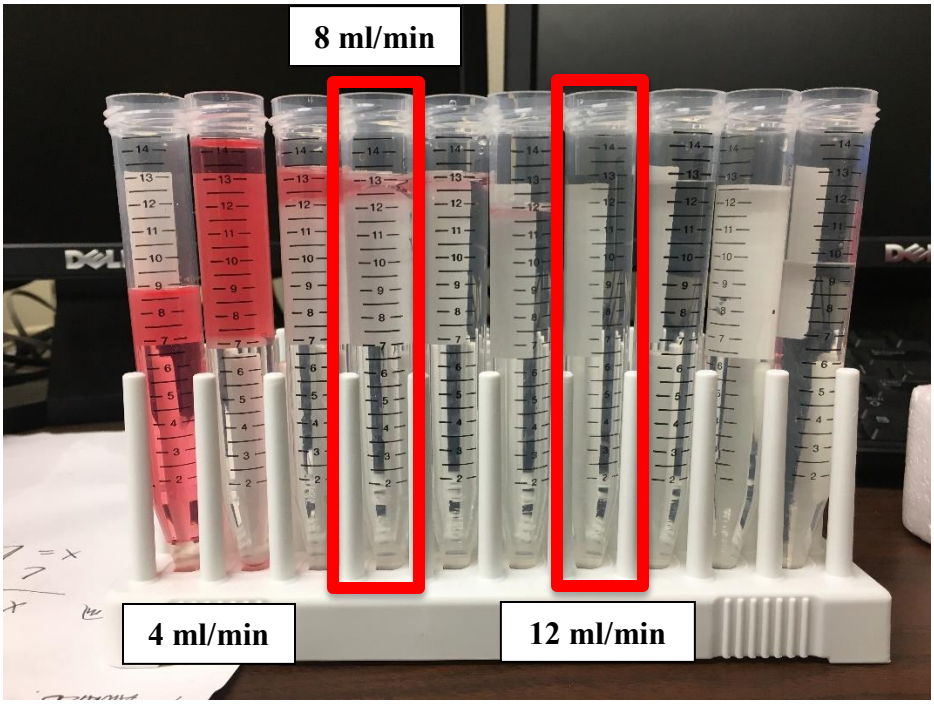


Figure 4.3: Example of effluent from residual oil saturation procedure. The red rectangles around the centrifuge indicate a change in flow rate.

## 4.5 RESULTS

| **Summary of Coreflood Experiments in Chapter 4** | | | | | | | | |
|---|---|---|---|---|---|---|---|---|
| Experiment Type | Core | SS | $\phi$ | k (mD) | Initial Saturation | Injected Fluids | Flow Rate (mL/min) | Percentage Recovery (%) |
| Effects of Sonicated Emulsion Flow-rate on Effective Permeability Reduction and Pressure Response – Low Flow Rate | A | Boise | 0.27 | 785 | Brine | Sonicated Pentane Emulsion (NP) | 0.25 | - |
| Effects of Sonicated Emulsion Flow-rate on Effective Permeability Reduction and Pressure Response – High Flow Rate | A | Boise | 0.27 | 785 | Brine | Sonicated Pentane Emulsion (NP) | 0.5 | - |
| Effects of Beadpack Emulsion Droplet Size and Emulsifier on Effective Permeability Reduction and Pressure Response – Small Droplets | B | Boise | 0.33 | 429 | Brine | Beadpack Decane Emulsion (NP) | 0.5 | - |
| Effects of Beadpack Emulsion Droplet Size and Emulsifier on Effective Permeability Reduction and Pressure Response – Large Droplets | B | Boise | 0.33 | 429 | Brine | Beadpack Decane Emulsion (NP) | 0.5 | - |
| Effects of Beadpack Emulsion Droplet Size and Emulsifier on Effective Permeability Reduction and Pressure Response – Surfactant-stabilized | B | Boise | 0.33 | 429 | Brine | Beadpack Decane Emulsion (Surf) | 0.5 | - |
| Effects of Beadpack Emulsion Salinity on Dynamic Stability and Effective Permeability Reduction – High Salinity | C | Boise | 0.32 | 3572 | Brine | Beadpack Decane Emulsion (NP) | 0.5 | - |
| Effects of Beadpack Emulsion Salinity on Dynamic Stability and Effective Permeability Reduction– Low Salinity | C | Boise | 0.32 | 3572 | Brine | Beadpack Decane Emulsion (NP) | 0.5 | - |
| Effects of Sonicated Emulsion Salinity on Dynamic Stability and Effective Permeability Reduction – Low Salinity | D | Boise | 0.29 | 418 | Brine | Sonicated Pentane Emulsion (NP) | 0.5 | - |
| Effects of Sonicated Emulsion Salinity on Dynamic Stability and Effective Permeability Reduction – High Salinity | D | Boise | 0.29 | 418 | Brine | Sonicated Pentane Emulsion (NP) | 0.5 | - |
| Effects of Sonicated Emulsion Salinity on Residual Oil Recovery – Low Salinity | E | Boise | 0.33 | 2541 | Residual Mineral Oil and Brine | Sonicated Pentane Emulsion (NP) | 0.5 | 87% |

Table 4.2: Coreflood experiments conducted in this thesis.

| | | | | | | | | |
|---|---|---|---|---|---|---|---|---|
| Effects of Sonicated Emulsion Salinity on Residual Oil Recovery – High Salinity | E | Boise | 0.33 | 2541 | Residual Mineral Oil and Brine | Sonicated Pentane Emulsion (NP) | 0.5 | 89% |
| Effects of Sonicated Emulsion Salinity on Residual Oil Recovery – Low Salinity (redo) | E (redo) | Boise | 0.29 | 693 | Residual Mineral Oil and Brine | Sonicated Pentane Emulsion (NP) | 0.5 | 56% |
| Effects of Sonicated Emulsion Salinity on Residual Oil Recovery – High Salinity (redo) | E (redo) | Boise | 0.29 | 693 | Residual Mineral Oil and Brine | Sonicated Pentane Emulsion (NP) | 0.5 | 61% |
| Effects of Sonicated Emulsion Zeta-potential on Residual Oil Recovery – Low Magnitude Zeta-potential (PEG-coated Nanoparticles) | F | Boise | 0.34 | 3915 | Residual Mineral Oil and Brine | Sonicated Pentane Emulsion (NP) | 0.5 | 81% |
| Effects of Sonicated Emulsion Zeta-potential on Residual Oil Recovery – High Magnitude Zeta-potential (EOR 5xs Nanoparticles) | F | Boise | 0.34 | 3915 | Residual Mineral Oil and Brine | Sonicated Pentane Emulsion (NP) | 0.5 | 85% |

Table 4.2: Coreflood experiments conducted in this thesis.

### 4.5.1 Coreflood A: Effects of Sonicated Emulsion Flow-rate on Effective Permeability Reduction and Pressure Response

This coreflood experiment was designed to investigate the effect of emulsion injection rates on droplet-pore blocking effects and effective permeability reduction (i.e., conformance control). The emulsion injection rate has been shown to have a significant consequences for emulsion droplet-pore blocking and effective permeability reduction potential with surfactant-stabilized emulsions. Studies have shown that increases in injection rates often reduce the effectiveness of pore-throat blockage due to local increases in capillary effects (McAuliffe, 1973; Guillen *et. al*, 2011, 2012). It will be shown that with nanoparticle-stabilized emulsions that this may not always be the case.

***Emulsions***

Nanoparticle-stabilized pentane-in-water emulsions were generated using an aqueous 2 wt% PEG nanoparticle dispersion at 5 wt% API via a sonication gun at 100%

for 1 minute in 100 mL (total) volumes of 1:1 pentane to nanoparticle dispersion. A total of 400 mL of emulsion was generated for each flood. The sonication method resulted in emulsions with extremely small droplets. Droplet images of the emulsion are shown in Figure 4.4.

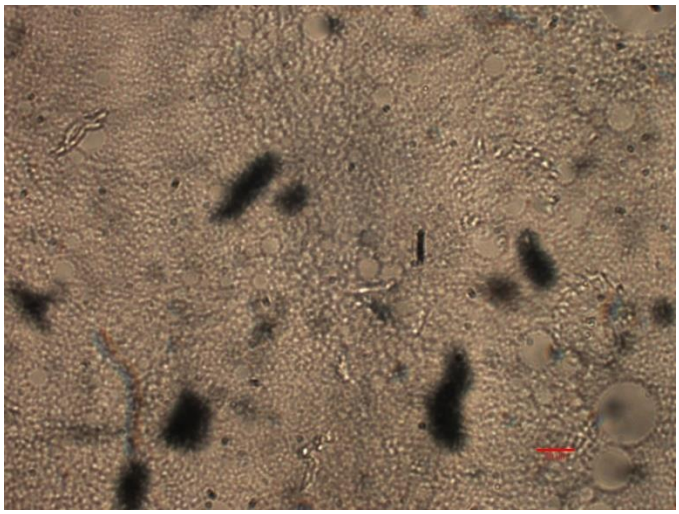

Figure 4.4: Microscopic images of pentane emulsion (1:1 phase ratio, 2 wt% PEG-coated nanoparticles, 5 wt% API) produced via sonication method at varying ionic concentrations. Red line represents scale bar of 20 microns. Median droplet diameter of 5.81 microns

The emulsion was so dense that it was difficult to obtain an image where the droplet edges were well-defined. Using some discretion when analyzing the droplet images, the median droplet size was determined to be roughly 6 microns. Due to the poor imaging capabilities, during the original analysis of these sonicated emulsions it was thought that the sonication process may have caused large nanoparticle aggregates to form in the emulsion phase. Furthermore, after allowing the emulsion used in these experiments to sit in a sealed container for several weeks, creaming and partial phase separation had resulted in an very viscous emulsion phase, which seemed to indicate nanoparticle aggregation as seen in bicontinuous gels generated at high salinities (as discussed in Chapter 3). Possible

nanoparticle aggregates formed by the sonication generation process were a major concern for coreflood experiments given that nanoparticle aggregates could irreversibly attach to grain surfaces or become stuck in pore throats, potentially leading to effective permeability reductions not resulting from pure droplet-pore throat blockage behavior.

However, after taking microscopic pictures of the compact emulsion phase, these concerns were alleviated – as well-defined droplets are shown in Figure 4.5 below. It was determined that the high packing density and small droplet size of these emulsions post-generation, makes clear images of individual droplets extremely hard to capture, as seen in the amorphous semi-spherical shapes dispersed between droplets in Figure 4.4. This occurs because multiple layers of droplets are continuously going in and out of focus, creating this effect. It should be noted that the median droplet size did not change transiently for this particular emulsion.

Figure 4.5: Microscopic image of pentane emulsion (1:1 phase ratio, 2 wt% PEG-coated nanoparticles, 5 wt% API) that has been allowed to cream and settle for two days in a sealed glass container (previously shown in Figure 4.5, immediately post generation. Red line represents scale bar of 20 microns. Median droplet diameter of 6.06 microns

To further confirm that no nanoparticle aggregates were formed during the sonication process, the effective size of the nanoparticles in the excess aqueous phase of the emulsion was measured using the Zetasizer DLS. The effective nanoparticle size in the excess phase was determined to be 24.08 nanometers (nm), which corresponds to the effective size of the nanoparticles in the 5 wt% API nanoparticle dispersion (~22 nm) that was used to generate this emulsion. .

***Rheology***

Rheology measurements of the sonicated emulsion made using the rheometer and methods described in section *3.1.4*. Figure 4.6 displays data from the rheology tests conducted on the nanoparticle-stabilized pentane emulsion used in these corefloods. What is interesting is that the emulsions generated via sonication differ from those generated in beadpacks, in that they are less viscous and are actually Newtonian. This phenomenon will be explored later in this section. The low shear rate plateau is desirable in oilfield applications, because an extremely large viscosity is avoided in very low shear conditions such as large distances from the wellbore.

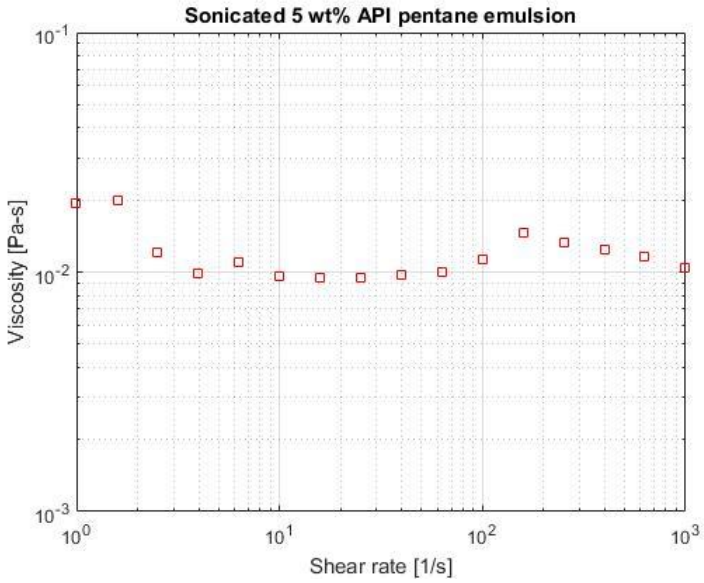


Figure 4.6: Rheology of 5% API, nanoparticle-stabilized pentane emulsion generated via sonication method to be injected into cores.

***Emulsion Injection and Pressure Responses***

The nanoparticle-stabilized pentane emulsion at 5 wt% API discussed in the previous section was injected at varying flow rates into a Boise sandstone core saturated with 5 wt% API brine. In the first coreflood, the emulsion was injected at 0.25 mL/min (~8 ft/day) for roughly four pore volumes. The core was then cleaned as described in the coreflood methods section and re-saturated to 5 wt% API brine. The second coreflood was then conducted by injecting, emulsion into the core at 0.5 mL/min (~16 ft/day) for roughly 5 pore volumes. The effluent and pressure drop were recorded for each.

Figure 4.7 displays the core properties and recorded pressure drop of the first coreflood at the lower injection rate (0.25 mL/min). Midway through the coreflood experiment the pressure transducer had to be switched. Originally, the pressure drop across the core was being recorded by the transducer calibrated for a pressure drop of less than 200 psi. Given the corefloods conducted by injecting nanoparticle-stabilized emulsions in

the past (Ahmad, 2015), a pressure drop exceeding 200 psi was not expected. However, in this case the sonicated emulsions with smaller droplets seem to be more effective in reducing the permeability of the core than emulsions generated via beadpack co-injection. The transducer was manually switched to the 1000 psi transducer at 1.75 pore volume of emulsion injection. This explains the sharp pressure drop seen in the pressure response at that time. The second dip in the pressure response is due to the injection of aqueous nanoparticle phase that had separated from the emulsion in the accumulator. Interestingly, the pressure drop never exceeded 200 psi after this. The extra presence of excess nanoparticle dispersion in the core is thought to have caused this decrease in effective permeability reduction.

| Coreflood A – Low Injection Rate | | | | | |
|---|---|---|---|---|---|
| k (mD) | ϕ | Pore Volume (mL) | $S_{or}$ | Flow Rate (mL/min) | Percent Recovery (%) |
| 785 | 0.27 | 42.11 | - | 0.25 | - |

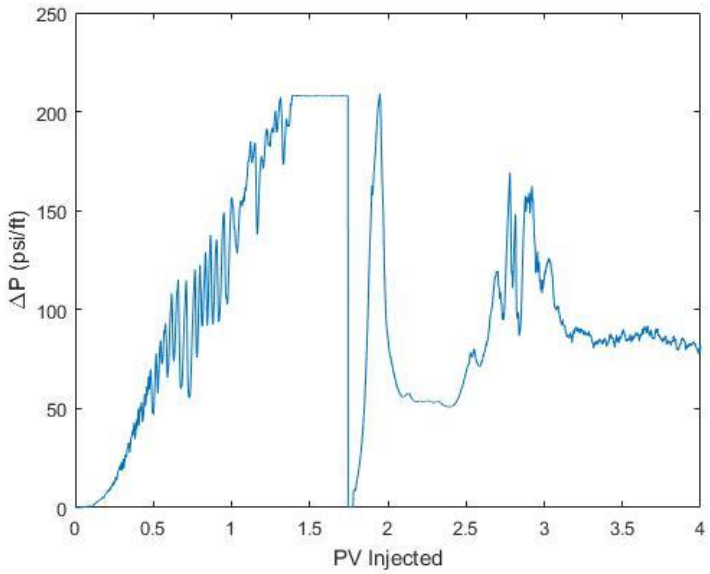


Figure 4.7: Coreflood A – 0.25 ml/min injection of sonicated emulsion into core saturated with 5 wt% API brine. The pressure transducer calibrated for recording pressures below 200 psi recorded maximum readings (~200 psi) from 1.4-1.75 PVs. The pressure transducer used to measure the pressure drop across the core was manually switched over to the 1000 psi transducer at 1.75 pore volumes injected. This transducer was used for the remainder of the coreflood.

At ambient conditions the pentane emulsions are unstable due to the high vapor pressure of pentane. Because the coreflood was conducted overnight, a camera was set up to record if and when emulsion breakthrough at the effluent end of the core occurred. Unfortunately, the camera malfunctioned during the emulsion flood at 0.25 ml/min, and it is uncertain whether emulsion breakthrough occurred. Breakthrough of pentane occurred after 1 pore volume of injection.

The core was cleaned and was saturated with 5 wt% API brine. No significant changes in permeability were observed. Emulsion was then injected at a higher rate, 0.5

mL/min, to observe any differences in pressure response and effluent liquids obtained. Figure 4.8 displays the core properties and recorded pressure drop for this second coreflood.

| Coreflood A – High Injection Rate | | | | | |
|---|---|---|---|---|---|
| k (mD) | $\phi$ | Pore Volume (mL) | $S_{or}$ | Flow Rate (mL/min) | Percent Recovery (%) |
| 778 | 0.27 | 42.11 | - | 0.5 | - |

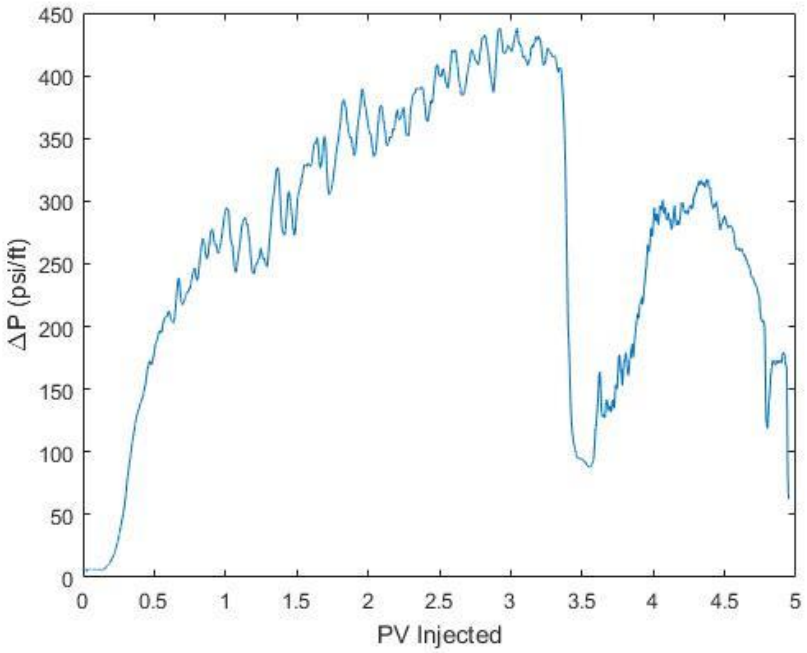


Figure 4.8: Coreflood A – 0.5 ml/min injection of sonicated emulsion into core saturated with 5 wt% API brine.

After roughly 3.5 pore volumes of emulsion injection at 0.5 mL/min, emulsion was produced in the effluent. It was originally thought that this drastic decrease in pressure drop across the core, coincided with emulsion breakthrough. After further review the occurrence of these events at the same time was mere coincidence. This drastic decrease in pressure drop is attributed to the injection of excess nanoparticle dispersion that has separated from

the emulsion, and is common in the many coreflood experiments in this study. Microscopic imaging of the effluent emulsion was conducted and is shown in Figure 4.9.

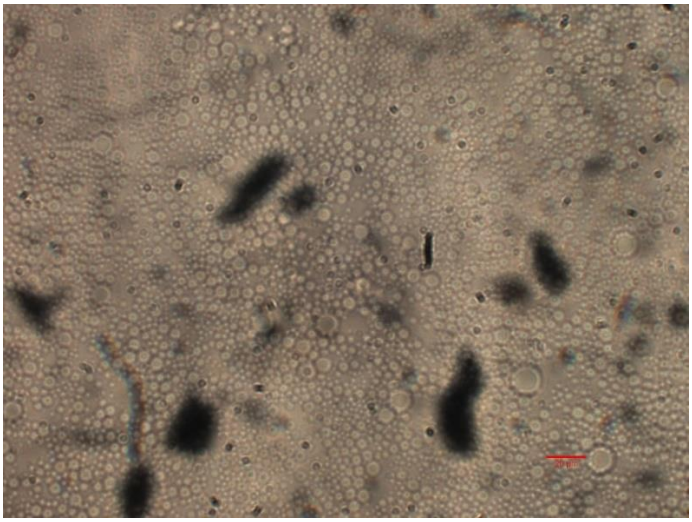

Figure 4.9: Microscopic image of effluent pentane emulsion from the injection of sonicated pentane emulsion at 0.5 mL/min. Red line represent scale bar of 20 microns. Median droplet size of 4.46 microns

The effluent emulsion possesses a noticeably lesser droplet-density then the injected emulsion. Furthermore, the median droplet size was 4.46 microns. Given the statistical information about the variance of the droplet sizes for the injected and effluent emulsion, there is not enough statistical significance to claim that the droplet size of the emulsions decreased after flowing through the core. Rather than individual droplets coalescing together and forming larger droplets, it is hypothesized that a small fraction of individual droplets coalesce resulting in an emulsion with less droplets per unit volume.

***Effective Permeability Reduction***

By way of Darcy's law it was expected that the pressure drop of the emulsion injected at a higher flow rate would have a larger pressure drop than that of the lower

injection rate. Furthermore, given the comparable work done on surfactant-stabilized emulsions (McAuliffe, 1973; Guillen *et. al*, 2011, 2012), it was expected that at lower flow rates or lower capillary numbers the emulsions would block pore-throats more effectively, due to lower hydrodynamic forces at pore-throats – leading to more extensive effective permeability reductions. In the case of this nanoparticle-stabilized emulsion coreflood experiments and the range of injection rates explored here, this effect was not observed. Reductions in effective permeability are shown in Figure 4.10 for the first ~1.5 pore volumes of emulsion injection.

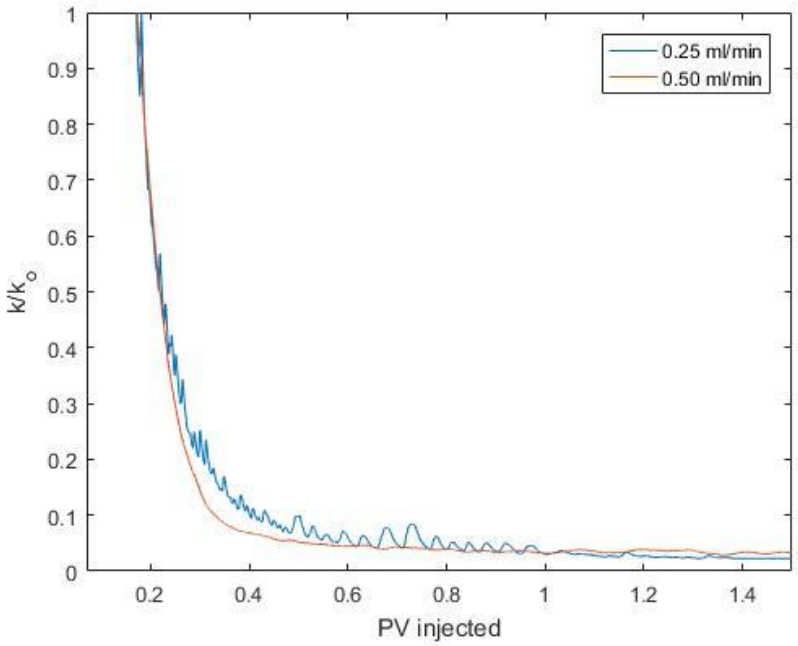


Figure 4.10: Reduction in core effective permeability as a function of pore volumes injected for emulsion injection experiments at 0.25 and 0.5 mL/min injection rates. $k_o$ is from the steady-state permeability measurements obtained using 5 wt% API brine.

Differences in behavior between surfactant-stabilized and nanoparticle-stabilized emulsions in porous media could include: not a wide enough range of capillary numbers

explored to observe a difference (not likely), nanoparticle-stabilized emulsion in-situ instability relative to ultra-robust surfactant-stabilized emulsions (likely), and differences in concentration of emulsion droplets per unit volume (likely). Furthermore, because the droplets are much smaller than the average pore throats (30-40 microns), the effectiveness of droplet-pore throat blockage is likely less of a function of local capillary forces and interstitial velocity, rather more dependent on concentration of emulsion droplets per unit volume which is held constant in this case.

Because of the effluent camera malfunction during the lower injection rate coreflood, the next paragraph serves as a discussion as to the possibility of effluent emulsion production. Since the effective permeability reduction seems constant over the range of injection rates considered, if breakthrough were to occur in the lower injection rate case, it would likely occur around the same pore volumes of injected emulsion in the observed high injection rate case. This is assuming that with these small droplet emulsions and the considered injection rates studied, there is little to no dependence on droplet velocity through pore throats, thus holding true for the non-dimensional time of pore volumes injected. Since everything else was held constant for these emulsions used in this experiment (emulsion type and in-situ stability, core properties, same resistance to flow, etc.), breakthrough of emulsion would likely occur at the same pore volume injected, regardless of the injection rate.

### 4.5.2 Coreflood B: Effects of Beadpack Emulsion Droplet Size and Emulsifier on Effective Permeability Reduction and Pressure Response

This coreflood experiment was designed to investigate the effects of relatively small changes in emulsion droplet size on pressure response and effective permeability reduction. Furthermore, the effect of emulsifying agents was investigated by comparing

the pressure response and stability of nanoparticle and surfactant-stabilized emulsions when injected into a Boise Sandstone core.

As seen in section *4.5.1* emulsions generated via sonication resulted in extremely small droplets (roughly 5 microns). Because these experiments were conducted in order to compare the effect of slight alterations in droplet size, the emulsions were generated via beadpack co-injection at varying flow rates. The size of the droplets in these emulsions were desired to be near the size of the median pore throat diameter of Boise sandstone, roughly 30-40 microns (Johnson, 2015).

***Emulsions***

PEG-coated nanoparticle dispersions at 2 wt% API were used to stabilize emulsions via co-injection with decane into a beadpack with 180 micron glass beads at flow rates of 12 and 75 mL/min. Droplet images were taken of the emulsions as shown in Figure 4.11.

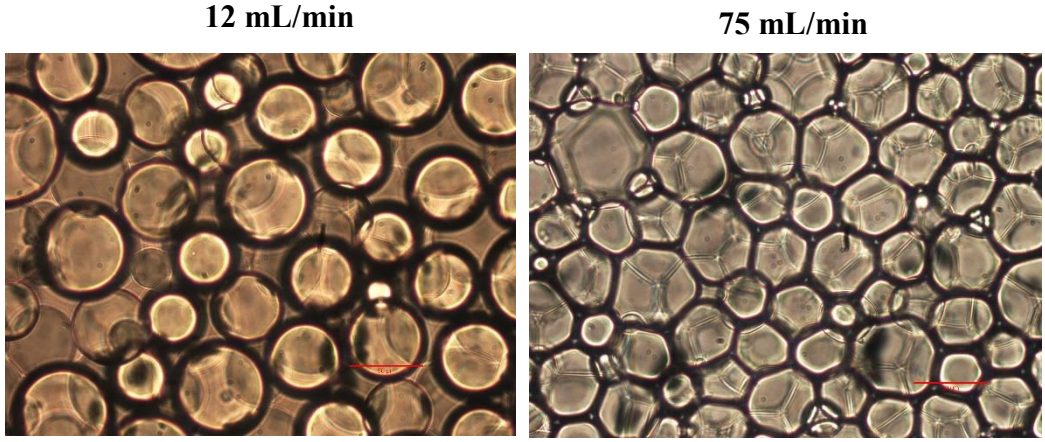


Figure 4.11: Microscopic images of decane emulsions (1:1 phase ratio, 2 wt% PEG-coated nanoparticles, 0 wt% API aqueous phase) generated via co-injection into beadback. Red line represent scale bars of 50 microns. At co-injection rates of 12 mL/min (left), median droplet diameter of 46.4 micron. At co-injection rates of 75 mL/min (red), median droplet diameter of 33.1 micron.

Emulsion droplet size was reduced by increasing the co-injection rate, hence the shear rate through the beadpack as explored and documented by Gabel (2014). At 12 mL/min co-injection rates, a nanoparticle-stabilized decane emulsion was generated with a median droplet size of 46. 4 micron; at 75 mL/min, a median droplet size of 33.1 microns.

Finally, a surfactant-stabilized decane emulsion was prepared, consisting of an aqueous phase of 2 wt% Sodium Dodecyl Sulfate (SDS), an anionic surfactant, at 2 wt% API. The surfactant-decane emulsion was generated via 1:1 co-injection into a beadpack at 12 mL/min. Droplet images were taken of this emulsion as shown in Figure 4.12. The median droplet size of this emulsion was 21.8 microns.

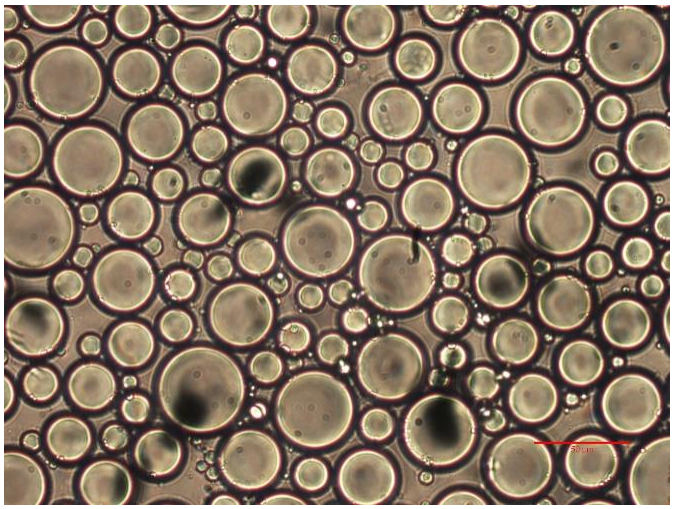

Figure 4.12: Microscopic image of surfactant-stabilized decane emulsion (1:1 phase ratio, 2 wt% SDS, 0 wt% API aqueous phase) generated via co-injection into beadback at 12 mL/min. Red line represent scale bars of 50 microns. Median droplet diameter of 21.8 microns.

It should be noted that even a six-fold increase in injection rate and shear rate in the beadpack did not cause a drastic change in emulsion droplet size for the nanoparticle-stabilized emulsions. Furthermore, in the case of the sonicated generation process,

emulsions with much smaller droplet sizes could be prepared, with median sizes of roughly 5 microns. In the future, beadpack generation of emulsions may not be desirable due to the lack of emulsion customizability using this method. It also should be noted that in an attempt to achieve comparable droplet size distributions to the nanoparticle-stabilized emulsions, co-injection rates were reduced for the surfactant emulsions, however resultant droplet sizes did not change significantly. This is attributed to the relative ease with which surfactants act as an emulsifying agent compared to nanoparticles.

***Rheology***

Rheology measurements of the emulsions at each co-injection rate and emulsifying agent were taken as shown in Figure 4.13.

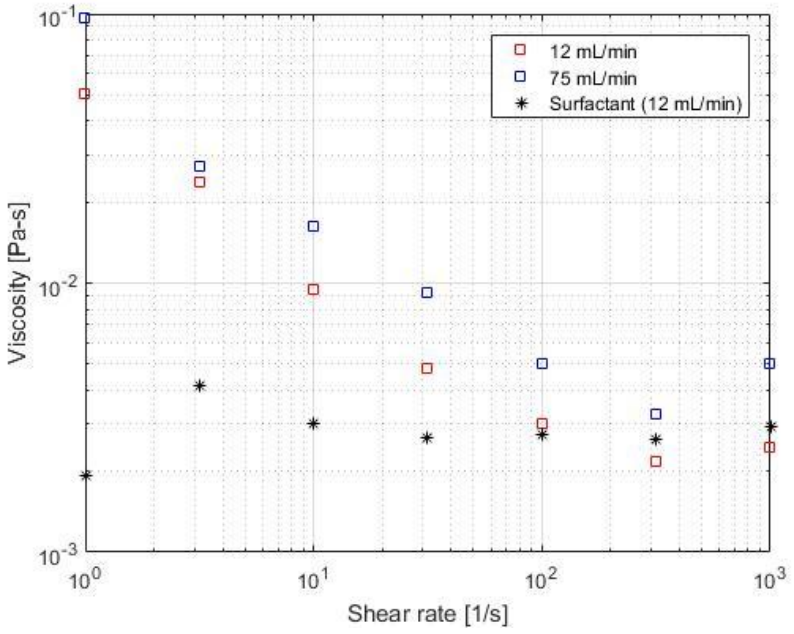


Figure 4.13: Rheology of nanoparticle-stabilized decane emulsions generated via different beadpack co-injection rates and emulsifying agents. The first two objects in the legend correspond to emulsions stabilized using nanoparticle dispersions.

The nanoparticle-stabilized emulsions generated via beadpack co-injection are shown to be highly-shear thinning power law fluids, as seen in *Chapter 3*. The nanoparticle-stabilized emulsion generated at higher co-injection rates is slightly more viscous, coinciding with smaller droplet sizes as has been documented by Gabel (2014). As will be shown in later sections, this theory that smaller droplet sizes causes more viscous emulsions will fall apart when emulsions are generated via the sonication method and in fact, display characteristics of Newtonian fluids. Likewise the surfactant-stabilized emulsion, with droplets half the size of the nanoparticle-stabilized emulsions, is much less viscous and displays Newtonian fluid characteristics.

***Emulsion Injection and Pressure Responses***

The nanoparticle-stabilized emulsion with the smaller median droplet size (75 mL/min co-injection rate, 33.1 microns median droplet size) was first injected at 0.5 mL/min, roughly 16 ft/day, into a Boise sandstone core saturated with 5 wt% API brine with a porosity of 0.33, permeability of 429 mD, and pore volume of 46.71 mL. Roughly 7 pore volumes of emulsion were injected, and the pressure drop across the core and effluent composition were recorded. No emulsion was produced in the effluent. The core was then cleaned as described in section *4.3.6*. The nanoparticle-stabilized emulsion with the larger median droplet size (12 mL/min co-injection rate, 46.4 microns median droplet size), was then injected at 0.5 mL/min, and the pressure drop across the core and effluent phases were recorded. No emulsion was produced in the effluent in this case, as well. Figure 4.14 compares the pressure response between the emulsions with different droplet sizes.

| Coreflood B – Effects of Beadpack Emulsion Droplet Size | | | | | |
|---|---|---|---|---|---|
| k (mD) | ϕ | Pore Volume (mL) | $S_{or}$ | Flow Rate (mL/min) | Percent Recovery (%) |
| 429 | 0.33 | 46.71 | - | 0.5 | - |

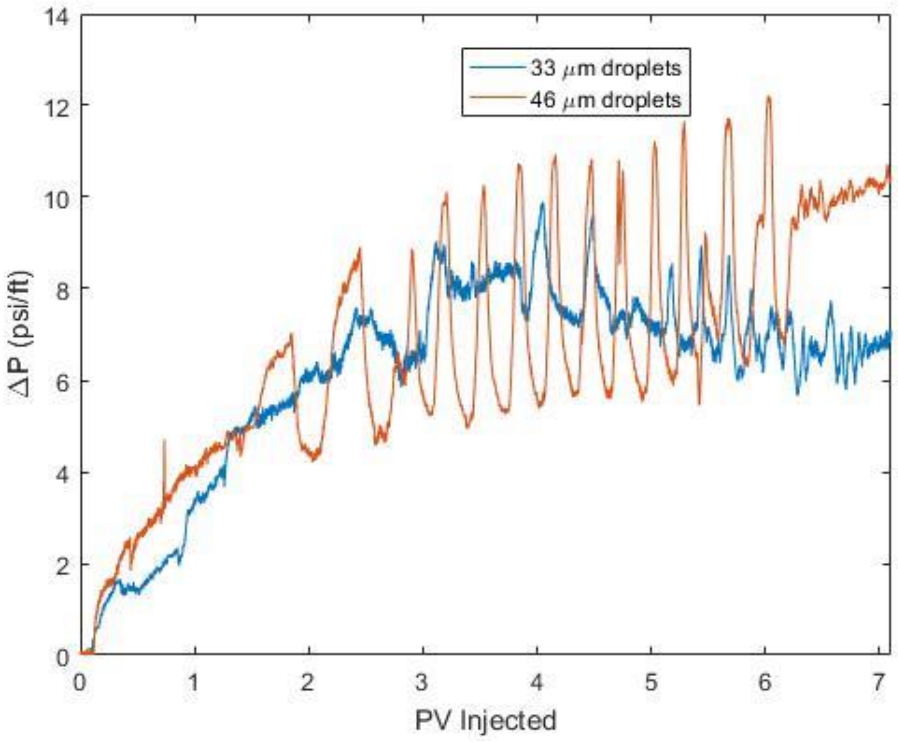


Figure 4.14: Coreflood B – Pressure response from coreflood experiments injecting nanoparticle-stabilized decane emulsions with varying median droplet sizes at 0.5 mL/min into Boise sandstone core saturated with 5 wt% API brine.

While each emulsion's median droplet size is certainly within the range of the average pore-throat size of Boise sandstones, there is a noticeable difference between the pressure responses for the relatively two emulsion floods. During the 46 micron emulsion coreflood, the amplitude of the pressure oscillations (~5 psi) is much greater than that of the pressure response during the 33 micron flood (~2.5 psi at most). This is a clear indication of more pore-throat blocking phenomenon. The 46 micron emulsion has a

greater percentage of emulsion droplets that can block the pore-throats through larger droplet-to-pore throat diameter ratios. Furthermore, given that the smaller droplet emulsion is more viscous, the increase in pressure drop in the case of the large droplet case must be due to increased pore throat blockage and effective permeability reduction.

***Effective Permeability Reduction***

It was expected that the emulsion with the larger droplets would result in a larger pressure drop, thus a larger decrease in effective permeability, due to increases in pore-throat blockage. As shown in Figure 4.15, these emulsions significantly reduce the permeability of the core.

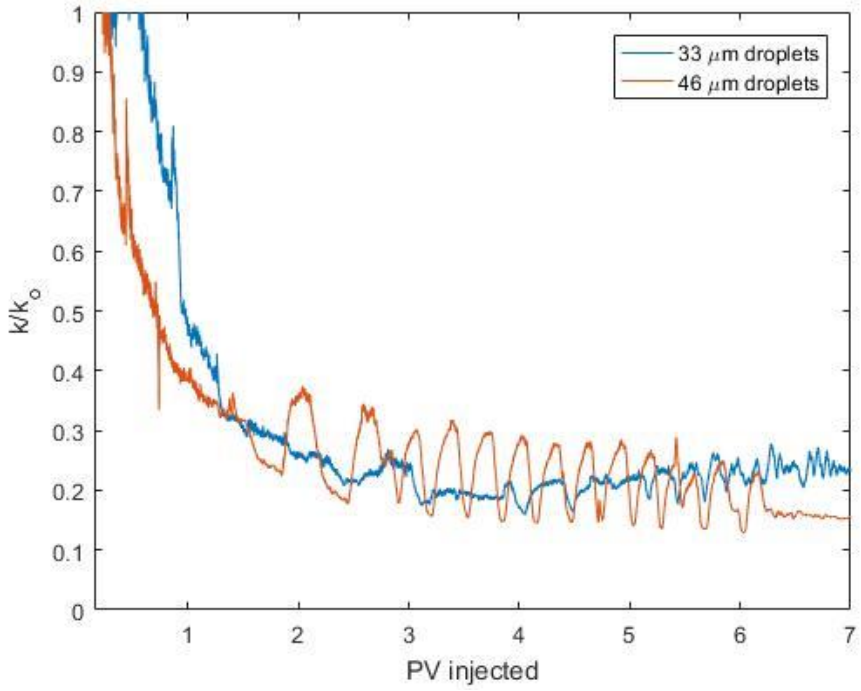


Figure 4.15: Reduction in core effective permeability as a function of pore volumes injected for emulsion injection experiments at varying droplet sizes. $k_o$ is from the steady-state permeability measurements obtained using 5 wt% API brine.

The larger droplets decrease the effective permeability of the core slightly more than the emulsion with the smaller droplets. One reason as to why this difference is not as pronounced as it was thought it would be may be due to the fact that differences in the emulsions' droplet distributions were not significant enough. Another reason could be due to the relative instability of the emulsions in-situ. As was stated before, no emulsion was produced in the effluent for either droplet size. Compared to the emulsions injected in Coreflood A, where the droplets were roughly 5 microns (generated via sonication) and were produced in the effluent, these emulsions having much larger droplets seem to be much more dynamically unstable. The slight increase in droplet size in the 46 micron emulsion, could cause the droplets to be significantly less stable than the 33 micron emulsion, resulting in only a small increase in pressure drop and decrease in effective permeability reduction. Furthermore, comparing the reductions in Coreflood A (Figure 4.10) and Coreflood B (Figure 4.15), it is apparent that while slight increases in droplet size at the pore-throat scale may enhance droplet pore-throat blockage, large reductions in droplet size (reducing droplet sizes to the ~5 micron scale) significantly increase the in-situ stability of the emulsions leading to greater reductions in effective permeability and effluent emulsion breakthroughs.

***Surfactant Comparison***

Finally, after conducting the 2$^{nd}$ nanoparticle-stabilized emulsion flood (46 micron median droplet size) the Boise sandstone core was cleaned and saturated with 5 wt% API brine. The surfactant-stabilized emulsion was then injected into the core at 0.5 mL/min. Roughly 6 pore volumes of emulsion were injected. After 1.95 pore volumes of injection, stable emulsion was produced the effluent. The pressure response of the surfactant-

stabilized emulsion flood is shown in comparison to the nanoparticle-stabilized emulsion floods in Figure 4.16.

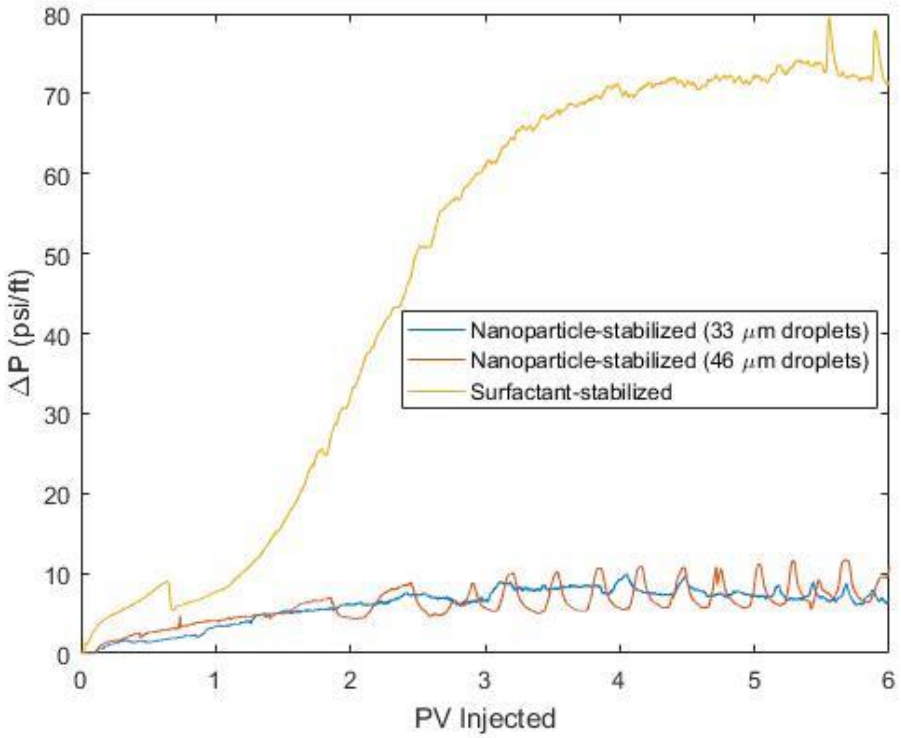


Figure 4.16: Coreflood B – Comparison of pressure responses from coreflood experiments injecting nanoparticle and surfactant-stabilized decane emulsions with varying median droplet sizes at 0.5 mL/min into Boise sandstone core saturated with 5 wt% API brine.

Despite having much smaller droplet-to-pore throat diameter ratios than the nanoparticle-stabilized emulsions, the surfactant-stabilized emulsion exhibits a much larger pressure drop due to its ability to maintain stability while flowing through porous media. At a roughly steady-state pressure drop, the surfactant-stabilized emulsion reduced the effective permeability reduction ratio to ~0.025. While it would seem that the larger, nanoparticle-stabilized droplets would increase droplet-pore throat blockage behavior, the instabilities of nanoparticle-stabilized emulsions in-situ are highlighted in this experiment.

These instabilities are likely due to a nanoparticle-stabilized droplets' poor resistance to coalescence and maintaining mechanical or kinetic (conditional) stability when experiencing large hydrodynamic and capillary forces at a clogged pore throat, in contrast to surfactant emulsions that are thermodynamically (unconditionally) stable.

Once steady-state surfactant emulsion production was achieved in the effluent, around 2.5 pore volumes of injection, samples were taken and analyzed under the microscope for droplet distribution measurements. The median droplet size in the effluent was determined to be 25.1 microns, very close to that of the injected emulsion (21.8 microns). At steady-state emulsion production it is hypothesized that little to no droplet coalescence is occurring. An image of effluent surfactant emulsion is shown in Figure 4.18.

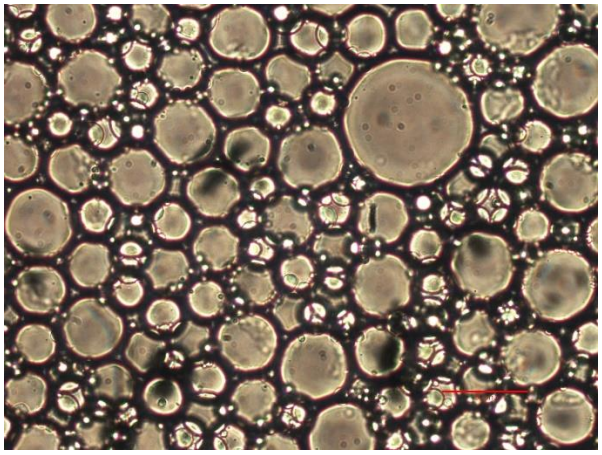

Figure 4.18: Microscopic image of surfactant-stabilized decane emulsion obtained in effluent of coreflood experiment. Red line represent scale bars of 50 microns. Median droplet size of 25.1 microns.

### 4.5.3 Coreflood C: Effects of Beadpack Emulsion Salinity on Dynamic Stability and Effective Permeability Reduction

#### *Emulsions*

The purpose of this experiment was to observe the effects of increasing beadpack-generated emulsion salinity on an emulsion's dynamic and in-situ stability, coreflood pressure response, and effective permeability reduction. Different emulsions were generated at varying beadpack co-injection rates and salinities to observe the effects that these variables had on droplet size and dynamic stability, as deduced from multi-step rheology tests. Emulsions were prepared at a 1:1 ratio of decane to 2 wt% PEG nanoparticle dispersion with varying salt concentration at 0 wt% and 10 wt% API brine. For 10 wt% API brine emulsions, phases were co-injected into the beadpack at 12, 25, 50, 75, and 100 ml/min per phase. Emulsion generated using 0 wt% API was injected at 100 ml/min per phase. Droplet size distributions of each emulsion were measured using microscopes stills and the ImageJ software. The microscope stills and droplet size distributions are shown in Figures 4.19 and 4.20, respectively.

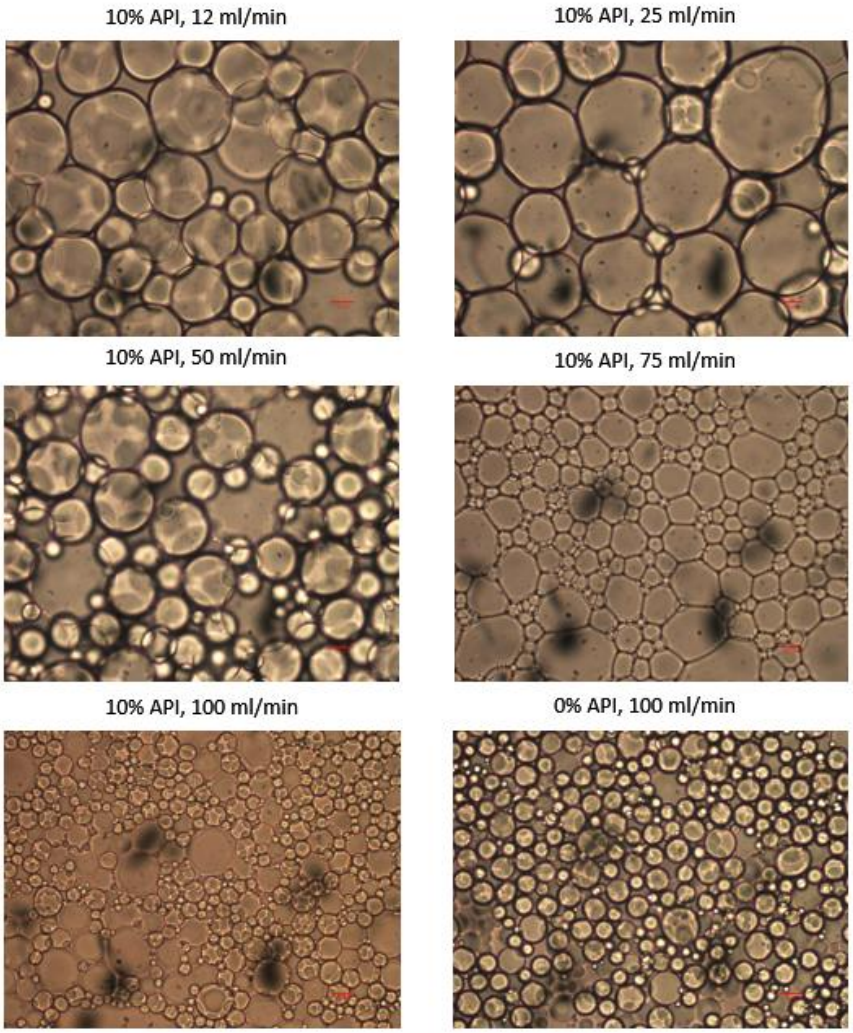


Figure 4.19: Microscopic images of nanoparticle-stabilized decane generated via beadpack co-injection at varying injection rates and salinities. Red lines represent scale bars of 50 microns.

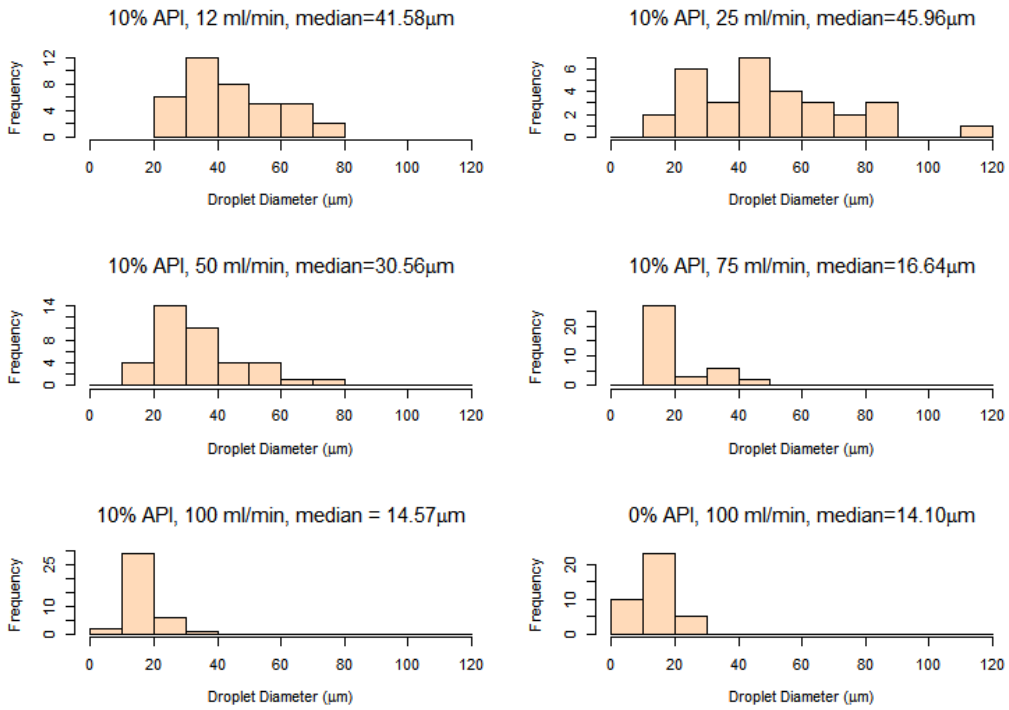


Figure 4.20: Histograms of droplet distributions for emulsions made at varying injection rates and salinities.

The 10 wt% API emulsions generated at varying injection rates served as a baseline to determine a consistent droplet size that could be generated using either 0 wt% or 10 wt% API nanoparticle phase. Because emulsions with smaller droplet sizes (i.e. sonicated emulsions) have been shown to be more stable during corefloods in this thesis, the 100 mL/min co-injected emulsions were chosen, with median droplet sizes of 14.10µm and 14.57µm at 0 wt% API and 10 wt% API, respectively. Interestingly, at this high co-injection rate, differences in aqueous phase salinity seemed to have little effect on the median droplet diameter of the emulsions.

***Rheology***

Rheology measurements of the 0 wt% and 10 wt% API emulsions were taken, including multi-step viscosity measurements where the tests were conducted sequentially without sample replacement. This was done to quantify what will be called dynamic stability for the remainder of this thesis. If droplet coalescence or breakage were to occur due to poor dynamic stability, a resultant less viscous rheology profile would occur in the second rheology test.

Figure 4.21 displays data from multi-step rheology tests conducted on the 0 wt% API emulsion. This emulsion was characterized as non-Newtonian with highly-shear thinning behavior. It is very clear that this emulsion had significant dynamic instability issues. The greatly reduced viscosity profile during the second step of the test is evidence of droplet coalescence under shear stress.

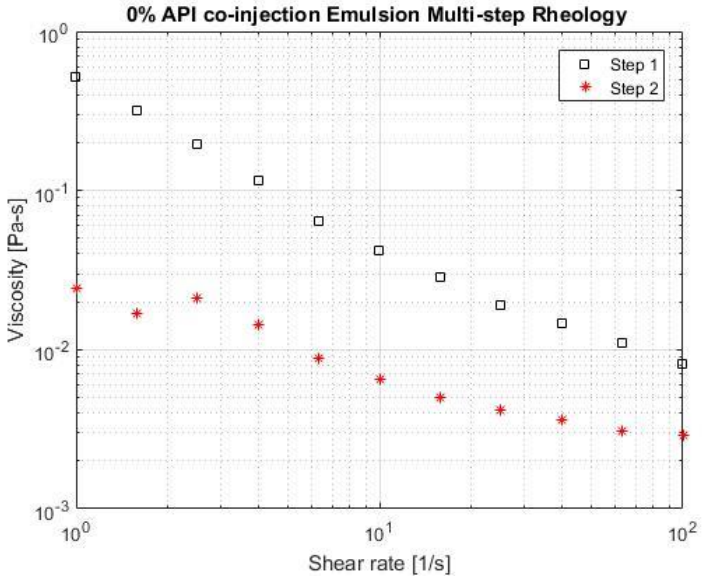


Figure 4.21: Rheology of 0 wt% API, PEG nanoparticle-stabilized decane emulsion generated via beadpack co-injection.

Figure 4.22 displays data from multi-step rheology tests conducted on the 10 wt% API emulsion. This emulsion was characterized as a non-Newtonian fluid with highly-shear thinning behavior. Unlike the 0 wt% API emulsions, the increased salinity seems to aid in greatly increasing the dynamic stability of the emulsion under shear stress.

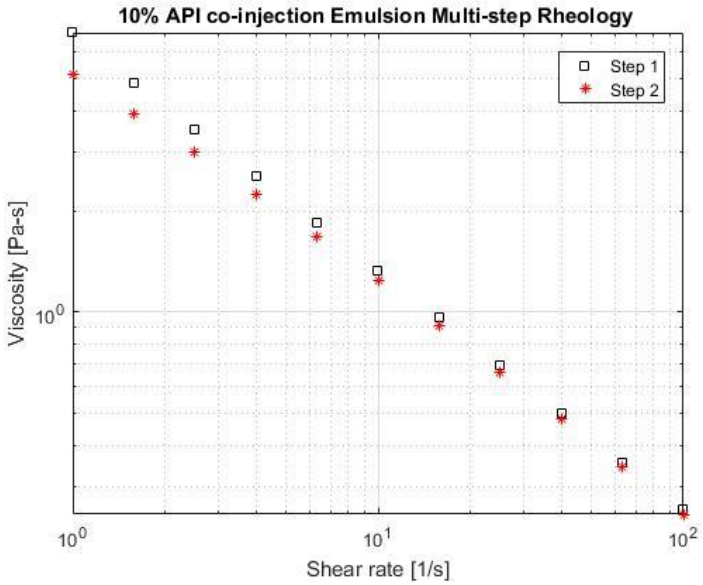


Figure 4.22: Rheology of 10 wt% API, PEG nanoparticle-stabilized decane emulsion generated via beadpack co-injection.

A comparison of the viscosity profiles of the two emulsions at different ionic concentrations is shown in Figure 4.23. The 10 wt% API emulsion was much more viscous, which was expected given the work done in *Chapter 2*. A 10 wt% API emulsion was generated as reference to show viscosity profiles of emulsions generated via different methods. The consequences of this will be detailed later.

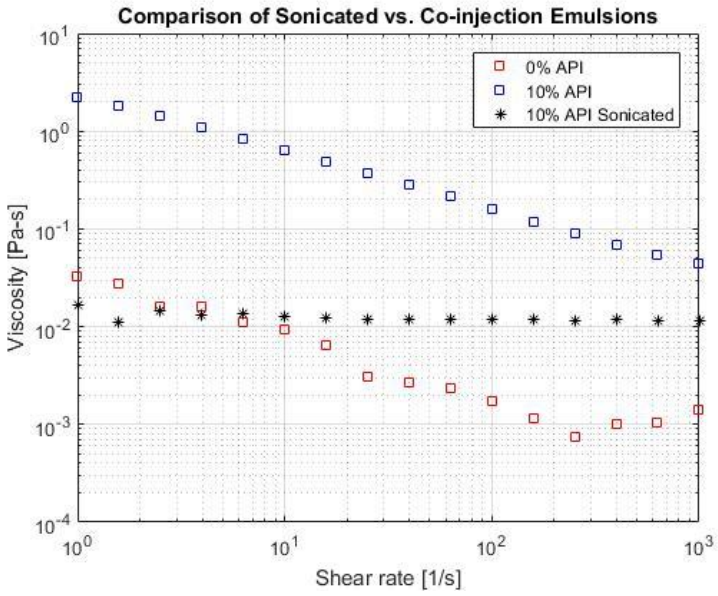


Figure 4.23: Rheological comparison of 0 wt% and 10 wt% API, PEG nanoparticle-stabilized decane emulsions generated via beadpack co-injection with reference to 10 wt% API decane emulsion generated via sonication method.

Differences in the dynamic stability of the two emulsions can be attributed to the formation of a network of interconnected droplets and aggregates in the high salinity emulsions as first proposed by Horozov et al. (2007). The aggregates bridging droplets adds to the integrity and resistance to coalescence of the droplets in high salinity emulsions. This is of increasing importance when considering flow through porous media, where asymmetrical hydrodynamic forces are applied on droplet interfaces. This is the likely reason as to why many nanoparticle-stabilized emulsions are not produced in the effluent of many corefloods or at least until extremely late pore volumes of injection. Thus, it was expected that when injected into a core, the 10 wt% API emulsion would exhibit larger effective permeability reductions than the 0 wt% API emulsion and would have a higher chance of being produced in the effluent.

***Emulsion Injection and Pressure Responses***

First, 4 pore volumes of 0 wt% API emulsion were injected at 0.5 ml/min, roughly 16 ft/day, into a Boise sandstone core saturated with 5 wt% API brine with a porosity of 0.32, permeability of 3572 mD, and pore volume of 45.35 mL. Unfortunately, the LABVIEW program recording the pressure drop crashed during the flooding procedure and no data was recorded. No emulsion was present in the effluent. The core was then cleaned as described in section *4.3.6* and saturated with 5 wt% API brine. 3.5 pore volumes of the 10 wt% API emulsion were injected at 0.5 ml/min. No emulsion was produced in the effluent. Core cleaning was conducted again and 4 pore volumes of 0 wt% API emulsion was injected into the core at 0.5 ml/min, again with no emulsion in the effluent. The pressure drops were recorded for the following experiments and are shown in Figure 4.24.

| Coreflood C – Nanoparticle-stabilized Emulsion Corefloods | | | | | |
|---|---|---|---|---|---|
| k (mD) | ϕ | Pore Volume (mL) | $S_{or}$ | Flow Rate (mL/min) | Percent Recovery (%) |
| 3572 | 0.32 | 45.35 | - | 0.5 | - |

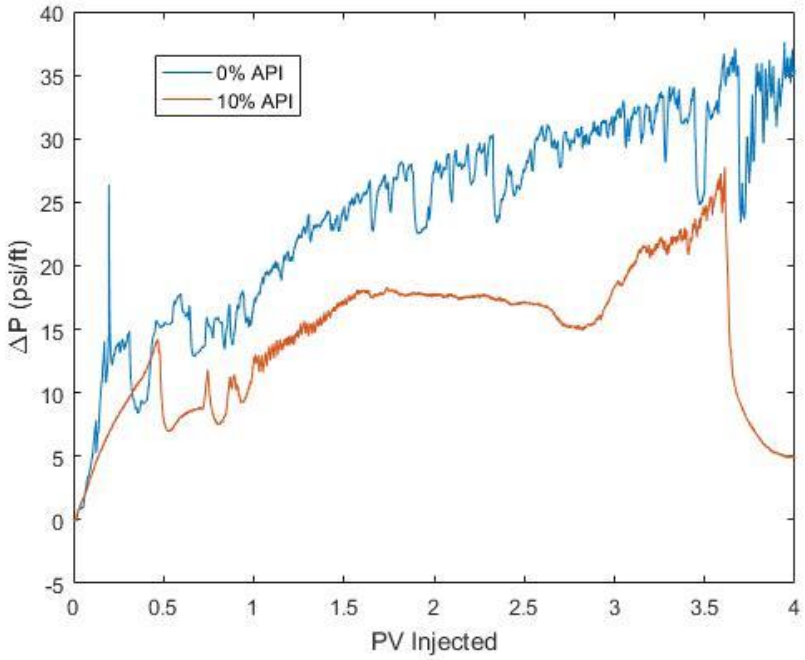


Figure 4.24: Coreflood C – Pressure response from injecting nanoparticle-stabilized decane emulsions with varying salinities at 0.5 mL/min into Boise sandstone core saturated with 5 wt% API brine.

Even though the 10 wt% API emulsion displayed enhanced dynamic stability in the rheology tests as shown in Figures 4.21 and 4.22, the pressure drop and effective permeability reductions were slightly larger for the 0 wt% API emulsion. Due to the fact that the 0 wt% API emulsion injection was the third coreflood conducted on the core and only a marginal increase in pressure drop was observed, the difference is probably statistically insignificant. Given the in-situ instabilities observed during previous corefloods of beadpack-generated emulsions as seen in the lack of effluent emulsion and relatively low pressure drops, it has been concluded that despite high salinity or high

emulsion generating shear rates (high beadpack co-injection rates), beadpack emulsions are inferior to sonicated emulsions in terms of in-situ stability. However, the significance of salinity on emulsion stability should not be ignored. In the following section, this significance will be explored by injecting sonicated emulsions at varying salinities into a brine saturated core.

### 4.5.4 Coreflood D: Effects of Sonicated Emulsion Salinity on Dynamic Stability and Effective Permeability Reduction

#### *Emulsions*

The purpose of this experiment was to observe the effects of increasing salinity on sonicated emulsion dynamic and in-situ stability, pressure response, and effective permeability reduction. Two emulsions were generated via the sonication method at 3 wt% and 10 wt% API, prepared at a 1:1 ratio of pentane to 2 wt% PEG nanoparticle dispersion. Microscopic images where captured to observe the effects of salinity on droplet size. Also, the effects of salinity on the emulsions' dynamic stability were deduced from multi-step rheology tests. Median droplet sizes of each emulsion were measured using microscopes stills and the ImageJ software. The microscope stills are shown below in Figure 4.25.

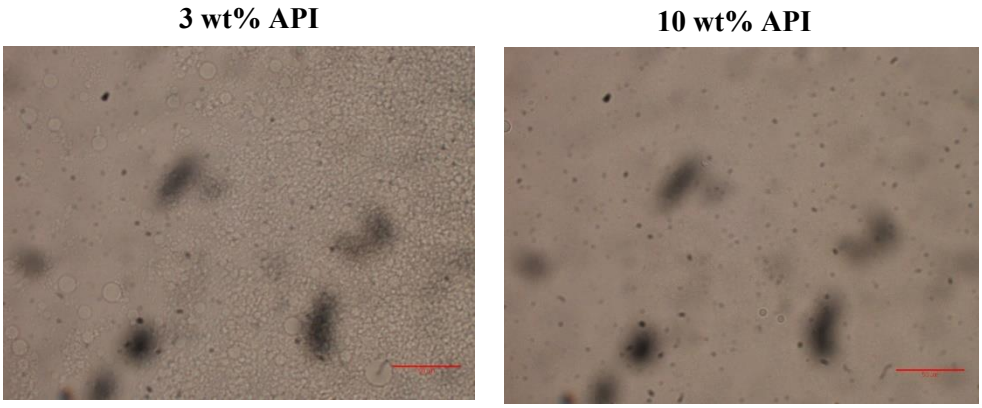


Figure 4.25: Microscopic images of nanoparticle-stabilized pentane emulsions (1:1 phase ratio, 2 wt% PEG-coated nanoparticles) produced via sonication method. Red lines represent scale bars of 50 microns. Median droplet diameters of 3.9 and 3.1 microns for 3 wt% and 10 wt% API emulsions, respectively.

There seemed to be little effect of salinity on emulsion droplet size or the emulsification process. The 3 wt% API emulsion had a median droplet diameter of 3.9 microns, while the 10 wt% API emulsion had a median droplet size of 3.1 microns.

***Rheology***

Rheology measurements of the emulsions at varying salinities were taken, including multi-step viscosity measurements where the tests were conducted sequentially without sample replacement. If droplet coalescence or breakage were to occur due to poor dynamic stability, a resultant less viscous rheology profile would occur in the second rheology test conducted. As seen in Coreflood A rheology tests, it was expected that the sonicated emulsions would exhibit Newtonian behavior and would exhibit increases in dynamic stability with increases in salinity due to droplet-droplet aggregate bridging.

Figure 4.26 displays data from multi-step rheology tests conducted on the 3 wt% API emulsion. This emulsion was characterized as non-Newtonian with slightly-shear thinning behavior. It is clear that this emulsion has significant dynamic instability issues.

The greatly reduced viscosity profile during the second step of the test is evidence of droplet coalescence under shear stress. In the 1-10 $s^{-1}$ region the fluid behaves like a Newtonian fluid, however becomes slightly shear-thinning as the shear rate increased. In fact, this shear-thinning behavior is likely due to droplet coalescence, unlike the true shear-thinning beadpack emulsions. Thus, the emulsion could be viewed as a pseudo-Newtonian fluid with instabilities at high shear rates.

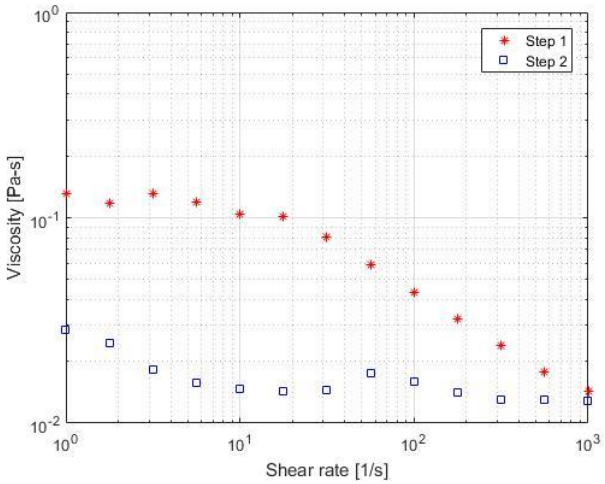


Figure 4.26: Rheology of 3 wt% API, PEG nanoparticle-stabilized pentane emulsion generated via sonication method.

Figure 4.27 displays data from multi-step rheology tests conducted on the 10 wt% API emulsion. This emulsion was characterized as a Newtonian fluid. Unlike the 3 wt% API emulsion, the increased salinity seemed to greatly increase the dynamic stability of the emulsion under shear stress.

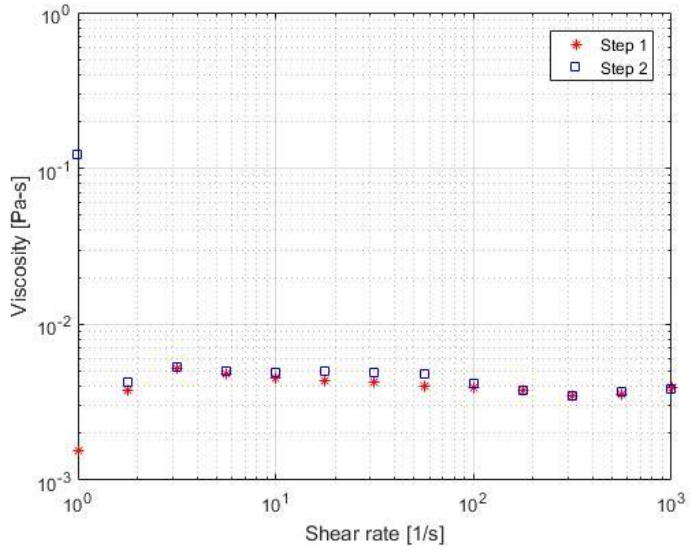


Figure 4.27: Rheology of 10 wt% API, PEG nanoparticle-stabilized pentane emulsion generated via sonication method.

A comparison of the viscosity profiles of the two emulsions at different ionic concentrations during the first step of the multi-step rheology tests is shown in Figure 4.28.

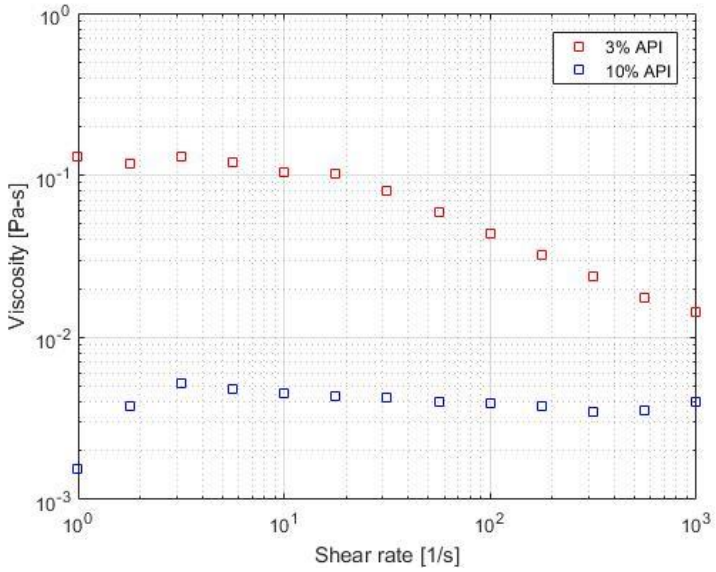


Figure 4.28: Rheological comparison of 3 wt% and 10 wt% API, PEG nanoparticle-stabilized pentane emulsions generated sonication method.

The 3 wt% API emulsion was much more viscous which was unexpected given the work done on (beadpack) emulsion rheology *Chapter 2*. It is not entirely understood why sonicated emulsion rheology behavior differs from that generated in the beadpack, however it was likely due to the ability of the sonicating tip to impart more energy into the emulsion generation process and form smaller droplet sizes. What can be concluded is that the differences in dynamic stability of the two emulsions is due to the formation of a network of interconnected droplets and aggregates in the high salinity emulsions. It was expected that when injected into a core, the 10 wt% API emulsion would exhibit larger effective permeability reductions and have a higher chance of being present in the effluent compared to the 3 wt% API emulsion.

It was also observed that the 10 wt% API emulsion was relatively less opaque compared to the 3 wt% API emulsion, as shown in Figure 4.29.

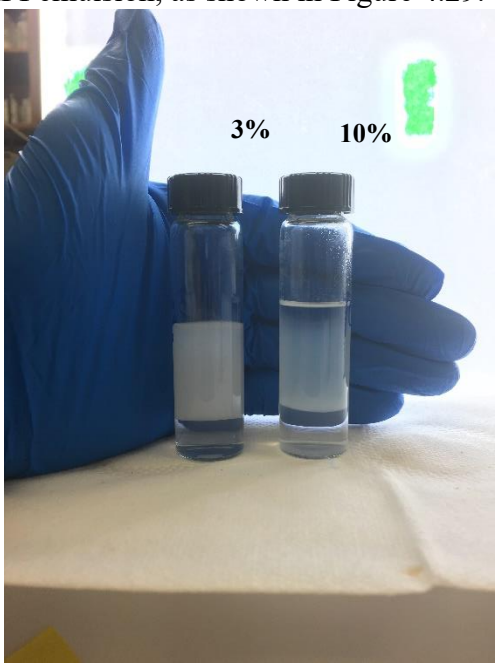


Figure 4.29: Relative comparison of opaqueness of 3 wt% and 10 wt% API, PEG nanoparticle-stabilized pentane emulsions generated sonication method. Corresponding wt% API is displayed as "%" value above vial.

Note that thermodynamically-stable surfactant microemulsions (droplet diameters 10-100 nm) that form droplets without imposed external shear forces, often appear transparent or clear due to small droplet sizes (smaller than the wavelength of light) allowing light to pass through without any refraction (Z. Sun et al., 2005). Although the droplet sizes were nearly the same for these two emulsions and are not in the nanometer range, the differences in opaqueness, may give some observational insight into the conditional stability of each emulsion. Like a transparent surfactant microemulsion, the less opaque 10 wt% API emulsion may be more conditionally stable as already seen in multi-step rheology tests, and the refractivity of an emulsion may serve as a relative and qualitative indicator for in-situ emulsion stability.

***Emulsion Injection, Pressure Responses and Effective Permeability Reductions***

First, roughly 7.5 pore volumes of 3 wt% API emulsion were injected at 0.5 ml/min, roughly 16 ft/day, into a Boise sandstone core saturated with 5 wt% API brine with a porosity of 0.29, permeability of 418 mD, and pore volume of 45.39 mL. The core was then cleaned as described in the coreflood procedure section *4.3.6* and saturated with 5 wt% API brine. Roughly 5.5 pore volumes of the 10 wt% API emulsion were injected at 0.5 ml/min. No emulsion was produced in the effluent for either coreflood, and pentane breakthrough occurred at approximately 1.2 pore volumes for both injected emulsions. The pressure drops were recorded for the following experiments and are shown in Figure 4.30.

| Coreflood D – Nanoparticle-stabilized Emulsion Corefloods | | | | | |
|---|---|---|---|---|---|
| k (mD) | ϕ | Pore Volume (mL) | $S_{or}$ | Flow Rate (mL/min) | Percent Recovery (%) |
| 418 | 0.29 | 45.39 | - | 0.5 | - |

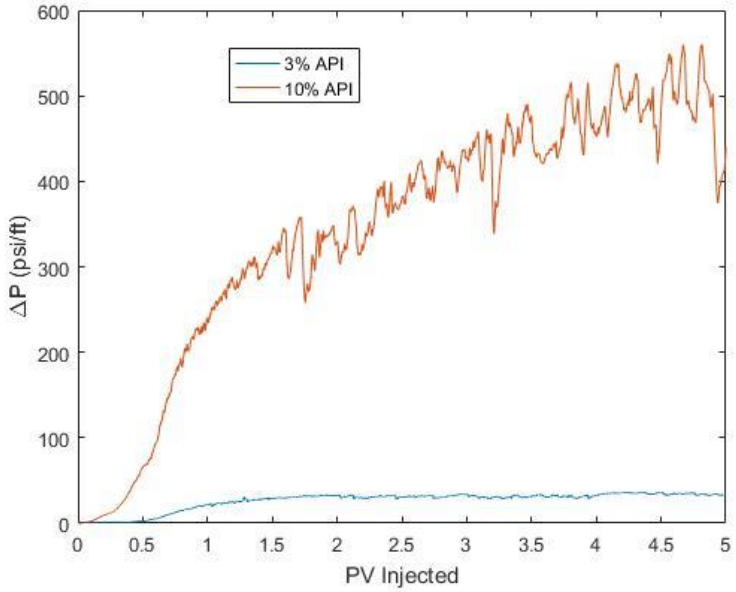


Figure 4.30: Coreflood D – Pressure response from coreflood experiments injecting nanoparticle-stabilized pentane emulsions generated via sonication at varying salinities at 0.5 mL/min into Boise sandstone core saturated with 5 wt% API brine.

Although no emulsion was produced in the effluent, the differences in pressure response for the low and high salinity emulsions generated via sonication is drastic. The 3 wt% API emulsion reaches a steady state of approximately 30 psi at 1.5 pore volumes injected with very few oscillations, whereas the 10 wt% API emulsion exhibits large pressure fluctuations (indicative of pore-throat blockage and release mechanisms), and an increasing pressure drop of over 500 psi at 5 pore volumes injected. Despite the order of magnitude reduction in viscosity for the 10 wt% API emulsion, there is an enormous increase of in-situ stability indicated by the large relative increase in pressure drop. This is

likely due to strengthening in emulsion stability from droplet-droplet bridging. Also, as will be detailed more extensively in the following section for Coreflood E, the increase in salinity may enhance droplet attachment to grains due to reduction in electrostatic repulsive forces via DLVO theory, otherwise known as droplet capture in filtration theory. Despite the large increase in resistance to flow (and inferred increased in-situ stability), no emulsion was present in the effluent of the high salinity coreflood. This could be attributed to not enough pore volumes injected in the high salinity case. Furthermore a steady-state pressure drop was never reached, indicative of a continuous process of increased droplet-pore blockage. While pentane and excess nanoparticle dispersion broke through in the effluent at 1.2 pore volumes and were continually produced, this could represent a fraction of the droplets that have coalesced and not captured or filtered by the core.

The increase of in-situ emulsion stability can also be quantified in terms of effective permeability reduction as shown in Figure 4.31. The 3 wt% API emulsion reduces the effective permeability reduction ratio to roughly 7% while the 10 wt% emulsion reduces the ratio to 0.4%. While drastically reducing the permeability may not be completely practical in field use, permeability ratios are suitable for judging emulsion stability. In reality, practical application of dense emulsions such as these could be alternating injection of emulsion and water for enhanced conformance control by plugging high permeability regions.

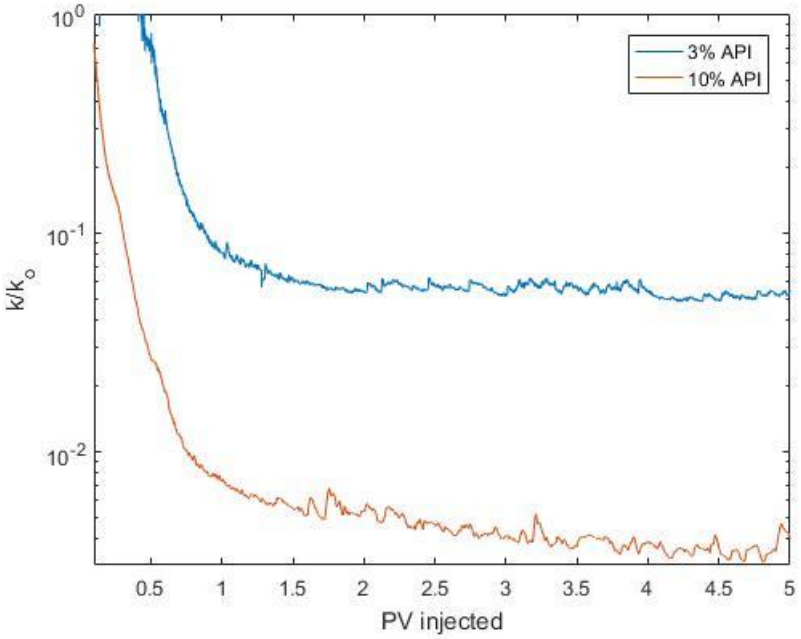


Figure 4.31: Coreflood D - Reduction in core effective permeability as a function of pore volumes injected for emulsion injection experiments at varying salinities. $k_o$ is from the steady-state permeability measurements obtained using 5 wt% API brine. Note semilog y-axis.

### 4.5.5 Coreflood E: Effects of Sonicated Emulsion Salinity on Residual Oil Recovery

These coreflood experiments were designed to investigate the effects of salinity on residual oil recovery during nanoparticle-stabilized emulsion injection. In *Chapter 3* PEG-coated nanoparticles were shown to serve as stable emulsifiers in static conditions (or pressurized in case of volatile pentane oil phase). As emulsion droplets flow through porous media, shear forces are imparted on the emulsion droplets and may even cause the droplets to break or coalesce. In dynamic conditions like these, emulsions that were previously characterized as statically stable, may in fact be unstable under shear and uneven hydrodynamic forces. While increases in ionic concentration have shown to destabilize and cause sedimentation of certain types of nanoparticles, PEG-coated silica nanoparticles have proven to be stable over a wide range of ionic concentrations and types

of ions. If the nanoparticles can tolerate increases in salinity, resultant emulsions possess greater dynamic and in-situ stability due to the formation of a three-dimensional network of interconnected droplets and aggregates, (Horozov et al., 2007). In this experiment two emulsions at varying salinities were injected into a Boise sandstone core for the purpose of observing the effects of salinity on recovering residual light mineral oil via nanoparticle-stabilized emulsions.

As shown in the preceding experiments, emulsions generated via the sonication gun with droplet sizes within the 1-10 micron range were much more stable as they flowed through porous media. With a droplet to average pore throat diameter below one, pore throat blockage and diversion of flow at the pore-scale cannot be attributed to the simple straining of droplets, rather pore-throat clogging via droplet bridging or aggregation can occur. At these small droplet to pore throat radius ratios, blockage may be dominated by interception effects (Soo, 1983) where droplets become attached to grains due to surface interactions. Interception effects could manifest in blockage mechanisms such as droplet bridging or aggregation at pore throats, as shown in Figure 2.7 (Dressaire and Sauret, 2017). Extended DLVO theory may help optimize this interception phenomenon to plug high permeability areas and divert flow elsewhere. DLVO theory can be used to describe both droplet-droplet interactions and droplet-surface interactions. The particular interaction of interest for optimizing interception phenomenon is the relationship between the droplet-surface. Most simply put, DLVO theory describes the competition between van der Waals attractive forces and electrostatic double layer repulsive forces as shown below:

$$W_t(h) = W_{vdW}(h) + W_{edl}(h) \tag{9}$$

where $W_t$ is the sum of the two opposing energies, $W_{vdW}$ is Waals potential, $W_{edl}$ is the electrostatic double layer potential, and $h$ is the distance between the droplet and grain

surface. The van der Waals attractive energy between a droplet and surface is expressed below:

$$W_{vdW}(h) = -\frac{AR}{6h}, \tag{10}$$

where $A$ is the Hamaker constant and $R$ is the droplet diameter. Being a function of the material of the droplet and surface, the Hamaker constant will be considered invariable for the purposes of this discussion. The electrostatic double layer energy can be expressed as the following:

$$W_{edl} = \Psi_o \exp(-\kappa h), \tag{11}$$

where $\Psi_o$ is the Stern potential, and $\kappa$ is the Debye-Hückel parameter as defined by:

$$\kappa = \left(\frac{2Ne^2I}{\varepsilon_o \varepsilon_r k_B T}\right)^{0.5}, \tag{12}$$

where $N$ is Avogadro's number, $e$ is the protonic charge, $I$ is the ionic strength of the electrolyte solution, $\varepsilon_o$ is the permittivity of the vacuum, $\varepsilon_r$ is the relative permeability of the electrolyte concentration, $k_B$ is the Boltzmann constant, and $T$ is temperature. While the Stern potential ($\Psi_o$) cannot be measured directly, zeta potential (ζ) can be measured and is taken to be identical to the Stern potential in this case. Figure 4.32 shows both the sum of van der Waals and electrostatic repulsion potentials as a function of separation difference between droplets and grain surfaces as well as the effects ionic concentration on the total potential. Minima in the total potential curves represent droplet-surface distances at which droplets become reversibly (secondary minimum) or irreversibly (primary minimum) attached at grain surfaces. By increasing the ionic concentration of the emulsion, chances of droplet attachment increase, enhancing droplet-pore throat blocking mechanisms. It has been hypothesized that droplets are reversibly attached to grain surfaces in the secondary minimum energy well.

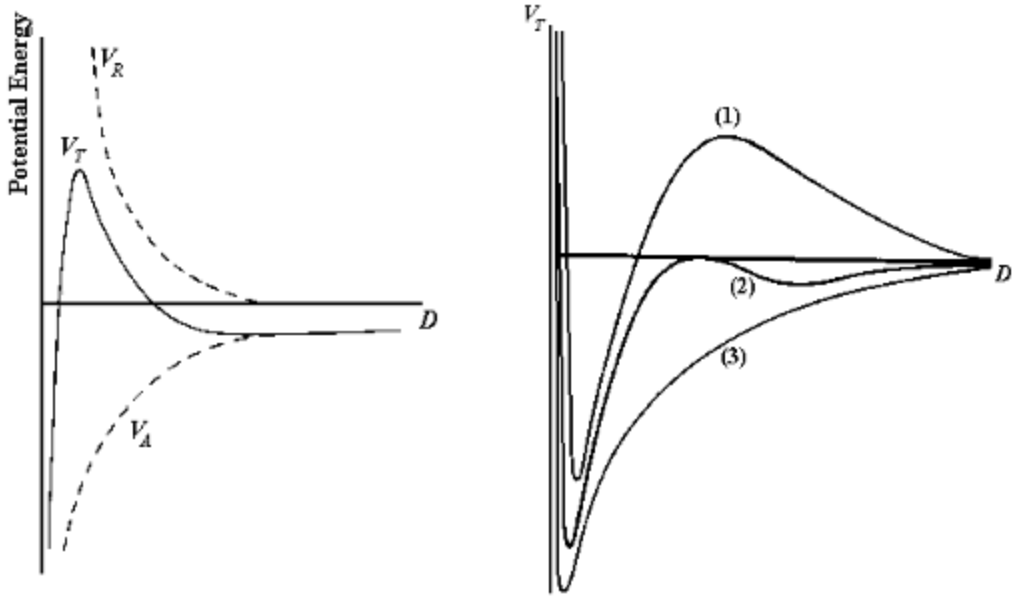


Figure 4.32: Total potential energy of interaction ($V_T$): sum of attractive van der Waals ($V_A$) and electrostatic repulsive ($V_R$) potentials as a function of separation distance (left). Total potential at varying ionic concentrations (right): (1) low, (2) intermediate, and (3) high ionic concentrations. (Cooper, 1999)

In the scope of these coreflood experiments the van der Waals forces could not be modified unless the material of nanoparticle was changed, however the repulsive forces can be reduced by increasing the ionic strength of the emulsions. By decreasing the repulsive force between the droplet-grain surfaces, interception effects can be enhanced and it is thought better sweep efficiencies and displacement profiles will be achieved. In this particular experiment, increasing the ionic concentration of the emulsion did just that. In some sense, strong repulsive forces between droplets are desired to prevent coalescence and phase separation (separation maintained mechanically by droplet-aggregate bridging at high salinities). However, weak repulsive forces between droplets and grains are desired to aid in interception and pore blockage phenomenon.

***Emulsions***

Two emulsions were generated via the sonication method at 3 wt% and 10 wt% API, prepared at a 1:1 ratio of pentane to 2 wt% PEG nanoparticle dispersion. Microscopic images where captured to observe the effects of salinity on droplet size. Droplet images were taken of the emulsions as shown in Figure 4.33. Because the emulsions were so dense, a bandpass filter was applied to the 10 wt% API emulsion image in ImageJ to aid in seeing droplet boundaries and obtain median droplet diameters.

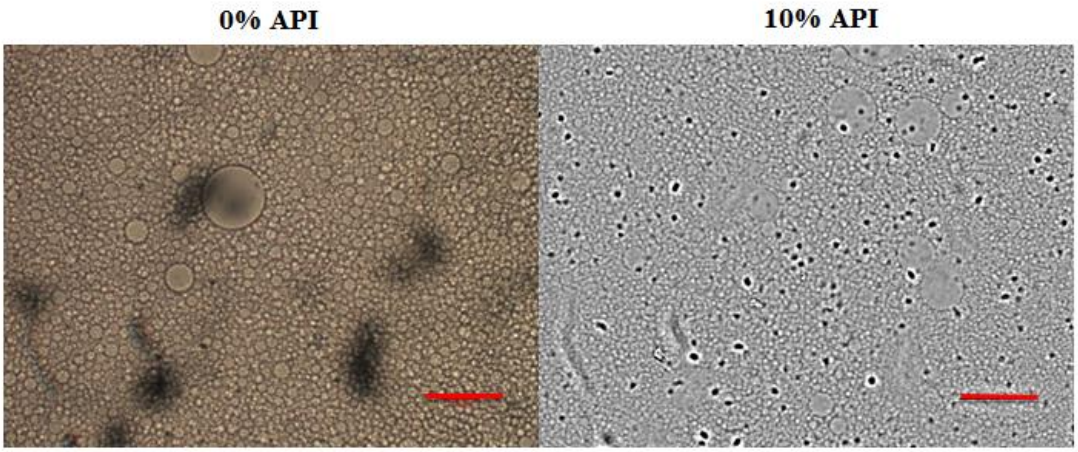


Figure 4.33: Microscopic images of pentane emulsions (1:1 phase ratio, 2 wt% PEG-coated nanoparticles) produced via sonication method at varying ionic concentrations. Red lines represent scale bars of 50 microns. Median droplet diameters of 4.7 and 4.9 microns for 3 wt% and 10 wt% API emulsions, respectively.

There seemed to be little effect of salinity on the droplet size or the emulsification process. The 0 wt% API emulsion had a median droplet diameter of 4.7 microns, while the 10 wt% API emulsion had a median droplet diameter of 4.9 microns.

***Rheology***

Rheology measurements of the sonicated emulsions at each ionic concentration were taken, including multi-step viscosity measurements where the tests were conducted sequentially without sample replacement. If droplet coalescence or breakage were to occur due to poor dynamic stability, a less viscous rheology profile would occur in the second rheology test conducted.

Figure 4.34 displays data from multi-step rheology tests conducted on the 0 wt% API emulsion. This emulsion was characterized as a non-Newtonian fluid with slightly-shear thinning behavior. It was difficult to ascertain whether this behavior was due to droplet coalescence (deduced from the reduction in viscosity profile during 2$^{nd}$ step) or if the emulsion was truly shear-thinning due to droplet-droplet deformation.

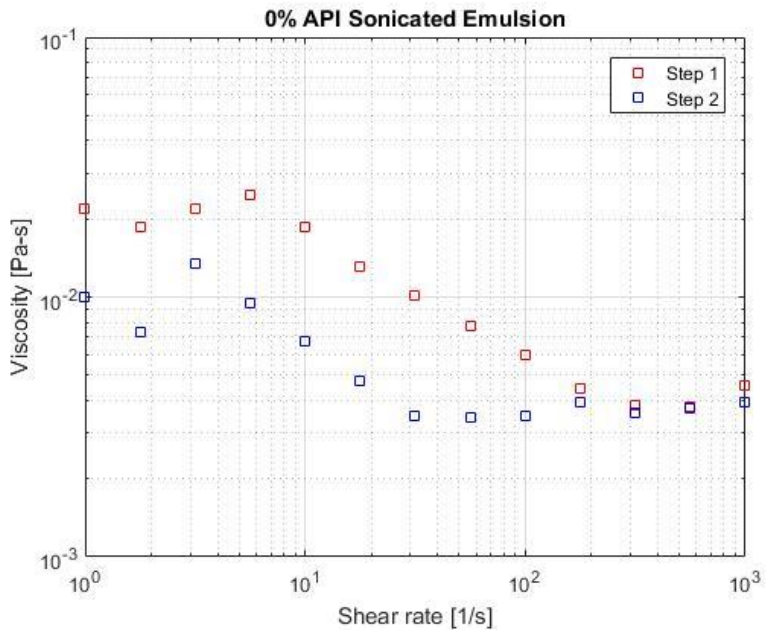


Figure 4.34: Rheology of 0 wt% API, PEG nanoparticle-stabilized pentane emulsion generated via sonication method to be injected into core for residual oil recovery experiments.

Figure 4.35 displays data from multi-step rheology tests conducted on the 10 wt% API emulsion. This emulsion was characterized as a Newtonian fluid. Furthermore, the droplets are stable under large imparted shear stresses as seen, in the lack of change in viscosity profiles during both steps of the multi-step test.

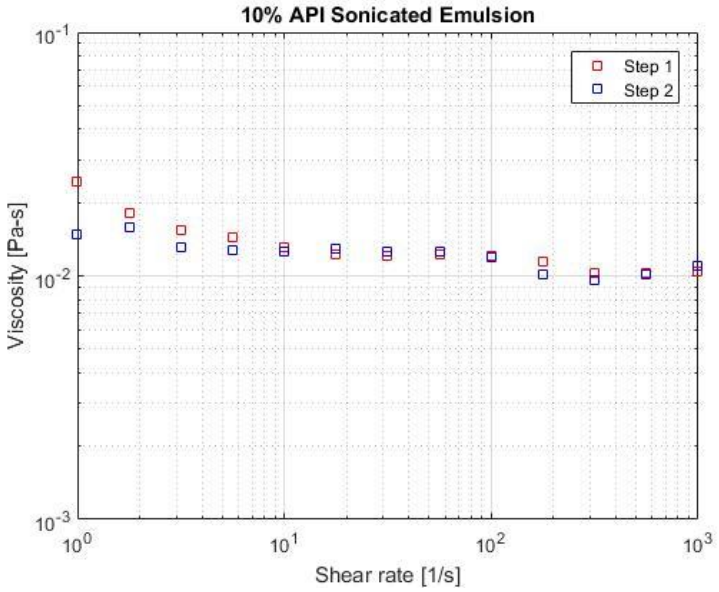


Figure 4.35: Rheology of 10 wt% API, PEG nanoparticle-stabilized pentane emulsion generated via sonication method to be injected into core for residual oil recovery experiments.

A comparison of the viscosity profiles of the two emulsions at different ionic concentrations is shown in Figure 4.36. While the emulsions display similar viscosity profiles at low shear rates, the 0% API emulsion begins to exhibit non-Newtonian shear-thinning behavior at ~10 $s^{-1}$, indicative of the dynamic instabilities and droplet coalescence.

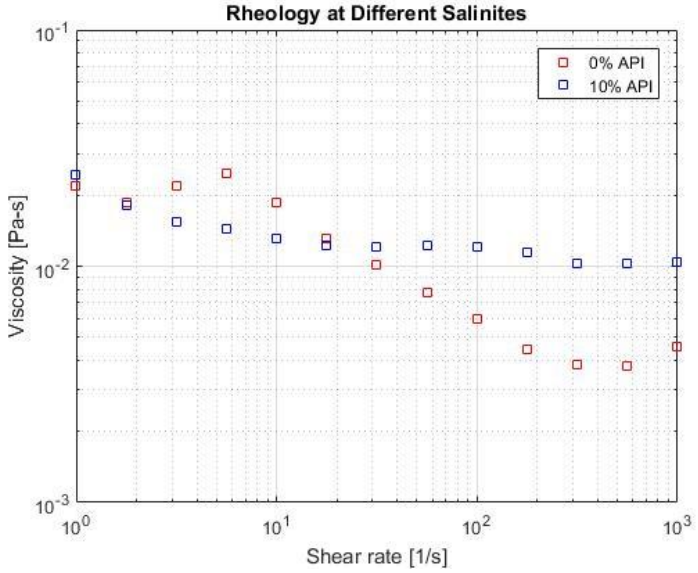


Figure 4.36: Rheological comparison of 0 wt% and 10 wt% API, PEG nanoparticle-stabilized pentane emulsion generated via sonication method to be injected into core for residual oil recovery experiments.

Again, formation of a network of interconnected droplets and aggregates as first proposed by Horozov et al. (2007) aids in the dynamic stability of the high-salinity 10 wt% API emulsion. While the increase in ionic concentration aids dynamic stability of emulsions through droplet-aggregate bridging, exponential decreases in electrostatic double layer forces between droplets and grains were expected to increase interception phenomenon, effective permeability reductions, sweep efficiencies, and ultimately, residual oil recovery.

***Emulsion Injection and Pressure Responses***

0 wt% API emulsion was injected into a Boise sandstone core at residual mineral oil saturation which had been previously waterflooded with 5% API brine as described in the coreflood experimental methods section. It was injected at a flow rate of 0.5 mL/min (~16 ft/day) to observe the effects of using nanoparticle-stabilized emulsions at low salinities for residual oil recovery. It was thought that the presence of the resident 5% API

brine from waterflooding procedures would prevent clay-swelling as the emulsion was injected, through the diffusion of ions into the aqueous phase of the emulsion. Roughly 8 pore volumes of emulsion were injected.

Figure 4.37 displays the effluent from the core during the first three pore volumes of emulsion injection and pressure drop across core for eight pore volumes of injection. The residual mineral oil was initially colorless, but it is thought that some oil-soluble red dye from a previous coreflood was not entirely flushed from the flow lines, leading to some of the oil picking up a red tint. The pressure drop was observed to increase until approximately 30 psi at 2.5 pore volumes, then the pressure dropped drastically to 5 psi. This rapid pressure decrease has been attributed to the injection of a slug of excess aqueous nanoparticle phase that had separated from the emulsion in the accumulator. Pressure began to build again at a similar rate, reaching a pseudo steady-state at approximately 6.5 pore volumes at which the pressure oscillated at a maximum between 50 and 15 psi with an average of roughly 43 psi. These oscillations are indicative of droplet pore-throat blockage and deformation (eventually flowing through throat). However because no emulsion was produced in the effluent, the emulsion is breaking at some point within the core due to its dynamic instability as detailed in the preceding rheology section.

| Coreflood E – 0 wt% API Emulsion Residual Oil Recovery | | | | | |
|---|---|---|---|---|---|
| k (mD) | ϕ | Pore Volume (mL) | $S_{or}$ | Flow Rate (mL/min) | Percent Recovery (%) |
| 2541 | 0.33 | 46.43 | 0.23 | 0.5 | 87 |

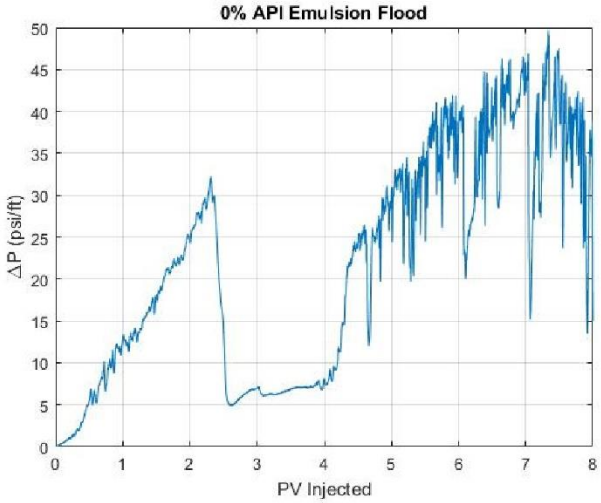


Figure 4.37: Coreflood E – 0 wt% API emulsion flood. Residual oil recovery of mineral oil through injection of ~8 pore volumes of emulsion at 0.5 mL/min. Aqueous phase-mineral oil interphase identified by red lines in picture of effluent collected. Tan water phase is the result of produced solids, which can be seen at the bottom of the test tubes.

Before injection of the emulsion, the residual oil saturation ($S_{or}$) was calculated to be 0.23 which indicated that at a pore volume 46.43 mL there was 10.67 mL of oil available for recovery. 9.3 mL of mineral oil was recovered from the core following the emulsion injection resulting in 87.2% of residual oil recovery. This residual oil was produced within the first two pore volumes of emulsion injection. After the first two pore volumes of emulsion injection, roughly 1:1 nanoparticle dispersion to pentane was produced in the effluent (otherwise, broken emulsion). No emulsion was ever present in the effluent. There is likely some increase in mobility control and sweep efficiency in section of the core near the inlet as the pressure drop suggests pore-throat blockage and effective permeability reduction, however the dominating mechanism of oil recovery is likely due to increases in miscibility of the displacing front due to the pentane that has broken from the emulsion.

The test tubes shown above were left in a fume hood for 48 hours to allow the pentane to evaporate from the oil phase to obtain accurate measurements of residual mineral oil recovery. This explains why several of the test tubes have less than 12-13 mL of fluid. The first test tube has less due to the timing of the start of emulsion injection and the timer on the fractional collector. The tan, turbid aqueous phases in tubes 5-8 are indicative of produced solids from unpredicted clay-swelling. In the future, 0 wt% API emulsions will not be used in coreflood experiments.

While there was likely an increase in pore volume due to the amount of solids produced in the effluent of the 0 wt% API emulsion flood, permeability tests were conducted after the core had been cleaned as described in the methods section and the post-emulsion flood core permeability was within 6% of the original permeability. Because of this it was assumed that the production of solids in the first flood would have negligible effects during the residual oil recovery experiments for the 10 wt% API emulsion flood.

10 wt% API emulsion was injected into the cleaned Boise sandstone core at residual mineral oil. Like the 0 wt% API emulsion flood, it was injected at a flow rate of 0.5 mL/min (~16 ft/day) to observe the effects of using nanoparticle-stabilized emulsions at high salinity for residual oil recovery. Roughly 8 pore volumes of emulsion were injected.

Figure 4.38 displays the effluent from the core during the first three pore volumes of emulsion injection and the pressure drop across the core for eight pore volumes of injection. The residual mineral oil is dyed red, and the picture of the effluent centrifuge tubes was taken after allowing the pentane to evaporate for 48 hours. The pressure drop was observed to increase until approximately 700 psi at roughly 5 pore volumes of injection until the pressure decreased drastically to 100 psi. This rapid pressure decrease has been attributed to the injection of a slug of excess aqueous nanoparticle phase that had separated from the emulsion in the accumulator. Pressure increased again at a similar rate, however no pseudo steady-state was reached as in the 0 wt% API emulsion flood. The pressure drop continued to rise reaching a maximum pressure of ~1000 psi at the peak of the oscillations. As discussed before, these oscillations are indicative of droplet pore-throat blockage and droplet deformation (eventually flowing through the throat at large enough pressures). Emulsion broke through at approximately at 1.5 pore volumes of injection. After that continuous production of emulsion was continued until the end of the flood. This continuous rise in pressure is indicative of extreme effective permeability reduction as emulsion droplets continue to propagate into new pore-throats that have yet to be blocked.

| Coreflood E – 10 wt% API Emulsion Residual Oil Recovery | | | | | |
|---|---|---|---|---|---|
| k (mD) | ϕ | Pore Volume (mL) | $S_{or}$ | Flow Rate (mL/min) | Percent Recovery (%) |
| 2541 | 0.33 | 46.43 | 0.32 | 0.5 | 89 |

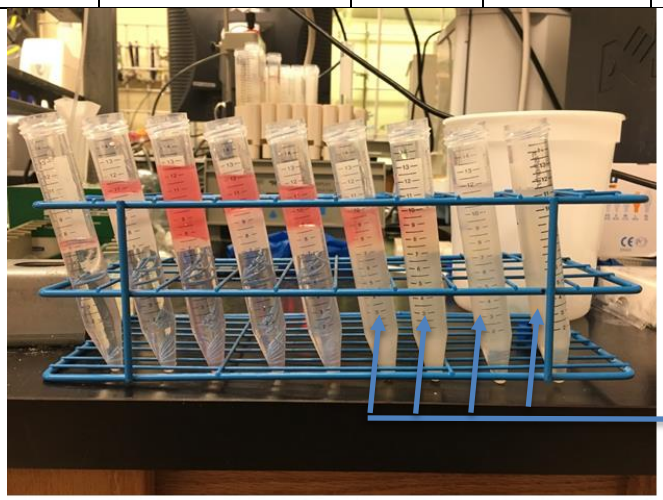


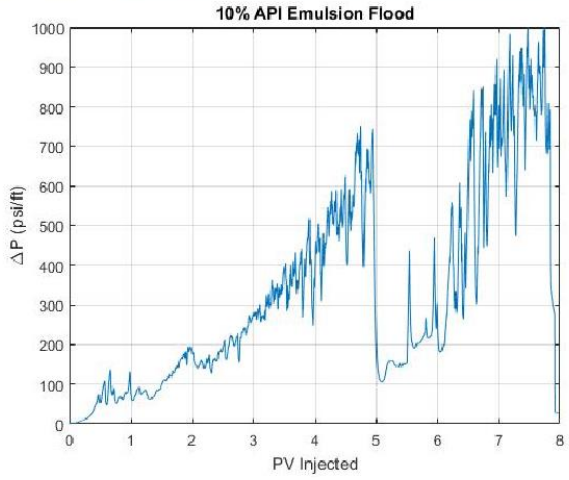


Figure 4.38: Coreflood E – 10 wt% API emulsion flood. Residual oil recovery of mineral oil through injection of ~8 pore volumes of emulsion injection at 0.5 mL/min. Emulsion breakthrough at 1.5 pore volumes, indicated by blue arrows.

Before injecting the emulsion, the residual oil saturation ($S_{or}$) was calculated to be 0.32 which indicated that at a pore volume 46.43 mL there was 15.04 mL of oil available for recovery. 13.4 mL of mineral oil was recovered from the core following the high salinity emulsion injection resulting in 89% recovery of residual mineral oil. Residual

mineral oil was produced within the first 1.5 pore volumes of emulsion injection. After this, emulsion was produced in the effluent until the termination of the test. Emulsion samples were taken from the effluent centrifuge tubes for microscopic imaging and rheology tests.

Droplet images were taken of effluent emulsion at different pore volumes and the median droplet diameters were found to be the same as the injected emulsion. An example of a microscopic image of the effluent emulsion is shown in Figure 4.39, taken from an emulsion sampled at 2.5 pore volumes with a median droplet size of 5.0 microns. Recall, the median droplet diameter of the injected emulsion was 4.9 microns.

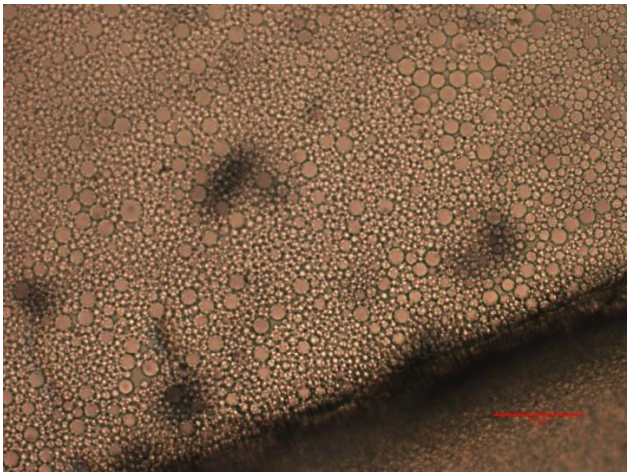

Figure 4.39: Microscopic image of droplets from effluent emulsion during 10 wt% API emulsion injection coreflood for residual oil recovery. Red scale bar of 50 microns. Median droplet diameter of 5.0 microns

The consistency in droplet size between the injected and produced emulsions demonstrates substantial increases in dynamic stability by simply increasing the ionic concentration in the aqueous nanoparticle dispersion used to generate the emulsions. It appears that the formation of a three-dimensional network of droplets and aggregates is critical to the

dynamic stability needed to keep droplets from coalescing while flowing through porous media.

Rheological tests were performed on effluent emulsion samples for multiple reasons. Comparisons between injected and effluent emulsion rheology serve as a convenient way of analyzing how flow through the porous media has changed characteristics such as bulk viscosity and dynamic stability. Effluent emulsion samples were taken from test tubes corresponding to 2, 2.5, and 3 pore volumes injected. Because it was a concern that some of the mineral oil had become emulsified in the produced emulsion and would impede on making accurate estimates of residual oil recovery, a mineral oil emulsion was generated to serve as a reference for rheological tests. Stabilized by the 10 wt% API PEG-coated nanoparticle dispersion, the mineral oil emulsion was generated via the same sonication method used to generate the injected pentane emulsion. Viscosity profiles of the injected emulsion and those discussed above are shown in Figure 4.40.

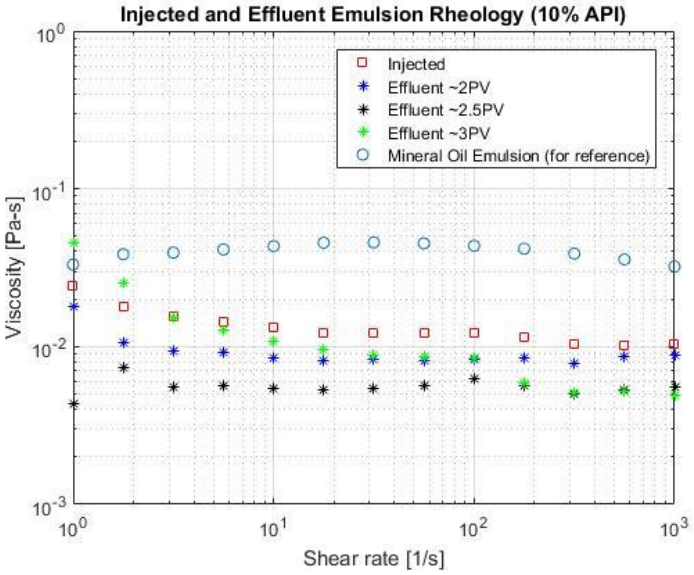


Figure 4.40: Rheology of injected 10 wt% API nanoparticle-stabilized pentane emulsion compared to effluent emulsion from residual coreflood experiment. Sonicated 10 wt% API nanoparticle-stabilized mineral oil emulsion included for reference.

Slight decreases in effluent emulsion viscosity are apparent and are likely due to minor droplet coalescence during flow through the core. It is difficult to tell from effluent emulsion microscope images whether droplet density per unit volume decreased in the effluent, due to droplets overlaying one another on the microscope slide. However with the viscosity profiles and general knowledge of the stability of nanoparticle-stabilized emulsions in-situ, it is safe to assume that either some droplet coalescence or retention occurred. From a rheology standpoint, if any mineral oil was present in the oleic phase of the effluent emulsions, the viscosity profile should be greater than that of the injected pentane emulsion. From a visual standpoint, no red or pink hue was seen in the effluent emulsion, which would have indicated the presence of dye that was present in the mineral oil (assuming no partitioning can occur through the aqueous phase and into pentane droplets). Finally, after the produced fluids from this experiment were allowed to evaporate

and/or separate, there was no indication of emulsified mineral oil emulsion in the effluent. This was expected given the large shear rates needed to initially generate emulsions. Furthermore, effluent emulsions possessed the same dynamic stability of the injected emulsion as shown in the multi-step rheology test in Figure 4.41. Although very slight reductions in bulk viscosity were observed between the injected and produced emulsions, it seems that any alteration that occurred due to flow through the core has not affected the dynamic stability of effluent emulsions.

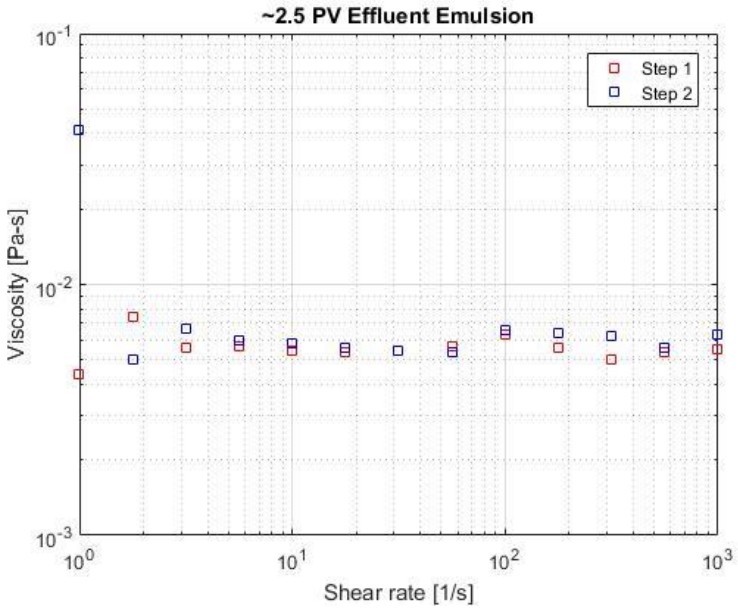


Figure 4.41: Multi-step dynamic stability rheology test of produced emulsion after 2.5 pore volumes of 10 wt% API nanoparticle-stabilized pentane emulsion injection for residual oil recovery experiment.

It is apparent that the high-salinity emulsion possesses advantages for residual oil recovery purposes compared to the low-salinity emulsion. From a dynamic stability perspective, high salinity emulsions are more robust as seen in the multi-step rheology tests, breakthrough in effluent, and as reflected in the pressure drop across the core during

injection. Furthermore, increases in oil recovery are likely due to the increases in interception phenomenon leading to greater effective permeability reduction and larger sweep efficiencies. The order of magnitude difference in pressure drop reflects the effects of increased ionic concentration in the reduction of repulsive electrostatic double layer forces between droplets and grain surfaces, as described by DLVO theory. Finally, while the presence of pentane droplets at the emulsion front increases the miscibility of the displacing front, no emulsification of mineral oil occurred with excess nanoparticle dispersion due to low injection rates (i.e. low shear rates). From a practicality standpoint this is great because nanoparticle-stabilized mineral oil emulsions are hard to separate at standard conditions due to the high viscosity of the oil phase. This test will be repeated given the clay-swelling and production of solids from 0 wt% API emulsion flood, instead using a 3 wt% API pentane emulsion. Similar results were expected.

***Repeating the Experiments***

Due to the unexpected clay-swelling and production of solids in the 0 wt% API emulsion flood during the previous experiments in Coreflood E, the experiment was repeated using 3 wt% and 10 wt% API pentane emulsions. The emulsions were sonicated at these salinities and were found to have nearly the same characteristics of the emulsions of those generated for Coreflood D (*Section 4.5.4*). The emulsions had median droplet diameters of ~3.6 microns, and nearly exact rheologies as seen in Figures 4.26, 4.27, and 4.28, where the 3 wt% API emulsion was much more viscous, but dynamically unstable. Similarities in the relative opaqueness of the emulsions were also observed, as seen in Figure 4.29.

First, roughly 6 pore volumes of 3 wt% API emulsion were injected at 0.5 ml/min, roughly 16 ft/day, into a Boise sandstone core at residual mineral oil saturation with a

porosity of 0.29, permeability of 693 mD, and pore volume of 44.08 mL. The core was then cleaned as described in the coreflood procedure section *4.3.6* and returned to residual mineral oil saturation. Roughly 6 pore volumes of the 10 wt% API emulsion were then injected at 0.5 ml/min. No emulsion was produced in the effluent for either coreflood, and pentane breakthrough occurred at approximately 1 pore volumes for both coreflood experiments.

Figure 4.42 displays the effluent from the core during the first 2.5 pore volumes of emulsion injection and pressure drop across the core for six pore volumes of injection. The residual mineral oil was dyed red. The pressure drop was observed to increase until approximately 24 psi at 1 pore volume, then gradually settle to 11 psi. Oscillations were indicative of droplet pore-throat blockage and deformation (eventually flowing through throats). No emulsion was produced in the effluent. The emulsion is likely breaking at some point within the core due to its dynamic instabilities. 56% of the residual mineral oil was recovered and was produced within the first two pore volumes of emulsion injected.

| Coreflood E (redo) – 3 wt% API Emulsion Residual Oil Recovery | | | | | |
|---|---|---|---|---|---|
| k (mD) | ϕ | Pore Volume (mL) | $S_{or}$ | Flow Rate (mL/min) | Percent Recovery (%) |
| 693 | 0.29 | 44.08 | 0.31 | 0.5 | 56 |

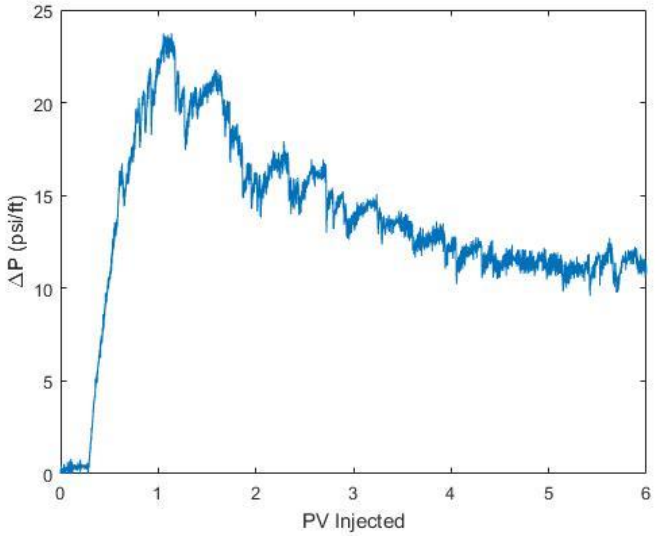


Figure 4.42: Coreflood E (redo) – 3 wt% API emulsion flood. Residual oil recovery of mineral oil through injection of ~6 pore volumes of emulsion injection at 0.5 mL/min. Effluent from first 2.5 pore volumes of injection shown.

The core was cleaned and returned to residual oil saturation. Then, roughly 6 pore volumes of 10 wt% API emulsion were injected into the core at residual mineral oil

saturation at 0.5 mL/min. Figure 4.43 displays the effluent from the core during the first 5 pore volumes of emulsion injection and pressure drop across core for six pore volumes of injection. The residual mineral oil was dyed red. The pressure drop gradually increased to 50 psi at the end of the flood. Oscillations are indicative of droplet pore-throat blockage and deformation (eventually flowing through throats). No emulsion was produced in the effluent, however residual mineral oil production was continued for nearly five pore volumes, contrasting one pore volume in the low salinity case.

| Coreflood E (redo) – 3 wt% API Emulsion Residual Oil Recovery | | | | | |
|---|---|---|---|---|---|
| k (mD) | ϕ | Pore Volume (mL) | $S_{or}$ | Flow Rate (mL/min) | Percent Recovery (%) |
| 693 | 0.29 | 44.08 | 0.31 | 0.5 | 61 |

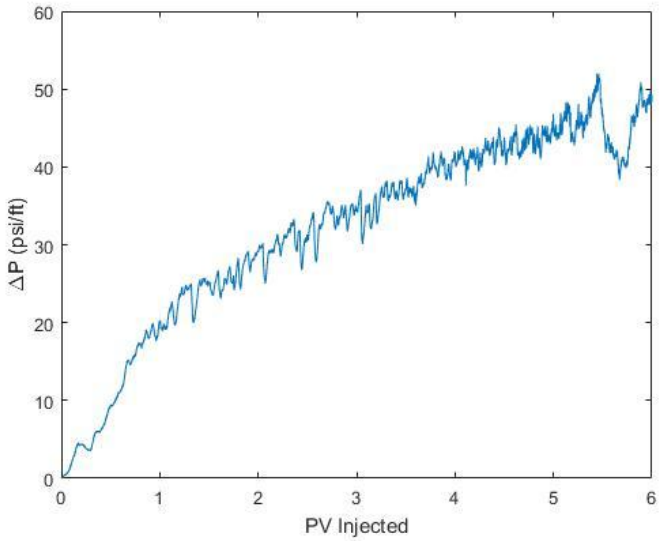


Figure 4.43: Coreflood E (redo) – 10 wt% API emulsion flood. Residual oil recovery of mineral oil through injection of ~6 pore volumes of emulsion injection at 0.5 mL/min. Effluent from first 5 pore volumes of injection shown.

Figure 4.44 displays reductions in effective permeability from the 3 and 10 wt% API emulsion floods, obtained from the pressure drop data.

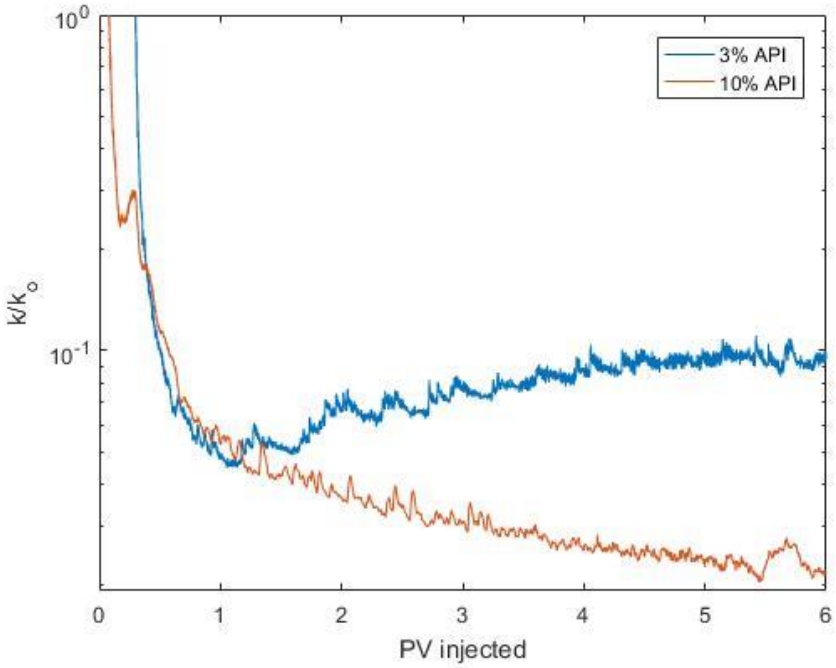


Figure 4.44: Coreflood E (redo) - Reduction in core effective permeability as a function of pore volumes injected for emulsion injection experiments at varying salinities. $k_o$ is from the steady-state permeability measurements obtained using 5 wt% API brine. Note semilog y-axis.

As discussed in the original Coreflood E experiments, it was apparent that high-salinity emulsions possess advantages for residual oil recovery purposes. Compared to the original set of corefloods, much more oil was recovered than in the repeated experiments. This is likely due to a lower permeability core, however the relative increases in pressure drop and residual oil recovered with increasing salinity indicate the advantages of higher salinity emulsions. A more in-depth analysis of why this is so can be found in the last paragraph before the start of this section.

### 4.5.6 Coreflood F: Effects of Sonicated Emulsion Zeta-potential on Residual Oil Recovery

This coreflood experiment was designed to investigate the effects that the zeta-potential of the emulsions had on heavy residual oil recovery during a nanoparticle-stabilized emulsion injection. Two brands of nanoparticles were used in these experiments, both PEG-coated with similar pH and nanoparticle size, however differing magnitudes in zeta-potential. The emulsion injected first in these experiments was generated using the PEG-coated nanoparticle dispersion that have been used in the previous experiments in this thesis. The second emulsion injected was generated using EOR 5xs from Nissan Chemicals, another PEG-coated concentrated nanoparticle dispersion (20 wt%) with similar effective nanoparticle size and pH. The concentrated nanoparticle dispersions were diluted to 2 wt% nanoparticles and 3 wt% API brine. These dispersions were used to generate pentane emulsions using the sonication method. Comparisons of the two dispersions are shown in Table 4.3 below:

| **Dispersion** | pH | Effective Nanoparticle Size (nm) | Zeta-potential (mV) |
|---|---|---|---|
| **PEG-coated** | 8.699 | 18 | -1.6 |
| **EOR 5xs** | 8.705 | 18 | -32.53 |

Table 4.3: Properties of aqueous nanoparticle dispersions used to generate pentane emulsions possessing different zeta-potential for residual oil recovery experiments. Effective nanoparticle size recorded at salinity of 3 wt% API and 2 wt% nanoparticles. Zeta-potential measurements taken at 0 wt% API and 2 wt% nanoparticles.

Amazingly, at the same dilution specifications (3 wt% API, 2 wt% nanoparticles) the two dispersions possessed the same effective nanoparticle size measured using the

Malvern Zetasizer DLS. Furthermore, the pH of each blend at this dilution was nearly identical. The zeta-potential of the two emulsions generated using these nanoparticle dispersions was measured at using the Zetasizer with no ionic concentration (0 wt% API) due to the limitations of the instrument in the presence of salinity. The decreases in zeta-potential with a marginal addition of salinity are believed to be inconsequential for the purposes of this experiment. To measure the zeta potential of the emulsions, the dense emulsion phase was diluted to a 0.1 wt% concentration in each respective 2 wt% nanoparticle dispersion used to generate the emulsions. This method was suggested from a Malvern representative due to issues with dense emulsion and excess aqueous and/or oleic phases separating in the folded capillary tube used by this instrument. The dilution of emulsion droplets gave a more accurate representation of droplet-droplet zeta-potential. As seen in Table 4.2, the emulsion generated using the EOR 5xs dispersion has a larger zeta-potential magnitude. This is indicative of larger repulsive forces between droplets and surfaces that they may come into contact with.

***Emulsions***

Each nanoparticle dispersion was used to generate roughly 250 mL of pentane emulsion via sonication for 45 seconds at an amplitude of 100%. A total of 50 mL of fluid was sonicated at a time. Droplet images were taken of the emulsions as shown in Figure 4.45.

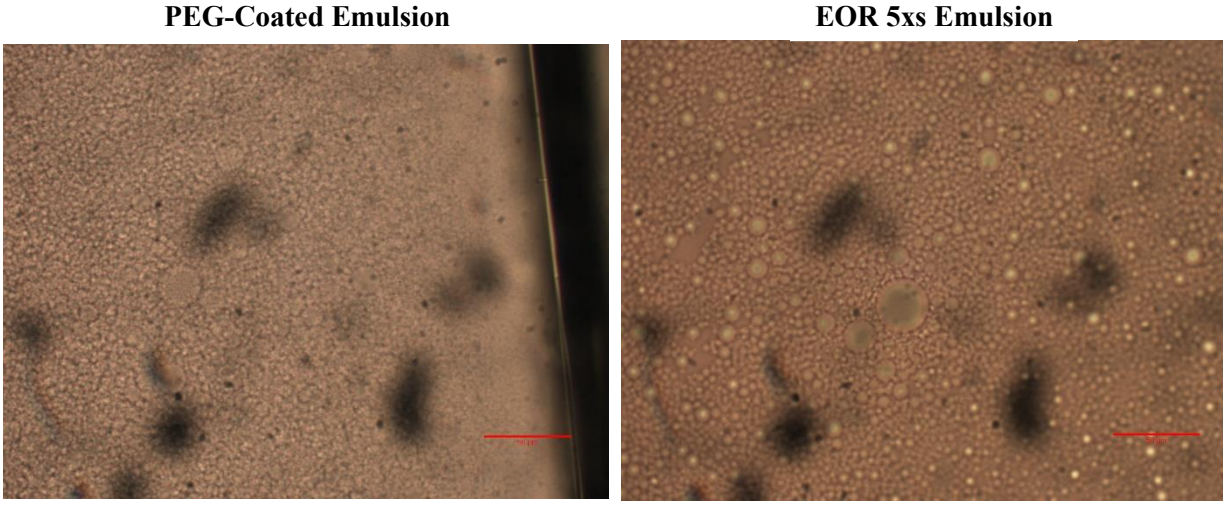


Figure 4.45: Microscopic images of pentane emulsions (1:1 phase ratio, 2 wt% nanoparticles, 3 wt% API) produced via sonication method with varying nanoparticle dispersion possessing different zeta-potential magnitude. Red lines represent scale bars of 50 microns. Median droplet diameters of 4.2 microns for both emulsions.

There seemed to be little effect of zeta-potential or nanoparticle dispersion type on the droplet size or the emulsification process. The emulsion generated with the previously used PEG-coated nanoparticles (low zeta-potential) and EOR 5xs nanoparticles (high zeta-potential) each had median droplet diameters of 4.2 microns.

***Rheology***

Rheology measurements of the sonicated emulsions generated using each type of nanoparticle dispersion were taken, including multi-step viscosity measurements where the tests were conducted sequentially without sample replacement. If droplet coalescence or breakage were to occur due to poor dynamic stability, a less viscous rheology profile would result in the second step of the test.

Figure 4.46 displays data from multi-step rheology tests conducted on the emulsion generated with the PEG-coated nanoparticle dispersion, otherwise the emulsion with the

smaller magnitude zeta-potential (-1.6 mV). This emulsion was borderline non-Newtonian, with slightly-shear thinning behavior. It possessed dynamic stability, displaying nearly the same viscosity profile in the multi-step test.

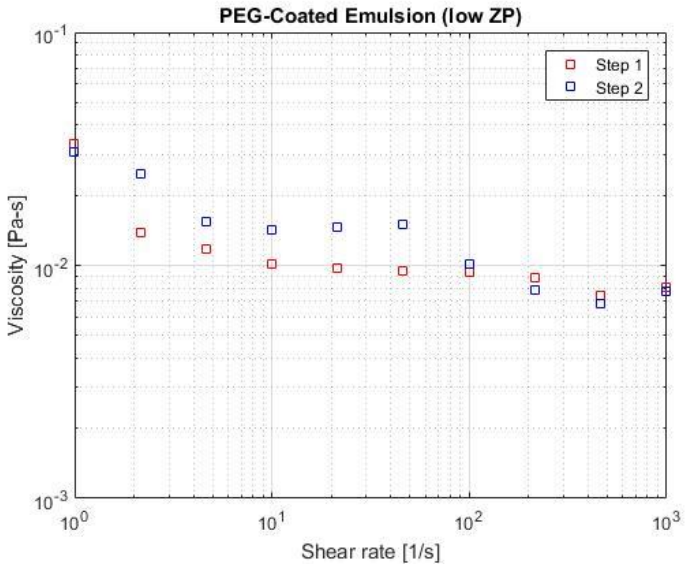


Figure 4.46: Rheology of 3 wt% API, PEG-coated nanoparticle-stabilized pentane emulsion generated via sonication method to be injected into core for residual oil recovery experiments. Of the two emulsions used in this experiment, this emulsion possessed a smaller magnitude zeta-potential of -1.6 mV.

Figure 4.47 displays data from the multi-step rheology tests conducted on the emulsion stabilized with the EOR 5xs emulsion, otherwise the emulsion with the larger magnitude zeta-potential (-32.53 mV). This emulsion was characterized as a Newtonian fluid. Furthermore, the droplets were stable under large imparted shear stresses as seen in the matching viscosity profiles in both steps of the multi-step test.

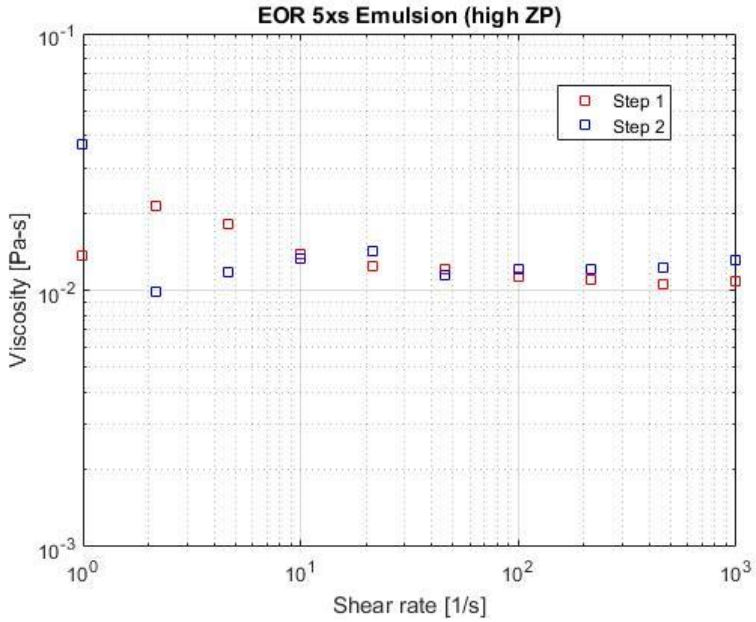


Figure 4.47: Rheology of 3 wt% API, EOR 5xs nanoparticle-stabilized pentane emulsion generated via sonication method to be injected into core for residual oil recovery experiments. Of the two emulsions used in this experiment, this emulsion possessed a larger magnitude zeta-potential of -32.53 mV.

A comparison of the viscosity profiles of the two emulsions with different nanoparticle dispersions and varying zeta-potentials is shown in Figure 4.48. The emulsion generated with the EOR 5xs seemed to be slightly more viscous, however for the purpose of this experiment, the rheology of each emulsion was considered equal.

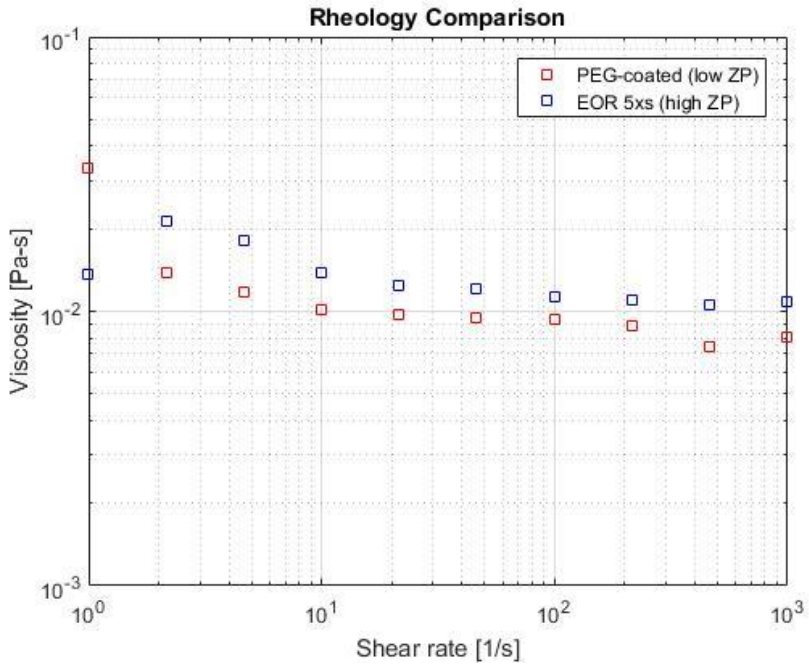


Figure 4.48: Rheology of pentane emulsions generated with PEG-coated and EOR 5xs aqueous nanoparticle dispersions at 3 wt% API, via sonication method, to be injected into core for residual oil recovery experiments. The emulsion stabilized by the PEG-coated nanoparticles had a zeta-potential of -1.6 mV, while the emulsion stabilized by the EOR 5xs nanoparticles had a larger zeta-potential of -32.53 mV.

***Emulsion Injection***

The low zeta-potential pentane emulsion stabilized by PEG-coated nanoparticles was injected into a Boise sandstone core at residual mineral oil saturation which had been previously waterflooded with 5% API brine as described in the coreflood experimental methods section. The emulsion was injected at a flow rate of 0.5 mL/min (~16 ft/day) to observe the effects of using nanoparticle-stabilized emulsions at low zeta-potential for residual oil recovery. Roughly 5 pore volumes of emulsion were injected.

Figure 4.49 displays the effluent from the core during the 5 pore volumes of emulsion injection and the pressure drop during that period. The residual mineral oil was dyed red. The pressure drop was observed to increase to approximately 130 psi at 1.4 pore

volumes of emulsion injection and then the pressure drop decreased drastically to 5 psi. This rapid pressure decrease has been contributed the injection of a slug of excess aqueous nanoparticle phase that had separated from the emulsion in the accumulator. Roughly 1.8 pore volumes of excess nanoparticle phase were then injected. Pressure then began to build again at a slower rate until five total pore volumes were injective. Again, oscillations seen in the pressure drop across the core are indicative of droplet pore-throat blockage and deformation (eventually flowing through throat). No emulsion was present in the effluent. This is indicative of the emulsion's dynamic instabilities while flowing through the core. For this blend of PEG-stabilized nanoparticles, a higher salinity aqueous nanoparticle phase is needed to form the robust droplet-aggregate network seen in the high salinity emulsion in Coreflood E.

| Coreflood F – PEG-coated 3 wt% API Emulsion | | | | | |
|---|---|---|---|---|---|
| k (mD) | ϕ | Pore Volume (mL) | $S_{or}$ | Flow Rate (mL/min) | Percent Recovery (%) |
| 3915 | 0.34 | 41.07 | 0.24 | 0.5 | 81 |

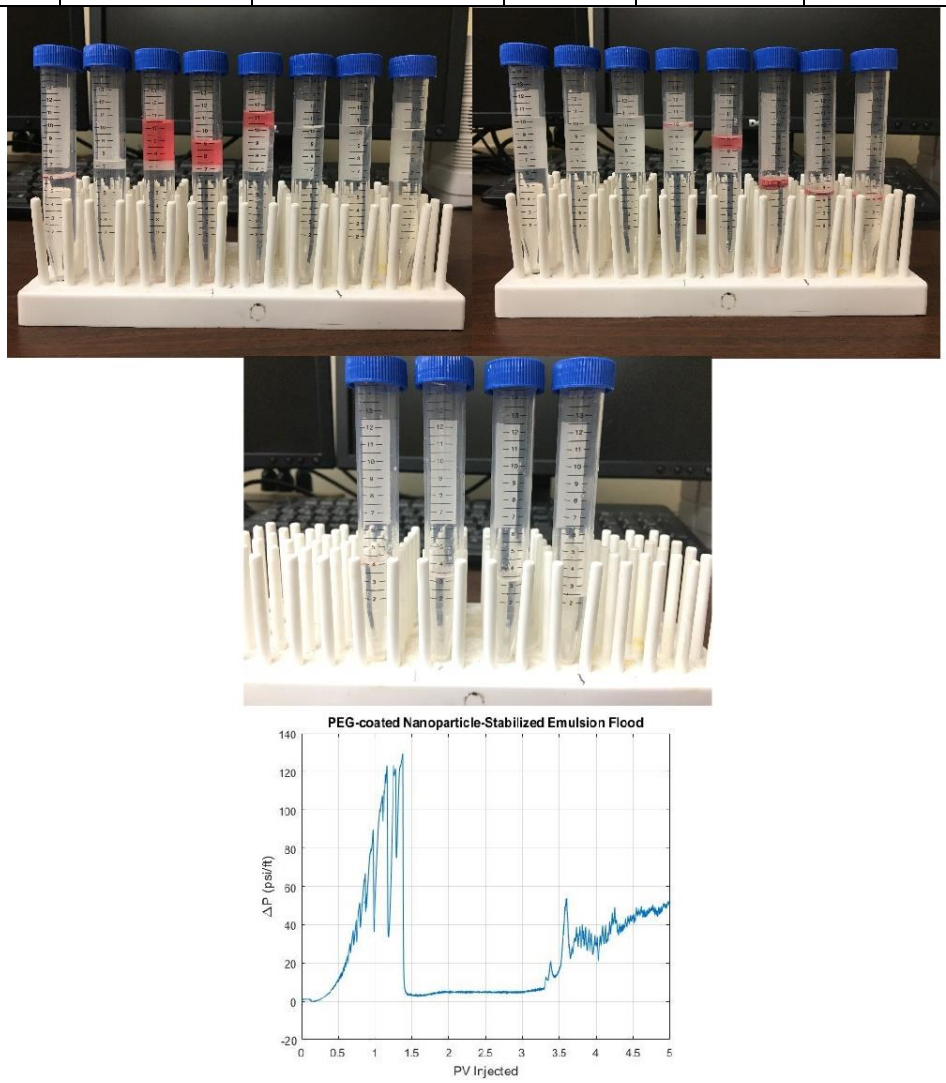


Figure 4.49: Coreflood F –PEG-stabilized pentane emulsion flood. Residual oil recovery of mineral oil through injection of ~5 pore volumes of emulsion at 0.5 mL/min.

Before injecting the emulsion, residual oil saturation ($S_{or}$) was calculated to be 0.24 which indicated that at a pore volume of 41.07 mL there was 9.73 mL of oil available for

recovery. 7.9 mL of mineral oil was recovered during emulsion injection resulting in a residual oil recovery of 81%. It seemed as though all of the oil was going to be produced within the first pore volume of injection, however after the unintended interval of excess nanoparticle phase injection, several additional mL's of oil where produced. This interval of nanoparticle dispersion injection is designated in centrifuge tubes 6-11 in Figure 4.49 where solely nanoparticle dispersion was injected and produced. Once emulsion injection starts again around 3.4 pore volumes, mineral oil production resumed and 1:1 ratio of nanoparticle dispersion to pentane (broken emulsion) was produced in the effluent. This is indicated in test tube 14 with the dyed mineral oil and missing volume due to pentane evaporation. Increases in residual oil recovery were likely due to enhanced mobility control and sweep efficiencies in the section of the core near the inlet as the pressure drop suggests pore-throat blockage and effective permeability reduction. As the emulsion propagates through the core, the dominating mechanism of oil recovery is likely due to increased miscibility of the displacing front due to pentane that has broken from the emulsion.

After cleaning the core as detailed in the coreflood procedures section and returning to residual mineral oil saturation, EOR 5xs nanoparticle-stabilized pentane emulsion was injected into the core. Like the PEG-coated nanoparticle-stabilized emulsion flood, it was injected at a flow rate of 0.5 mL/min (~16 ft/day) to observe the effects of using emulsions at varying zeta-potentials. Roughly 5 pore volumes of emulsion were injected.

Figure 4.50 displays the effluent from the core during 5 pore volumes of emulsion injection and the pressure drop during that period. The residual mineral oil was dyed red. The pressure drop was observed to increase to ~230 psi at 2.8 pore volumes of emulsion injection until the pressure drop decreased drastically to 30 psi. This rapid pressure decrease has been attributed to the injection of a slug of excess aqueous nanoparticle phase that had separated from the emulsion in the accumulator. Roughly 1.2 pore volumes of

excess nanoparticle phase were then injected. Pressure increased at an extremely fast rate and reached 250 psi, where the pressure began to oscillate again until five total pore volumes were injective. These oscillations seen in the pressure drop across the core are indicative of droplet pore-throat blockage and deformation. Emulsion was present in the effluent. In this case, the nanoparticle blend with the higher zeta-potential possessed better in-situ stability. Effluent emulsion was produced at approximately 1.5 pore volumes of injection. It appears that for the higher zeta-potential EOR 5xs aqueous nanoparticle dispersion, a high ionic concentration is not needed to stabilize and propagate emulsion through the core.

| Coreflood F – EOR 5xs-coated 3 wt% API Emulsion | | | | | |
|---|---|---|---|---|---|
| k (mD) | ϕ | Pore Volume (mL) | $S_{or}$ | Flow Rate (mL/min) | Percent Recovery (%) |
| 3915 | 0.34 | 41.07 | 0.25 | 0.5 | 85 |

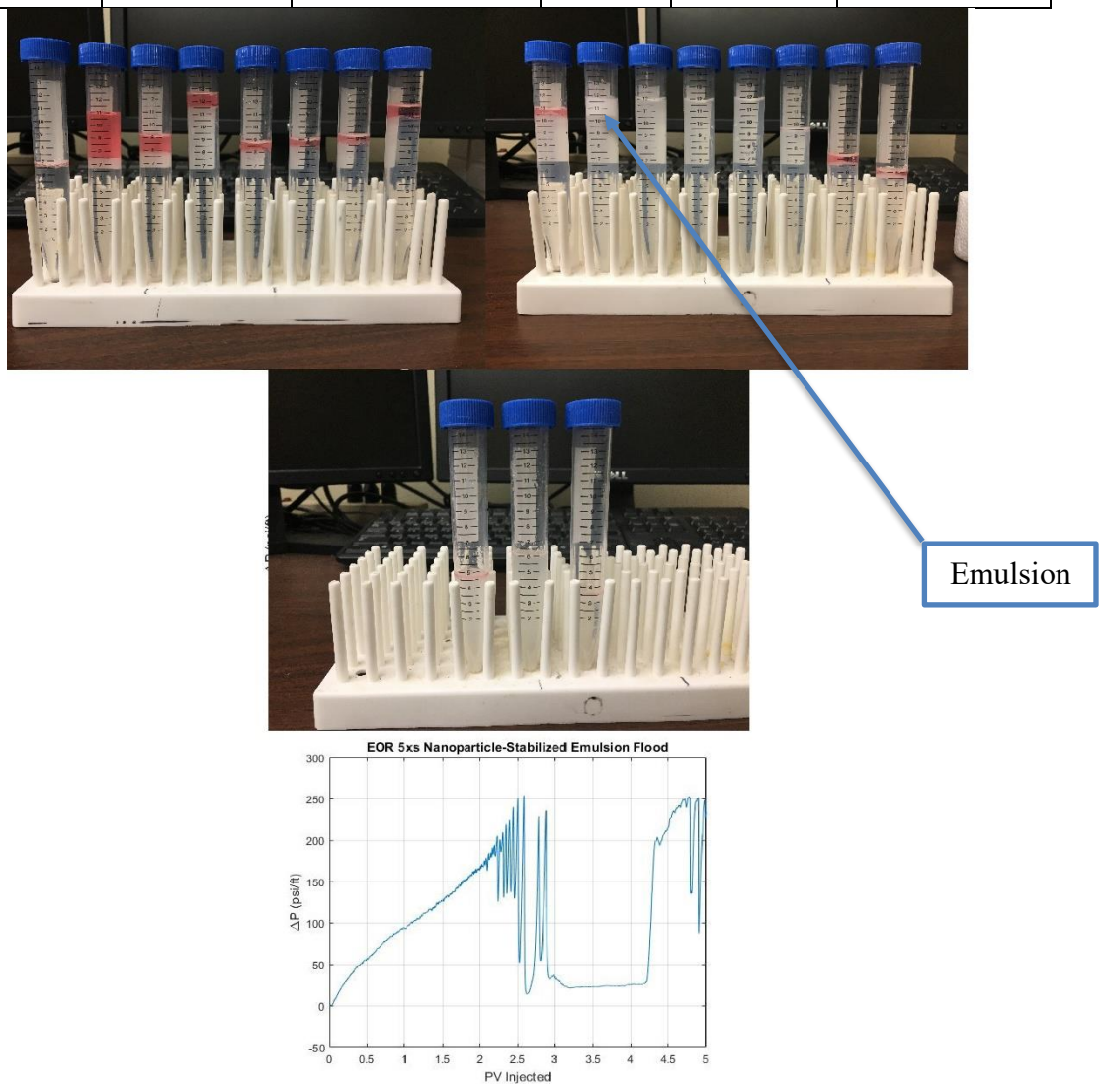


Figure 4.50: Coreflood F –EOR 5xs nanoparticle-stabilized pentane emulsion flood. Residual oil recovery of mineral oil through injection of ~5 pore volumes of emulsion at 0.5 mL/min

Before injection of the emulsion, the residual oil saturation ($S_{or}$) was calculated to be 0.24 which indicated that at a pore volume 41.07 mL there was 11.32 mL of oil available for recovery. 9.6 mL of mineral oil was recovered from the core following emulsion injection resulting in a residual oil recovery of 85%. In this case, it seemed as though all of the oil was going to be produced within the first two pore volume of emulsion injection, however after the unintended interval of excess nanoparticle phase injection, several additional mL's of oil where produced. The interval of nanoparticle dispersion injection is designated in centrifuge tubes 11-14 in Figure 4.50, where solely nanoparticle dispersion was produced. Once emulsion injection resumed, around 4.2 pore volumes injected, mineral oil and emulsion production resume. This is indicated in the dyed mineral oil in tube 14 and missing volume due to pentane evaporation. After pentane evaporation, a small fraction of very viscous emulsion remained stable counteracting the volatile pentane evaporation as highlighted in Figure 4.50.

Droplet images of effluent emulsions were taken at different pore volumes and median droplet diameters were consistent at 2.5 microns. A droplet image taken of the effluent emulsions is shown in Figure 4.51.

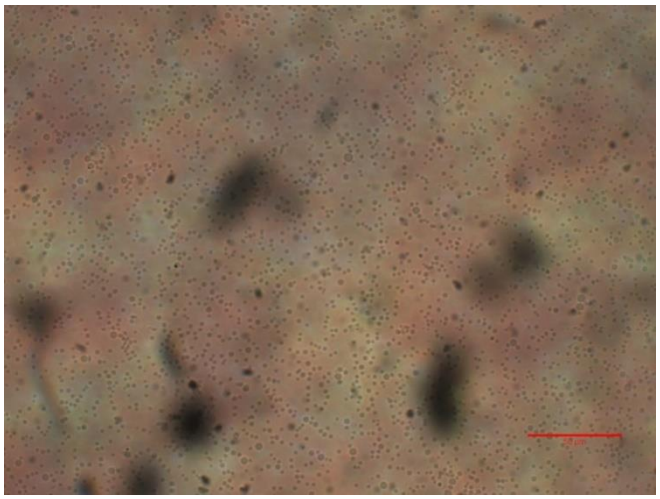

Figure 4.51: Microscopic images of effluent EOR 5xs pentane produced during residual oil recovery coreflood experiment. Red line represents scale bars of 50 microns. Median droplet diameter of 2.5 microns.

Unlike the dense injected emulsion, the effluent emulsion droplets were much less dense. These droplets were also smaller than those of the injected emulsion (4.2 microns). Unfortunately, the rheometer was under repair during this time period, and rheology measurements of the volatile pentane emulsion were unable to be made. The larger droplets have either broken or are entrapped in pore throats. In this case, increased residual oil recovery was likely due to enhanced mobility control and sweep efficiency throughout the entire section of the core as the pressure drop suggests pore-throat blockage and effective permeability reduction.

Figure 4.52 displays a comparison between the pressure responses of the injected emulsions in Coreflood F residual oil recovery experiments.

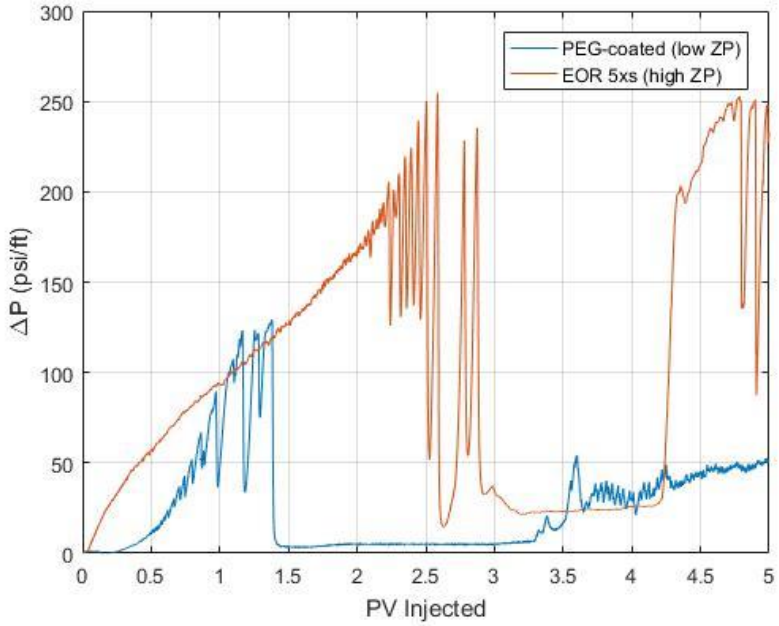


Figure 4.52: Coreflood F – comparison between PEG-coated and EOR 5xs emulsion pressure drops obtained during residual oil recovery experiments.

Although the EOR 5xs, high zeta-potential emulsion recovers only ~3% more residual oil, there is a significant reduction in effective permeability as shown in the larger pressure drop. In Coreflood E increased salinity aided in the emulsion's dynamic and in-situ stability. Furthermore, it is though that increases in salinity aid droplet-grain surface interception capture through exponential decreases in electrostatic double layer repulsive forces. Because the emulsions used in Coreflood F experiments were generated at low salinities, changes in zeta-potential only have a linear effect on the change in electrostatic double layer repulsive forces, per DLVO theory. Furthermore, it should be noted that simplifications were made in explaining extended DLVO theory in porous media. In reality, interactions between droplets and complex grain-surface geometries from the perspective of a single droplet make it difficult to ascertain what the dominant surface force imparted on a droplet. However, it is concluded that in the case of the high zeta-potential

emulsion (at low salinity), the droplets are repulsed via electrostatic repulsive forces rather than mechanical bridging of aggregates between droplets. Furthermore, the increase in pressure drop in the high zeta-potential case occurs due to the droplets having more resistance to flow through a pore throat due to increased repulsive forces between droplets and grains encountered at tight constrictions. Twofold, the increase in stability between droplets and local increases in the capillary pressure needed to force high zeta-potential droplets through a pore throat explain the increase in pressure drop and marginal increases in percent of residual oil saturation recovered.

## 4.6 CONCLUSION

As shown in Coreflood A, varying the injection rate for sonicated emulsions did not have a significant effect on an emulsion's ability to block pore throats as reflected in nearly identical effective permeability reduction ratios. Contrasting with surfactant-stabilized emulsions, where lower injection rates have shown to lead to more extensive effective permeability reductions, differences in the behavior of nanoparticle-stabilized emulsions could be contributed to: not a wide enough range of capillary numbers explored to observe a difference, in-situ instability relative to ultra-robust surfactant-stabilized emulsions, and differences in concentration of emulsion droplets per unit volume. Furthermore, because the droplets were much smaller than the average pore throats, the effectiveness of droplet-pore throat blockage is likely less of a function of local capillary forces and interstitial velocity, rather dependent on concentration of emulsion droplets per unit volume (held constant in this case).

In Coreflood B, beadpack-generated nanoparticle-stabilized emulsions of varying droplet size where injected to observe the effects of droplet size on effective permeability reduction and in-situ stability. Surfactant-stabilized emulsion was also injected to observe

the effects that the emulsifying agent had on these properties. It was concluded that beadpack emulsions with larger droplet-to-pore-throat ratios exhibit increased pore-throat blockage, as deduced from pressure responses and effective permeability reduction plots. Surfactant proved to be a much more effective emulsifier, exhibiting in-situ stability (no nanoparticle-stabilized emulsion was produced in the effluent during these tests) and as a consequence displaying more effective pore-throat blocking abilities as seen in much larger effective permeability reduction ratios.

In Coreflood C, the effects of increasing salinity on beadpack-generated emulsions' dynamic and in-situ stability, coreflood pressure response, and effective permeability reduction were observed. The high salinity emulsion displayed enhanced dynamic stability in the rheology tests, however the pressure drop and effective permeability reductions were slightly larger for the low salinity emulsion. The difference in these responses was likely statistically insignificant. The in-situ instabilities observed during this and previous corefloods of beadpack-generated emulsions, as seen in the lack of effluent emulsion and relatively low pressure drops, have led to the conclusion that despite high salinity or high emulsion generating shear rates (high beadpack co-injection rates), beadpack emulsions are inferior to sonicated emulsions in terms of in-situ stability.

In Coreflood D, the effects of increasing salinity on sonicated emulsions' dynamic and in-situ stability, coreflood pressure response, and effective permeability reduction were observed. Although no emulsion was produced in the effluent, the difference in pressure response for the low and high salinity emulsions generated via sonication was drastic. Despite the order of magnitude reduction in viscosity for the high salinity emulsion, there is an enormous increase of in-situ stability indicated by the large relative increase in pressure drop. This is likely due to strengthening in emulsion stability from droplet-droplet

bridging and enhanced droplet-grain attachment due to reductions in electrostatic repulsive forces via DLVO theory, otherwise known as droplet capture in filtration theory.

In Coreflood E, the effects of sonicated emulsion salinity on heavy residual oil recovery were observed. High salinity emulsions were more dynamically stable as seen in the multi-step rheology tests, breakthrough in effluent, and as reflected in the pressure drop across the core during injection. Furthermore, increases in oil recovery are likely due to increases in interception phenomenon leading to greater effective permeability reduction and better sweep efficiencies. The order of magnitude difference in pressure drop reflects the reduction in repulsive electrostatic double layer forces between droplets and grain surfaces as ionic concentration is increased.

In Coreflood F, the effects of emulsion zeta-potential on heavy residual oil recovery were observed. The high zeta-potential emulsion, resulted in marginal increases in residual oil recovery (~3%) and significant reductions in effective permeability. It was concluded that at high zeta-potentials, emulsion droplets are repulsed via electrostatic repulsive forces rather than mechanical bridging of aggregates between droplets. The increase in pressure drop in the high zeta-potential case occurs due to the droplets' increased resistance to flow through a pore throat, a product of increased repulsive forces between droplets and grains encountered at tight constrictions. Twofold, the increase in stability between droplets and local increases in capillary pressure needed to force high zeta-potential droplets through pore throats explain the increase in pressure drop and marginal increases in percent residual oil saturation recovered.

# Chapter 5

# Conclusions and Future Work

## 5.1 Conclusions

### 5.1.1 Static Stability of Nanoparticle-Stabilized Natural Gas Liquid-in-Water Emulsions

The salinity was varied from 0-20 wt% (API brine) for both the DP9711 and PEG-coated nanoparticle dispersions and a noticeable increasing trend in hydrodynamic diameter was observed. Increased nanoparticle aggregation was explained by the reduction in repulsion potential between particles from decreased electrostatic double layer forces due to increasing ionic concentrations.

Significant decreases in median droplet size were observed for pentane-in-water emulsions when the salinity was increased from 5 wt% to 10 wt% API, but less distinct trends were observed for salinities greater than 10 wt% API. For all salinities pentane emulsions were shown to remain stable if pressurized at 100 psi. When kept at room temperature and pressure, the emulsions would destabilize within 2 days, except for the emulsions at 20 wt% salinity due to the formation of a bicontinuous gel consisting of nanoparticle aggregates, high-salinity water, and residual amounts of trapped pentane. Pentane emulsion rheology was observed to be strongly shear-thinning. As the salinity of the emulsions increased, an increase in effective viscosity was observed.

Butane emulsions were generated using nanoparticle dispersions ranging from 5-20 wt% API salinity. As the salinity was increased, increases in fraction of emulsion phase, stability, and viscosity were observed.

### 5.1.2 Coreflood Experiments through Sandstone Cores

Nanoparticle-stabilized emulsions were injected into Boise sandstone cores to quantify and optimize in-situ emulsion stability for residual oil recovery purposes. For sonicated emulsions, varying the injection rate did not have a significant effect on an emulsion's ability to block pore throats, contrary to surfactant-stabilized emulsions, where lower injection rates have shown to lead to more extensive effective permeability reductions. Differences in this behavior could be contributed to: not a wide enough range of capillary numbers explored to observe a difference, in-situ instability relative to ultra-robust surfactant-stabilized emulsions, and differences in concentration of emulsion droplets per unit volume. Because the sonicated emulsion droplets were much smaller than the average pore throats of Boise sandstone, pore throat blockage phenomenon is likely dependent on the concentration of emulsion droplets per volume, rather than interstitial velocity and local capillary forces.

Beadpack-generated nanoparticle-stabilized emulsions of varying droplet size were injected into a sandstone core to observe the effects on effective permeability reduction and in-situ stability. It was concluded that beadpack emulsions with larger droplet-to-pore-throat ratios exhibit increased pore-throat blockage and effective permeability reduction. Surfactant-stabilized emulsion was injected and displayed increased in-situ stability, and as a consequence exhibited greater pore-throat blocking and effective permeability reduction abilities.

Beadpack-generated nanoparticle-stabilized emulsions of varying salinity were injected to observe the effects on effective permeability reduction and in-situ stability. While the high salinity beadpack emulsion displayed enhanced dynamic stability in the rheology tests, no significant increases in in-situ stability or effective permeability reductions were observed. The in-situ instabilities of beadpack-generated emulsion

corefloods like this, led to the conclusion that despite high salinity or high emulsion generating shear rates (high beadpack co-injection rates), beadpack emulsions are inferior to sonicated emulsions in terms of in-situ stability.

Sonicated nanoparticle-stabilized emulsions of varying salinity were injected to observe the effects on effective permeability reduction and in-situ stability. Despite an order of magnitude reduction in viscosity for the high salinity emulsion, an enormous increase of in-situ stability was indicated by the large relative increase in pressure drop. This was likely due to strengthening in emulsion stability from droplet-droplet bridging and enhanced droplet-grain attachment due to reductions in electrostatic repulsive forces via DLVO theory, otherwise known as droplet capture in filtration theory. Next, the same sonicated emulsions were injected into a sandstone core at residual oil saturation. Marginal increases in oil recovery were observed for the high salinity emulsion. The order of magnitude difference in pressure drop for low and high salinity emulsions reflected a decrease in repulsive electrostatic double layer forces between droplets and grain surfaces as the ionic concentration was increased.

Finally, sonicated nanoparticle-stabilized emulsions of varying zeta-potentials were injected to observe the effects on in-situ stability, effective permeability reduction, and residual oil recovery. Marginal increases in oil recovery, significant reductions in effective permeability, and in-situ stability were observed for the high zeta-potential emulsion. It was concluded that at high zeta-potentials, emulsion droplets are repulsed via electrostatic repulsive forces rather than mechanical bridging of aggregates between droplets, as in high salinity emulsions. The increase in pressure drop in the high zeta-potential case occurs due to the droplets' increased resistance to flow through a pore throat, a product of increased repulsive forces between droplets and grains encountered at tight constrictions. Two fold increase in stability between droplets and local increases in capillary pressure needed to

force high zeta-potential droplets through pore throats explained the increase in pressure drop and marginal increases in percent residual oil saturation recovered.

## 5.2 Future Work

Potential objectives for the expansion of this research are listed below:

- Glass micromodel experiments made to model single and/or multiple pore throats to visualize the effects of emulsifier, salinity, droplet size, and zeta-potential on pore-blocking potential. Extended DLVO and filtration theory may be useful in explaining observed phenomena.
- The effects of nanoparticle stability after encountering crude oils should be studied. Extending this, corefloods should be performed with heavy crude oils as the residual oil phase using nanoparticle-stabilized natural gas liquid emulsions as the displacing fluid.
- Different surface coatings or nanoparticle materials could be applied on nanoparticles to optimize residual oil recovery and in-situ emulsion stability. Optimizing both nanoparticle surface coatings, materials, and emulsion characteristics for different downhole environments is the ultimate objective.
- Nanoparticle-stabilized emulsions should be injected into different cores to observe how different permeability, pore size distribution, grain chemistry, etc. effect emulsion flow through porous media. Eventually, corefloods should be conducted with field cores rather than outcrop cores to see if this affects nanoparticle and emulsion in-situ stability.
- Temperature effects on emulsions and nanoparticles with different surface coatings should be explored.
- Aforementioned suggestions should also be evaluated with water-in-oil emulsions.

# References


Ahmad, Y. K. (2016). *Nanoparticle-Stabilized Oil-in-Water Emulsions for Residual Oil Recovery.* University of Texas at Austin, Austin. (M.S.E. Thesis).

Esmaeeli Azadgoleh, J., Kharrat, R., Barati, N., & Sobhani, A. (2014). Stability of Silica Nanoparticle Dispersion in Brine Solution: An Experimental Study. *Iranian Journal of Oil & Gas Science and Technology*, *3*(4), 26-40.

Binks, B. P. (2002). Particles as surfactants—similarities and differences. *Current opinion in colloid & interface science*, *7*(1), 21-41.

Binks, B. P., & Lumsdon, S. O. (2000). Influence of particle wettability on the type and stability of surfactant-free emulsions. *Langmuir*, *16*(23), 8622-8631.

Binks, B. P., & Lumsdon, S. O. (2000). Effects of oil type and aqueous phase composition on oil–water mixtures containing particles of intermediate hydrophobicity. *Physical Chemistry Chemical Physics*, *2*(13), 2959-2967.

Bragg, J. R. (1999). *U.S. Patent No. 5,910,467*. Washington, DC: U.S. Patent and Trademark Office.

Cates, M. E., & Clegg, P. S. (2008). Bijels: a new class of soft materials. *Soft Matter*, *4*(11), 2132-2138.

Cobos, S., Carvalho, M. S., & Alvarado, V. (2009). Flow of oil–water emulsions through a constricted capillary. *International Journal of Multiphase Flow, 35*(6), 507-515.

Cooper, S. C., (1999). Interfaces, Colloids, and Gels [html]. Retrieved from http://community.dur.ac.uk/sharon.cooper/lectures/colloids/interfacesweb1.html#_Toc449417599

Derjaguin, B., and Landau, L. (1993). Theory of the stability of strongly charged lyophobic sols and of the adhesion of strongly charged particles in solutions of electrolytes. *Progress in Surface Science, 43*(1-4), 30-59.

Dickinson, E. (1992). *Introduction to food colloids.* Oxford University Press.

Dressaire, E., & Sauret, A. (2017). Clogging of microfluidic systems. *Soft Matter*, *13*(1), 37-48.

Fu, X. (2012). *Enhanced Oil Recovery of Viscous Oil by Injection of Water-in-Oil Emulsion Made with Used Engine Oil* (Doctoral dissertation, Texas A&M University).

Gabel, S. T. (2014). *Generation, stability, and transport of nanoparticle-stabilized oil-in-water emulsions in porous media.* University of Texas at Austin, Austin. (M.S.E. Thesis).

Hackley, V. A., & Clogston, J. D. (2011). Measuring the hydrodynamic size of nanoparticles in aqueous media using batch-mode dynamic light scattering. *Characterization of Nanoparticles Intended for Drug Delivery*, 35-52.

Horozov, T. S., Binks, B. P., & Gottschalk-Gaudig, T. (2007). Effect of electrolyte in silicone oil-in-water emulsions stabilised by fumed silica particles. *Physical Chemistry Chemical Physics*, *9*(48), 6398-6404.

Horozov, T. S. (2008). Foams and foam films stabilised by solid particles. *Current Opinion in Colloid & Interface Science, 13*(3), 134-140.

Kaminsky, R. D., Wattenbarger, R. C., Lederhos, J., & Leonardi, S. A. (2010). Viscous oil recovery using solids-stabilized emulsions. In *SPE Annual Technical Conference and Exhibition*. Society of Petroleum Engineers.

Keir, G., Jegatheesan, V., & Vigneswaran, S. (2009). Deep bed filtration: modeling theory and practice. *Water and Wastewater Treatment Technologies, V. Saravanamuthu, ed., Eolss Publishers, Oxford, UK*, 263-307.

Johnson, A. C. (2015) *Investigations of Porous Media using Nuclear Magnetic Resonance Secular Relaxation Measurements and Micro-CT Image Analysis*. University of Texas at Austin, Austin. (M.S.E. Thesis)

Kim, I., Taghavy, A., DiCarlo, D., & Huh, C. (2015). Aggregation of silica nanoparticles and its impact on particle mobility under high-salinity conditions. *Journal of Petroleum Science and Engineering*, *133*, 376-383.

Kobayashi, M., Juillerat, F., Galletto, P., Bowen, P., & Borkovec, M. (2005). Aggregation and charging of colloidal silica particles: effect of particle size. *Langmuir*, *21*(13), 5761-5769.

Lake, L. W. (1989). Enhanced oil recovery.

McAuliffe, C. D. (1973a). Oil-in-water emulsions and their flow properties in porous media. *Journal of petroleum technology*, *25*(06), 727-733.

McAuliffe, C. D. (1973b). Crude-oil-water emulsions to improve fluid flow in an oil reservoir. *Journal of Petroleum Technology*, *25*(06), 721-726.

Particle Sciences (2011) "Emulsion Stability and Testing." Technical Brief 2011, Vol. 2, Particle Sciences, Bethlehem, PA.

Pope, G. A. (2007). Overview of Chemical EOR, Center for Petroleum and Geosystems Engineering, The University of Texas at Austin, Casper EOR workshop.

Pickering, S. U. (1907). Cxcvi.—emulsions. *Journal of the Chemical Society, Transactions*, *91*, 2001-2021.

Pieranski, P. (1980). Two-dimensional interfacial colloidal crystals. *Physical Review Letters*, *45*(7), 569.

Pilapil, B. K., Jahandideh, H., Bryant, S. L., & Trifkovic, M. (2016). Stabilization of Oil-in-Water Emulsions with Noninterfacially Adsorbed Particles. *Langmuir, 32*(28), 7109-7116.

Saigal, T., Dong, H., Matyjaszewski, K., & Tilton, R. D. (2010). Pickering emulsions stabilized by nanoparticles with thermally responsive grafted polymer brushes. *Langmuir*, *26*(19), 15200-15209.

Saleh, N., Sarbu, T., Sirk, K., Lowry, G. V., Matyjaszewski, K., & Tilton, R. D. (2005). Oil-in-water emulsions stabilized by highly charged polyelectrolyte-grafted silica nanoparticles. *Langmuir*, *21*(22), 9873-9878.

Soo, H. (1983). *Flow of dilute, stable emulsions in porous media*. University of California, Berkeley. (Ph.D. Dissertation)

Stancik, E. J., & Fuller, G. G. (2004). Connect the drops: Using solids as adhesives for liquids. *Langmuir*, *20*(12), 4805-4808.

Stumm, W., & Morgan, J. J. (2012). *Aquatic chemistry: chemical equilibria and rates in natural waters* (Vol. 126). John Wiley & Sons.

Torres, L. G., Iturbe, R., Snowden, M. J., Chowdhry, B. Z., & Leharne, S. A. (2007). Preparation of o/w emulsions stabilized by solid particles and their characterization by oscillatory rheology. C*olloids and Surfaces A: Physicochemical and Engineering Aspects, 302*(1), 439-448.

Verwey, E. J. W., Overbeek, J. T. G., & Overbeek, J. T. G. (1999). *Theory of the stability of lyophobic colloids.* Courier Corporation.

Xu, K., Zhu, P., Colon, T., Huh, C., & Balhoff, M. (2016). A Microfluidic Investigation of the Synergistic Effect of Nanoparticles and Surfactants in Macro-Emulsion-Based Enhanced Oil Recovery. *SPE Journal.*

Zhang, T. (2009). *Emulsions Stabilized with Nanoparticles for Potential Conformance Control Applications*. University of Texas at Austin, Austin. (M.S.E. Thesis)

Zhang, T., Davidson, D., Bryant, S., and Huh, C., 2010, "Nanoparticle-Stabilized Emulsions for Applications in Enhanced Oil Recovery", SPE Improved Oil Recovery Symposium, SPE-129885-MS.

Zhang, T., Davidson, D., Bryant, S. L., & Huh, C. (2010, January). Nanoparticle-stabilized emulsions for applications in enhanced oil recovery. In *SPE improved oil recovery symposium*. Society of Petroleum Engineers.

Ziming Sun, J., Erickson, M. C., & Parr, J. W. (2005). Refractive index matching and clear emulsions. *International Journal of Cosmetic Science, 27*(6), 355-356.